

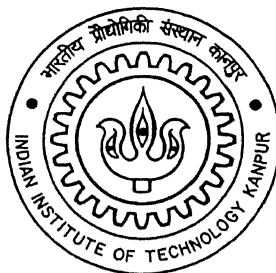
# **A novel duplex PSA and TSA cycle for fractionation of a binary gas mixture**

*A thesis submitted  
in partial fulfillment of the requirements  
for the degree of*

**MASTER OF TECHNOLOGY**

*by*

**PRAVEEN KUMAR**



*to the*

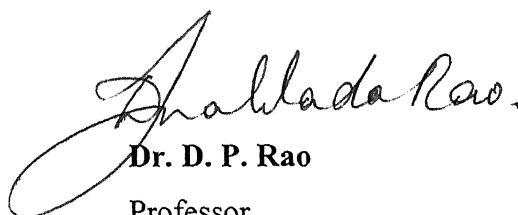
**DEPARTMENT OF CHEMICAL ENGINEERING  
INDIAN INSTITUTE OF TECHNOLOGY, KANPUR**

**July, 2005**

# CERTIFICATE

It is certified that the work contained in this thesis entitled "**A novel duplex PSA and TSA cycle for fractionation of a binary gas mixture**", by Praveen Kumar, has been carried out under my supervision and that this work has not been submitted elsewhere for a degree.

July, 2005

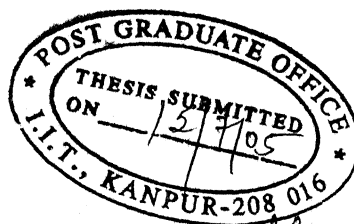
  
**Dr. D. P. Rao**

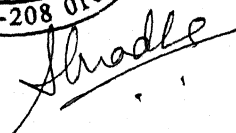
Professor

Department of Chemical Engineering

Indian Institute of Technology

Kanpur, 208016





TH  
CHE/2005/M  
K96n

12 SEP 2005 /CHE

मुख्योत्तम काशीनाथ केलकर पुस्तकालय  
भारतीय प्रौद्योगिकी संस्थान कानपुर  
अवधि क्र० 152791



A152791

*Dedicated*

*to*

*Grandmaa*



# Acknowledgement

I express my deep sense of gratitude to my thesis supervisor, Dr. D. P. Rao for his valuable guidance and encouragement throughout this work. I was very much inspired from his unending enthusiasm, complete devotion towards work and perfection in every respect.

I sincerely thank my lab senior Chetan who has given his valuable insights during the start of this work.

I thank all my labmates Murthy sir, Sivakumar, AChandra, Reddy, AmitG, Himmabindu, Milan, Surana, Prakash, Dinesh and especially to Kaushal for their cooperation in completing this work.

Special thanks to the group *bits@iitk* with members Rajeev sir, Rajiv, Arvind, Ravish, Sonali and me too. They provided me a lovely family atmosphere during my stay at IIT Kanpur. The fun time shared with them will always be a treasured memory.

I can't forget ever in my life the help and affection shown by Mishra, Ravi, Sachin, Chhavi, Kasturi, Sonny and especially by *bit@iitk* group, when I was bedridden in HC. I am unable to express my gratitude in words to all of them.

I would like to express my deep respect to my parents and BABA for their love, care and constant encouragement throughout my career. Without them nothing in life would have been possible.

*Finally, Thanks to 'ALMIGHTY' for Everything.*

Praveen Kumar

# *Contents*

	<b>Page No.</b>
Abstract	i
List of Figures	ii
List of Tables	viii
Nomenclature	ix
<b>1. Introduction</b>	<b>1</b>
1.1 Structure of the thesis	3
<b>2. Origin and Development of duplex PSA</b>	<b>4</b>
2.1 Duplex PSA: Origin and development	5
2.2 Literature review on duplex PSA	8
2.3 Numerical simulation studies on PSA	8
<b>3. Process Description: Duplex PSA and TSA</b>	<b>11</b>
3.1 Original duplex PSA	11
3.2 Modified version-I duplex PSA (MV-I duplex PSA)	13
3.3 Modified version-II duplex PSA (MV-II duplex PSA)	14
3.4 Duplex TSA	18
<b>4. Modeling and Simulation</b>	<b>21</b>
4.1 Mathematical model	21
4.2 Initial and boundary conditions	29
4.2.1 Original duplex and MV-I duplex PSA	30
4.2.2 MV-II duplex PSA	32
4.2.3 Duplex TSA	32
4.3 Parameters estimation	34
4.4 Method of solution	38

<b>5. Results and Discussion</b>	<b>46</b>
5.1 Fractionation of carbon dioxide-nitrogen (CO <sub>2</sub> -N <sub>2</sub> ) mixture	47
5.1.1 Original duplex PSA	49
5.1.2 Parametric study of Original duplex PSA	59
5.1.3 MV-I duplex PSA	61
5.1.4 Comparison of MV-I duplex and Original duplex PSA	64
5.1.5 MV-II duplex PSA	66
5.1.6 Parametric study of MV-II duplex PSA	73
5.1.7 Comparison of MV-II duplex and Original duplex PSA	77
5.2 Fractionation of methane-hydrogen (CH <sub>4</sub> -H <sub>2</sub> ) mixture	79
5.2.1 Effect of feed position	80
5.2.2 Original duplex and MV-I duplex PSA	82
5.2.3 Comparison of MV-I duplex and Original duplex PSA	85
5.2.4 MV-II duplex PSA	87
5.2.5 Parametric study of MV-II duplex PSA	90
5.2.6 Comparison of MV-II duplex and Original duplex PSA	91
5.3 Fractionation of nitrogen-oxygen (N <sub>2</sub> -O <sub>2</sub> ) mixture	94
5.3.1 Effect of feed position	96
5.3.2 Original duplex PSA	97
5.3.3 MV-II duplex PSA	103
5.3.4 Comparison of MV-II duplex and Original duplex PSA	110
5.4 Duplex TSA	111
<b>6. Conclusions</b>	<b>117</b>
6.1 Scope for Future Studies	118
<b>References</b>	<b>119</b>
<b>Appendix</b>	<b>123</b>

## **Abstract**

The conventional pressure swing adsorption (PSA) is used as an alternative to cryogenic distillation. It has not yet proved to be competitive with cryogenic processes for large units. Moreover it yields only one component as pure product and the other being impure. Recently a new PSA, called as duplex PSA, has been reported. Recent studies indicate that it yields two products but sharp separation is not possible. In this work, a modified duplex PSA has been proposed to obtain two products with purities in excess of 99%. Simulation studies were carried out to assess the performance of the original and the proposed duplex PSA for the  $\text{CO}_2\text{-N}_2$ ,  $\text{CH}_4\text{-H}_2$  and  $\text{N}_2\text{-O}_2$  systems. In the original duplex PSA, the maximum purity obtained of the heavy components ( $\text{CO}_2$  and  $\text{CH}_4$ ) was 90% and that of the light component ( $\text{N}_2$  and  $\text{H}_2$ ) was 95%. In the  $\text{N}_2\text{-O}_2$  system, maximum purity of both the products obtained was 75%. In contrast, the purity of both the products improved dramatically to 99+% or more for all the systems studied in the proposed duplex PSA. Further, the productivity is higher than the conventional PSA. The proposed duplex PSA finds application in the capture and sequestration of  $\text{CO}_2$  from flue gases, upgradation of natural gas and as an alternative to cryogenic distillation of gas mixtures like air.

# List of Figures

Figure		Page no.
Fig. 2.1	PSA process with stripping recycle	5
Fig. 2.2	PSA process with enriching recycle	6
Fig. 2.3	Duplex PSA process with intermediate feed inlet position	7
Fig. 3.1	Sequence of steps in Original duplex and MV-I duplex PSA in a cycle	12
Fig. 3.2	Pressure history in the bed in a cycle in Original duplex and MV-I duplex PSA	14
Fig. 3.3	Sequence of steps in MV-II duplex PSA in a cycle	16
Fig. 3.4	Pressure history in the bed in a cycle in MV-II duplex PSA	17
Fig. 3.5	Sequence of steps in duplex TSA in a cycle	18
Fig. 3.6	Temperature shift along the length of the bed undergoing cooling	19
Fig. 3.7	Temperature shift along the length of the bed undergoing heating	20
Fig. 4.1	Differential element of a section of the adsorber	21
Fig. 4.2	Flow-chart for simulation of Original duplex and MV-I duplex PSA cycle	39
Fig. 4.3	Flow-chart for simulation of MV-II duplex PSA cycle	42
Fig. 5.1	Adsorption isotherm of carbon dioxide on Zeolite 13X at 298.15 K	48
Fig. 5.2	Two modes of equalization and pressurization	49
Fig. 5.3	Mass balance sheet of Original duplex PSA with equalization and pressurization from CO <sub>2</sub> rich end (mode-I)	51
Fig. 5.4	Mass balance sheet of Original duplex PSA with equalization and pressurization from N <sub>2</sub> rich end (mode-II)	52
Fig. 5.5 (a)	Partial pressure and solid phase concentration profile of CO <sub>2</sub> in the bed undergoing blowdown from CO <sub>2</sub> rich end	53

Fig. 5.5 (b)	Partial pressure and solid phase concentration profile of CO <sub>2</sub> in the bed undergoing blowdown from N <sub>2</sub> rich end	53
Fig. 5.6 (a)	Gas phase concentration profile in the bed undergoing feed (Original duplex)	55
Fig. 5.6 (b)	Solid phase concentration profile in the bed undergoing feed (Original duplex)	55
Fig. 5.6 (c)	Gas phase concentration profile in the bed undergoing blowdown (Original duplex)	56
Fig. 5.6 (d)	Gas phase concentration profile in the bed undergoing blowdown (Original duplex)	56
Fig. 5.6 (e)	Gas phase concentration profile in the bed undergoing purge (Original duplex)	57
Fig. 5.6 (f)	Solid phase concentration profile in the bed undergoing purge (Original duplex)	57
Fig. 5.6 (g)	Gas phase concentration profile in the bed undergoing pressurization (Original duplex)	58
Fig. 5.6 (h)	Solid phase concentration profile in the bed undergoing pressurization (Original duplex)	58
Fig. 5.7	Effect of raffinate recycle ratio; $P_H=1\text{atm}$ , $P_L=0.3\text{atm}$	59
Fig. 5.8	Effect of feed; $P_H=1\text{atm}$ , $P_L=0.3\text{atm}$ , $R_R=0.2$	60
Fig. 5.9	Effect of desorption pressure; $F=60\text{mmol/half cycle}$ , $P_H=1\text{atm}$ , $R_R=0.4$	61
Fig. 5.10	Variation in mole fraction of CO <sub>2</sub> and cumulative amount with time in outgoing stream from purge; $F=100\text{mmol/half cycle}$ , $P_H=1\text{atm}$ , $P_L=0.3\text{atm}$ , $R_R=0.2$	62
Fig. 5.11	Mass balance sheet of MV-I duplex PSA	63
Fig. 5.12	Effect of raffinate recycle ratio; $F=60\text{mmol/half cycle}$ , $P_H=1\text{atm}$ , $P_L=0.3\text{atm}$	64
Fig. 5.13	Effect of feed; $P_H=1\text{atm}$ , $P_L=0.3\text{atm}$ , $R_R=0.2$	65
Fig. 5.14	Effect of desorption pressure; $F=60\text{mmol/half cycle}$ , $P_H=1\text{atm}$ , $R_R=0.4$	65
Fig. 5.15	Mass balance sheet of MV-II duplex PSA	67

Fig. 5.16 (a)	Gas phase concentration profile in the bed undergoing feed (MV-II duplex)	68
Fig. 5.16 (b)	Solid phase concentration profile in the bed undergoing feed (MV-II duplex)	68
Fig. 5.16 (c)	Gas phase concentration profile in the bed undergoing intermediate-blowdown (MV-II duplex)	69
Fig. 5.16 (d)	Solid phase concentration profile in the bed undergoing intermediate-blowdown (MV-II duplex)	69
Fig. 5.16 (e)	Gas phase concentration profile in the bed undergoing final-blowdown (MV-II duplex)	70
Fig. 5.16 (f)	Solid phase concentration profile in the bed undergoing final-blowdown (MV-II duplex)	70
Fig. 5.16 (g)	Gas phase concentration profile in the bed undergoing purge (MV-II duplex)	71
Fig. 5.16 (h)	Solid phase concentration profile in the bed undergoing purge (MV-II duplex)	71
Fig. 5.16 (i)	Gas phase concentration profile in the bed undergoing pressurization (MV-II duplex)	72
Fig. 5.16 (j)	Solid phase concentration profile in the bed undergoing pressurization (MV-II duplex)	72
Fig. 5.17	Effect of raffinate recycle ratio; $F=100\text{mmol/half cycle}$ , $P_H=1\text{atm}$ , $P_I=0.5\text{atm}$	73
Fig. 5.18 (a)	Gas phase concentration profile ( $R_R = 0.2$ )	74
Fig. 5.18 (b)	Gas phase concentration profile ( $R_R = 0.6$ )	74
Fig. 5.18 (c)	Gas phase concentration profile ( $R_R = 1.8$ )	74
Fig. 5.19	Effect of feed; $P_H=1\text{atm}$ , $P_I=0.5\text{atm}$ , $R_R=0.6$	75
Fig. 5.20	Effect of intermediate-desorption pressure; $F=60\text{mmol/half cycle}$ , $P_H=1\text{atm}$ , $R_R=0.4$	76
Fig. 5.21	Effect of raffinate recycle ratio; $F=100\text{mmol/half cycle}$ , $P_H=1\text{atm}$ , $P_I=0.5\text{atm}$ (MV-II), $P_L=0.3\text{atm}$ (Original)	77
Fig. 5.22	Effect of feed; $P_H=1\text{atm}$ , $P_I=0.5\text{atm}$ (MV-II), $P_L=0.3\text{atm}$ (Original) $R_R=0.6$ (MV-II), $R_R=0.2$ (Original)	78

Fig. 5.23	Effect of intermediate-desorption (MV-II) or desorption pressure (Original); $F=60\text{mmol/half cycle}$ , $P_H=1\text{atm}$ , $R_R=0.4$	78
Fig. 5.24	Adsorption isotherm of methane on Activated carbon at 298.15 K	80
Fig. 5.25	Variation in product purity with different position of feed; $F=60\text{mmol/half cycle}$ , $P_H=1\text{atm}$ , $P_L=0.5\text{atm}$ , $R_R=0.5$	81
Fig. 5.26	Final gas phase concentration profile of $\text{CH}_4$ in bed undergoing feed; $F=60\text{mmol/half cycle}$ , $P_H=1\text{atm}$ , $P_L=0.5\text{atm}$ , $R_R=0.5$	81
Fig. 5.27	Mass balance sheet of Original duplex PSA	83
Fig. 5.28	Mass balance sheet of MV-I duplex PSA	84
Fig. 5.29	Effect of raffinate recycle ratio; $F=60\text{mmol/half cycle}$ , $P_H=1\text{atm}$ , $P_L=0.4\text{atm}$	85
Fig. 5.30	Effect of feed; $P_H=1\text{atm}$ , $P_L=0.4\text{atm}$ , $R_R=0.4$	86
Fig. 5.31	Effect of desorption pressure; $F=60\text{mmol/half cycle}$ , $P_H=1\text{atm}$ , $R_R=0.4\text{atm}$	86
Fig. 5.32	Mass balance sheet of MV-II duplex PSA	88
Fig. 5.33 (a)	Gas phase concentration profile in the bed undergoing feed (MV-II duplex)	89
Fig. 5.33 (b)	Solid phase concentration profile in the bed undergoing feed (MV-II duplex)	89
Fig. 5.34	Effect of raffinate recycle ratio; $F=60\text{mmol/half cycle}$ , $P_H=1\text{atm}$ , $P_L=0.6\text{atm}$	90
Fig. 5.35	Effect of feed; $P_H=1\text{atm}$ , $P_L=0.5\text{atm}$ , $R_R=0.5$	90
Fig. 5.36	Effect of intermediate-desorption pressure; $F=60\text{mmol/half cycle}$ , $P_H=1\text{atm}$ , $R_R=0.4$	91
Fig. 5.37	Effect of raffinate recycle ratio; $F=60\text{mmol/half cycle}$ , $P_H=1\text{atm}$ , $P_L=0.6\text{atm}$ (MV-II), $P_L=0.4\text{atm}$ (Original)	92
Fig. 5.38	Effect of feed; $P_H=1\text{atm}$ , $P_L=0.5\text{atm}$ (MV-II), $P_L=0.4\text{atm}$ (Original) $R_R=0.5$ (MV-II), $R_R=0.4$ (Original)	92
Fig. 5.39	Effect of intermediate-desorption (MV-II) or desorption pressure (Original); $F=60\text{mmol/half cycle}$ , $P_H=1\text{atm}$ , $R_R=0.4$	93



Fig. 5.40 (a)	Adsorption isotherm of nitrogen-oxygen on Zeolite 5A at 298.15 K	95
Fig. 5.40 (b)	Solid phase composition vs. gas phase composition of N <sub>2</sub> at 298.15 K	95
Fig. 5.41	Variation in product purity with different position of feed; F=60 mmol/half cycle, P <sub>H</sub> =4 atm, P <sub>L</sub> =1.5 atm, R <sub>R</sub> =1.0	96
Fig. 5.42	Final gas phase concentration profile of CH <sub>4</sub> in bed undergoing feed; F=60 mmol/half cycle, P <sub>H</sub> =4 atm, P <sub>L</sub> =1.5 atm, R <sub>R</sub> =1.0	96
Fig. 5.43	Mass balance sheet of Original duplex PSA	98
Fig. 5.44 (a)	Gas phase concentration profile in the bed undergoing feed (Original duplex)	99
Fig. 5.44 (b)	Solid phase concentration profile in the bed undergoing feed (Original duplex)	99
Fig. 5.44 (c)	Gas phase concentration profile in the bed undergoing blowdown (Original duplex)	100
Fig. 5.44 (d)	Gas phase concentration profile in the bed undergoing blowdown (Original duplex)	100
Fig. 5.44 (e)	Gas phase concentration profile in the bed undergoing purge (Original duplex)	101
Fig. 5.44 (f)	Solid phase concentration profile in the bed undergoing purge (Original duplex)	101
Fig. 5.44 (g)	Gas phase concentration profile in the bed undergoing pressurization (Original duplex)	102
Fig. 5.44 (h)	Solid phase concentration profile in the bed undergoing pressurization (Original duplex)	102
Fig. 5.45	Mass balance sheet of MV-II duplex PSA	104
Fig. 5.46 (a)	Gas phase concentration profile in the bed undergoing feed (MV-II duplex)	105
Fig. 5.46 (b)	Solid phase concentration profile in the bed undergoing feed (MV-II duplex)	105
Fig. 5.46 (c)	Gas phase concentration profile in the bed undergoing intermediate-blowdown (MV-II duplex)	106
Fig. 5.46 (d)	Solid phase concentration profile in the bed undergoing intermediate-blowdown (MV-II duplex)	106

Fig. 5.46 (e)	Gas phase concentration profile in the bed undergoing final-blowdown (MV-II duplex)	107
Fig. 5.46 (f)	Solid phase concentration profile in the bed undergoing final-blowdown (MV-II duplex)	107
Fig. 5.46 (g)	Gas phase concentration profile in the bed undergoing purge (MV-II duplex)	108
Fig. 5.46 (h)	Solid phase concentration profile in the bed undergoing purge (MV-II duplex)	108
Fig. 5.46 (i)	Gas phase concentration profile in the bed undergoing pressurization (MV-II duplex)	109
Fig. 5.46 (j)	Solid phase concentration profile in the bed undergoing pressurization (MV-II duplex)	109
Fig. 5.47	Effect of feed; $P_H=4\text{atm}$ , $P_I=1.5\text{ atm}$ (MV-II), $P_L=1.5\text{ atm}$ (Original) $R_R=0.5$	110
Fig. 5.48	Adsorption isotherm of carbon dioxide on Zeolite 13X	112
Fig. 5.49	Cooling (feed) step in duplex TSA	113
Fig. 5.50 (a)	Temperature profile in the bed undergoing cooling	113
Fig. 5.50 (b)	Gas phase concentration profile in the bed undergoing cooling	114
Fig. 5.50 (c)	Solid phase concentration profile in the bed undergoing cooling	114
Fig. 5.51	Heating step in duplex TSA	115
Fig. 5.52 (a)	Temperature profile in the bed undergoing heating	115
Fig. 5.52 (b)	Gas phase concentration profile in the bed undergoing heating	116
Fig. 5.52 (c)	Solid phase concentration profile in the bed undergoing heating	116

## List of Tables

Table		Page no.
Table 5.1	Parameters used in simulation of fractionation of carbon dioxide-nitrogen mixture	47
Table 5.2	Parameters used in simulation of fractionation of methane-hydrogen mixture	79
Table 5.3	Parameters used in simulation of fractionation of nitrogen-oxygen mixture	94
Table 5.4	Parameters used in simulation of fractionation of carbon dioxide-nitrogen mixture (TSA)	111

# Nomenclature

$A$	cross-sectional area of the bed ( $m^2$ )
$a_s$	specific surface area of the adsorbent particle ( $m^{-1}$ )
$b_i$	Langmuir's constant of component $i$ ( $mol/m^3$ ) <sup>-1</sup>
$c_t$	total gas phase molar concentration ( $mol/m^3$ )
$c_i$	gas phase molar concentration of component $i$ ( $mol/m^3$ )
$C_{ps}$	specific heat of solid ( $J/kgK$ )
$C_{pg}$	specific heat of gas ( $J/kgK$ )
$D$	diameter of pipe ( $m$ )
$D_e$	effective diffusivity ( $m^2/s$ )
$D_L$	axial dispersion coefficient ( $m^2/s$ )
$D_{Lo}$	axial dispersion coefficient at reference pressure of 1 atm ( $m^2/s$ )
$D_M$	molecular diffusivity ( $m^2/s$ )
$d$	diameter of the adsorber ( $m$ )
$d_p$	diameter of the particle ( $m$ )
$E$	moles of extract
$F$	moles of feed
$f$	friction-factor for pressure drop
$G_g$	mass velocity of fluid, ( $kg/m^2s$ )
$h_p$	particle heat transfer coefficient, ( $W/m^2K$ )
$\Delta H$	heat of adsorption, ( $J/mol$ )
$k$	frac value
$K$	Kozeny constant
$k_i$	linear driving force mass transfer coefficient ( $s^{-1}$ )
$K_e^\circ$	effective thermal conductivity for quiescent bed, ( $W/mK$ )
$K_{e,ax}$	effective axial thermal conductivity of gas, ( $W/mK$ )
$K_g$	thermal conductivity of gas, ( $W/mK$ )
$K_s$	thermal conductivity of solid, ( $W/mK$ )

$L$	length of the bed ( $m$ )
$L_e$	equivalent length of the valve ( $m$ )
$M_{Ai}$	initial moles of heavy component in the bed
$M_{Bi}$	initial moles of light component in the bed
$M_{Af}$	final moles of heavy component in the bed
$M_{Bf}$	final moles of light component in the bed
$M_{Ti}$	initial total moles in the bed
$M_{Tf}$	final total moles in the bed
$N$	number of components
$n_{out}^{cycle}$	moles of gas outgoing from a bed in a cycle
$n_{in}^{cycle}$	moles of gas entering into a bed in a cycle
$P$	total pressure ( $atm$ )
$P_H$	Adsorption pressure ( $atm$ )
$P_L$	desorption or final-desorption pressure ( $atm$ )
$P_I$	intermediate-desorption pressure ( $atm$ )
$Pr$	Prandtl number
$q_i$	solid-phase molar concentration of component $i$ ( $mol/m^3$ )
$q_i^*$	solid-phase molar concentration in equilibrium with $c_i$ ( $mol/m^3$ )
$q_{s,i}$	saturation constant of component $i$ ( $mol/m^3$ )
$q_t$	total solid-phase molar concentration ( $mol/m^3$ )
$R$	moles of raffinate
$Re_p$	particle Reynolds number
$R_P$	particle radius, ( $m$ )
$R_R$	raffinate recycle ratio
$R_E$	extract recycle ratio
$t$	time ( $s$ )
$t_c$	cycle time, ( $s$ )
$T_g$	gas phase temperature, $K$
$T_s$	solid phase temperature, $K$

$v_f$	interstitial gas velocity, ( $m/s$ )
$Y_E$	extract purity
$Y_R$	raffinate purity
$Y_F$	mole fraction of heavy component in feed
$y_i$	mole fraction of $i^{th}$ component in gas phase
$Y_{out}^{icycle}$	composition of gas coming out from a bed in a cycle
$Y_{in}^{icycle}$	composition of gas entering into a bed in a cycle
$z$	axial distance ( $m$ )
$z_F^-$	bed position just before the feed inlet
$z_F^+$	bed position just after the feed inlet

## Greek letters

$\alpha$	effective axial thermal diffusivity of gas ( $m^2/s$ )
$\varepsilon$	bed voidage
$\varepsilon_p$	particle porosity
$\rho_g$	density of gas, ( $kg / m^3$ )
$\rho_s$	density of solid, ( $kg / m^3$ )
$\mu$	viscosity of gas ( $kg/m.s$ )

## Sub-scripts

B	blowdown
BI	intermediate-blowdown
BF	final-blowdown
C	cooling
E	extract
F	feed
FR	frozen
H	heating
$i$	component number
P	purge

<i>PR</i>	pressurization
<i>R</i>	raffinate

## Super-scripts

*	equilibrium condition
<i>icycle</i>	cycle number

### Introduction

A highly energy intensive cryogenic distillation was the only option available for many years to fractionate air. The cryogenic distillation has now been supplemented by energy efficient and economical non-cryogenic technologies such as pressure swing adsorption (PSA) and membrane separation systems. PSA is the first commercial non-cryogenic process to produce pure nitrogen or oxygen from air. PSA has gained importance not only in air separation but also in the petrochemical industries. Process improvements and new generations of carbon molecular sieves and zeolites have resulted in increased efficiency of PSA systems since they were first introduced for commercial applications about 25 years ago. Around 5000 PSA systems have been installed worldwide over the last two decades, indicating the tremendous growth of the technology (Keith, 1997).

Most of the conventional PSA processes developed so far are based on the Skarstrom cycle. These require a number of beds and large pressure ratio ( $P_H/P_L$ ) leading to a large capital and operating costs. As an alternate to the Skarstrom PSA cycles and its variants, a new type of PSA cycle has been proposed by Leavitt (1992) and Hirose (1994). These are referred to as dual-reflux or duplex PSA cycle. The feed in a duplex PSA is introduced at some intermediate point along the length of the bed unlike Skarstrom type PSA where the feed is introduced at either ends of the bed. There is an inherent recycle of both the rich stream as well as the lean stream.

In the conventional PSA, there is a narrow mass transfer zone which transverses along the length of the bed. The bed behind and ahead of the mass transfer zone is in equilibrium. This implies that at any time only a fraction of the bed is utilized for mass transfer. Whereas in the duplex PSA, mass transfer zone is extended throughout the bed length resulting in 5-10 times large productivity than that of the conventional PSA.

One key feature distinguishing the duplex PSA from the conventional PSA is the concentration profile in the bed. In the duplex PSA, the concentration profiles in the bed are not destroyed and reformed during each cycle unlike in the Skarstrom type PSA. They are only shifted marginally depending upon the pressure ratio that is employed.



To assess the performance of the duplex PSA, simulation studies have been carried out with systems like carbon dioxide-nitrogen ( $\text{CO}_2\text{-N}_2$ ) with nitrogen as non-adsorbing, methane-hydrogen ( $\text{CH}_4\text{-H}_2$ ) with hydrogen as non-adsorbing and nitrogen-oxygen ( $\text{N}_2\text{-O}_2$ ) where both the components are adsorbing. The Original duplex PSA was not able to give clean separation. We proposed two modifications to the Original duplex cycle based on the simulation studies. They are referred to as MV-I duplex and MV-II duplex PSA cycle.

The MV-I duplex, where the time of extract withdrawal has been modified, shows marginal improvement in the product purity over that of the Original duplex. Though it was a marginal improvement, it gave an insight to further modify the duplex cycle. In the MV-II duplex, where the step of extract withdrawal has been modified, the purity of both the products improved dramatically to 99+% with 99+% recoveries.

The parametric studies such as effect of feed inlet position, raffinate recycle ratio, gas flow rate and desorption pressure have been done to assess the comparative performance of the Original duplex, MV-I duplex and MV-II duplex PSA. The raffinate recycle ratio is defined as the ratio of amount of gas recycled to the amount of raffinate product drawn. The MV-II duplex PSA seems to have potential to fractionate any binary gas mixture into clean products.

Based on the analogy with the duplex PSA, another process with temperature swing, duplex TSA has been proposed and the possibility of separation has been explored with  $\text{CO}_2\text{-N}_2$  system ( $\text{N}_2$  is non-adsorbing).

## **1.1 Structure of the thesis**

**Chapter 2** presents origin and development of the duplex PSA, literature survey on duplex PSA and simulation studies on PSA.

**Chapter 3** explains the process description of the duplex PSA and duplex TSA

**Chapter 4** described mathematical modeling and method of simulation of duplex PSA and duplex TSA.

**Chapter 5** discusses the results of the simulation studies performed with duplex PSA and duplex TSA.

**Chapter 6** presents the conclusions of the study and also presents the scope for future work.

### Origin and Development of duplex PSA

The introduction of PSA processes is commonly attributed to Skarstrom and Guerin de Montgareuil and Domine in 1957-1958 (Ruthven, 1993). The Air Liquide process, developed by Montgareuil and Domine, utilized a vacuum swing, whereas the Esso process, pioneered by Skarstrom, used a low pressure purge to clean the adsorbent bed following the blowdown step. The first three applications of PSA namely air separation, air-drying and hydrogen purification were in fact foreseen and demonstrated by Skarstrom. These remain the most important practical applications for this technology, although newer processes such as carbon dioxide recovery and natural gas purification are gaining increased acceptance.

The Skarstrom cycle in its basic form utilizes two packed adsorbent beds and four steps, (1) pressurization, (2) high pressure adsorption, (3) blowdown and (4) low pressure purge. Both beds undergo these four steps in a cycle. The Skarstrom cycle was only viable to get less selectively absorbable component as pure product and generally not applicable for production of more selectively adsorbed component. To get the more selectively adsorbed component as product, Wilson (1982) developed a process that is superficially the inverse of the Skarstrom cycle. The Wilson cycle has four steps viz. (1) pressurization (2) purge at high pressure, (3) blowdown and (4) low pressure feed.

The PSA processes which are based on Skarstrom cycle are limited by a single product with low recovery. Sirkar (1977) and Knaebel (1989) modified the Skarstrom cycle by providing reflux of both the products to yield high purities of both the products at reasonably high recoveries.

A new type of PSA cycle has been proposed by Leavitt (1992) and Hirose (1994). These are referred to as duplex or dual-reflux PSA cycle. These cycles are characterized by feed at some intermediate point along the length of the bed unlike Skarstrom cycle and its variants which employ feed from end of the bed. Hirose et. al. (1992) has explained the principle behind the development of the dual-reflux PSA cycle and is explained below.

## 2.1 Duplex PSA: Origin and development

Generally, the objective of PSA processes is either to remove or to concentrate one or many components from a binary or multicomponent feed gas mixture. The conventional PSA scheme for the purpose of removal (or stripping) is illustrated in Figure 2.1, which shows the bed conditions during a half cycle (of Skarstrom cycle). The feed gas with mole fraction  $Y_F$  enters from the top of the high pressure bed and separated into a lean gas that leaves from bottom. A part of the lean gas is recycled to the low pressure bed as stripping recycle. The enriched gas leaves the low pressure bed from top. The mole fraction of heavy component in the lean gas,  $Y_L$  can be lowered to a value nearly equal to 0 when the operating conditions are selected properly. However, the mole fraction of the enriched gas,  $Y_E$  cannot be increased at the same time up to a value higher than the pressure ratio ( $P_H/P_L$ ). This restriction is a thermodynamic limitation because the upper limit is controlled by the adsorption isotherm, a thermodynamic limit. Thus, a conventional PSA process, utilizing stripping recycle as the mode of separation is suitable to produce only light component as pure.

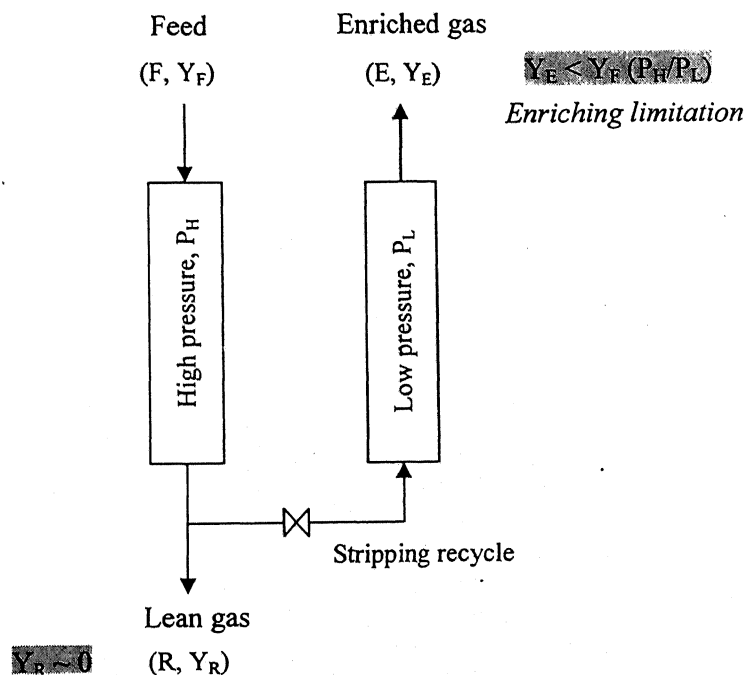


Fig. 2.1 PSA process with stripping recycle

The conventional PSA scheme for the purpose of concentration (or enriching) is illustrated in Figure 2.2, which shows the bed conditions during a half cycle (of Wilson cycle). The feed gas with mole fraction  $Y_F$  enters from the bottom of the low pressure bed. A part of the enriched gas from top of the low pressure bed is recycled to the high pressure bed as enriching recycle after compression. The lean gas leaves the high pressure bed from the top. The mole fraction of heavy component in the enriched gas,  $Y_E$  can be increased to a value nearly equal to 1 when the operating conditions are selected properly. However, the mole fraction of the lean gas,  $Y_R$  can not be lowered at the same time below a factor of the pressure ratio ( $P_L/P_H$ ) because of the thermodynamic limitation. Thus, a conventional PSA process, utilizing enriching recycle as the mode of separation is suitable to produce only heavy component as pure.

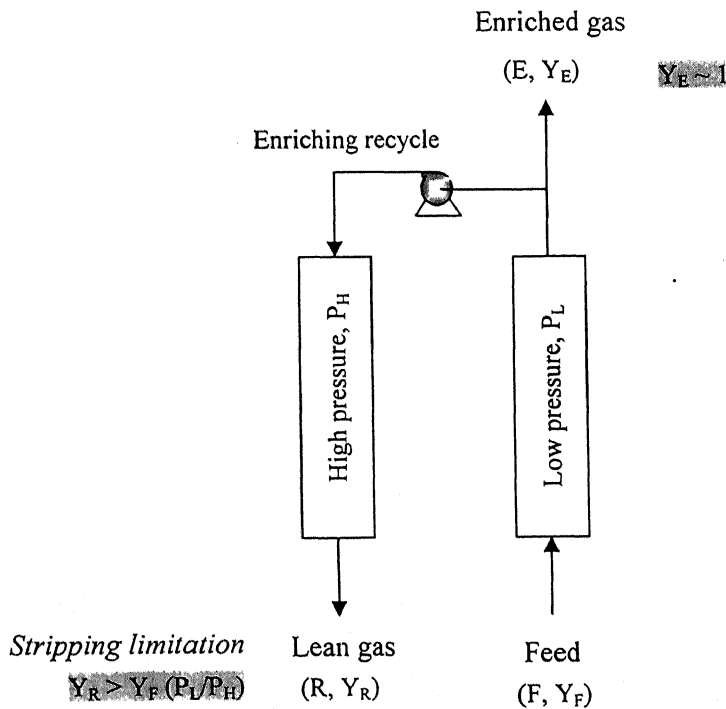


Fig. 2.2 PSA process with enriching recycle

The above two limitations can be overcome by reprocessing enriched gas leaving the stripping PSA in the enriching PSA, and lean gas leaving the enriching PSA in the stripping PSA. This concept leads to a new PSA process as shown in Figure 2.3 and

called as duplex or dual-reflux PSA process. It is a combination of the two conventional PSA processes represented by Figure 2.1 and 2.2. The feed gas is supplied at an intermediate position of the bed. By analogy to distillation, the feed inlet position divides each column into enriching and stripping sections, both at the same pressure. The length of the enriching and stripping section depends on the feed position. For an appropriate combination of operating variables, this process can give two types of high purity products- both enriched gas and lean gas.

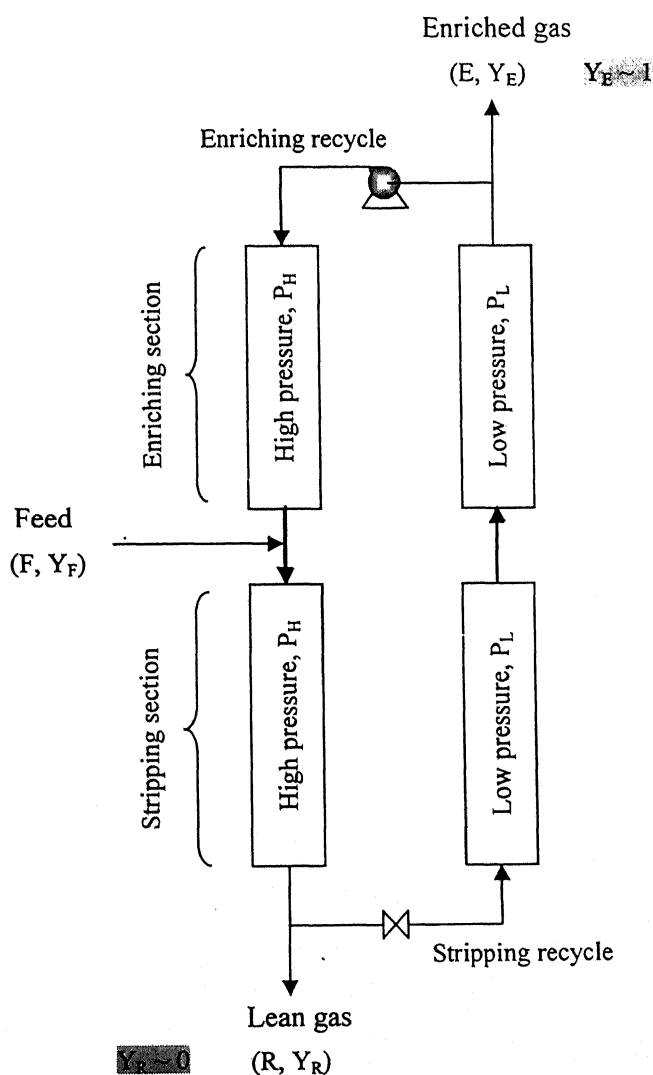


Fig. 2.3 Duplex PSA process with intermediate feed inlet position

## **2.2 Literature review on duplex PSA**

Though duplex PSA has been proposed in early 1990s, not much work is found in open literature. Hirose et. al. (1994) studied the removal and enrichment of carbon dioxide from the air-CO<sub>2</sub> mixtures. Zeolite 13X was used as the adsorbent and parametric studies such as effect of feed inlet position, reflux ratio, gas flow rates, and pressure ratio on the enriched product concentration or recovery as well as lean product concentration were experimentally investigated (Hirose et. al. 1995). They found that the optimum feed inlet position was at about middle of the bed. The first numerical analysis on duplex PSA was carried out by Hirose et. al.(1996) for simultaneous removal and concentration of carbon dioxide dilute gas from air. They developed a simple isothermal model with negligible axial dispersion and pressure drops through the bed to investigate the effects of various combinations of operating parameters. Ritter et. al. (2002) has carried out experimental studies for separation and concentration of a dilute feed of ethane in nitrogen using WestVaco BAX-1500 Activated carbon. The enrichment of useful trace components in air, such as Ne, Kr, Xe, etc. was studied by Ritter et. al. (2003) using only enriching reflux and parallel equalization. Equilibrium theory analysis of duplex PSA for separation of a binary mixture has been done by Ebner and Ritter (2004).

Molecular gate process described in Keller patent (1982) uses pistons to produce cyclic gas flow and pressure variations at the two end of the beds, while feed is admitted at an intermediate point. This process has not been commercialized because they are difficult to scale up to commercialized size (Leavitt 1992). Farooq et. al. (2002) studied the performance of piston PSA process with feed at the end of the bed unlike Molecular gate process where feed was at intermediate point of the bed.

## **2.3 Numerical simulation studies on PSA**

Most of the early simulation studies were carried out using the equilibrium model (Hill and Wong (1981); Knaebel and Hill (1985)). The equilibrium model provides valuable information about the dynamic behavior of the adsorption processes. Raghavan and Ruthven (1987) presented numerical simulation of PSA in the recovery of trace adsorbable from an inert carrier using the linear equilibrium and linear rate expressions. They also assumed that during pressure changes (blowdown and pressurization) there

was no mass transfer between the fluid and adsorbent. Raghavan and Ruthven discussed numerical simulation for a simple two bed PSA process in which effects of kinetics and changes in flow rate due to adsorption are significant. Alpay and Scott (1992) used the linear driving force (LDF) model to describe the adsorption and desorption kinetics in spherical particles. Chahbani and Tondéur (2000) discussed the mass transfer kinetics in PSA. They showed that the choice of the pore diffusion model plays a key role for obtaining reliable simulations. They compared their results with other models like LDF and equilibrium model. Kvamsdal and Hertzberg (1995) showed the effect of mass transfer during the blowdown step. According to their results, the frozen solid assumption is valid only in certain cases, and taking into account the mass transfer during the blowdown step gives a better overall model performance in the studied cases. Meunier and Huberson et al. (1992) studied a general non-isothermal model describing a single-component gas adsorption during pressurization with two mass intraparticle diffusions (macropore-micropore) and axial flow in the column. They found that the adsorption kinetics are not always a secondary effect and that they play an important role in the column dynamics as well as do the adsorption equilibrium properties. Lu and Rodrigues (1993) simulated a three- step one-column pressure swing adsorption process in isothermal and adiabatic cases for separation of a binary mixture. The bed dynamics at the cyclic steady state have been studied in the three individual steps (pressurization, feed and blowdown) by looking at the axial profiles and histories of the process parameters at four positions inside the bed. Modeling PSA leads to a nonlinear dynamic partial differential equation system, which is difficult to solve. The parameters in PSA models affecting the behavior of the process are highly coupled to each other. The model equations were solved by orthogonal collocation and by finite difference methods by Raghavan and Ruthven (1985). Matz and Knaebel (1988) employed method of characteristics and found the effects of incomplete purge in PSA. Sun and Meunier (1991) introduced a solution adaptive gridding technique (SAG) combined with a four point quadratic upstream differencing scheme to satisfactorily resolve very sharp concentration and temperature variations occurring in the case of small dispersing effects. Wen and Chou (1995) simulated a PSA process for air-5A zeolite system using the Moving Finite Element Method (MFEM) using the property of moving nodes in MFEM



with small weighting factors. The use of small weighting factors corresponds to the strong action of the penalty function. They discussed the effects of the weighting factors and boundary conditions on the implementation of the MFEM. Sun et al. (1996) suggested an improved finite-difference method for simulation of diffusion-limited PSA process. They concluded that this method of solution adaptive gridding was well suited for describing the sharp transitions as it exhibits much less oscillations and false diffusion. Morbidelli et al. (1997) used the orthogonal collocations on moving finite elements for simulating the PSA process. Hirose et. al. (2002) used a simple isothermal model for dual reflux PSA with negligible axial dispersion and pressure drop through the bed and validated it with experimental results.

## Process Description: Duplex PSA and TSA

This chapter presents the description of the Original duplex PSA, the MV-I duplex PSA, the MV-II duplex PSA and the duplex TSA. These are cyclic processes and are carried out in two identical beds. The beds are cylindrical vessel packed with adsorbent particles. The adsorbent preferentially adsorbs or retains one of components (heavy) over the other (light). The amount adsorbed increases with pressure and decreases with temperature. The process gets reversed (i.e. amount gets desorbed) on decreasing the pressure or increasing the temperature. So, by swinging the pressure (pressure swing) or temperature (temperature swing) inside the beds and arranging them in a sequence of steps, a gas mixture can be fractionated into the clean products.

The process details of the Original duplex, the MV-I duplex, the MV-II duplex PSA and the duplex TSA is given below.

### 3.1 Original duplex PSA

Original duplex PSA process consists of four steps in a cycle. Figure 3.1 shows the steps involved.

**Step 1:** In this step, the feed is introduced into bed-1 and both the end products are drawn simultaneously (raffinate from bottom of the bed-1 and extract from top of the bed-2). Table below shows the status of the beds.

	<i>Bed-1</i>	<i>Bed-2</i>
<i>Pressure</i>	$P_H$	$P_L$
<i>Status</i>	<i>Feed</i>	<i>Purge</i>

Feed is introduced at an intermediate point along the length of bed-1. The heavy component gets adsorbed inside the bed. A part of the outgoing stream, rich in light component is drawn from the bottom as raffinate product. The remaining part is recycled to the bottom of bed-2 as raffinate recycle. This will purge off the heavy component from

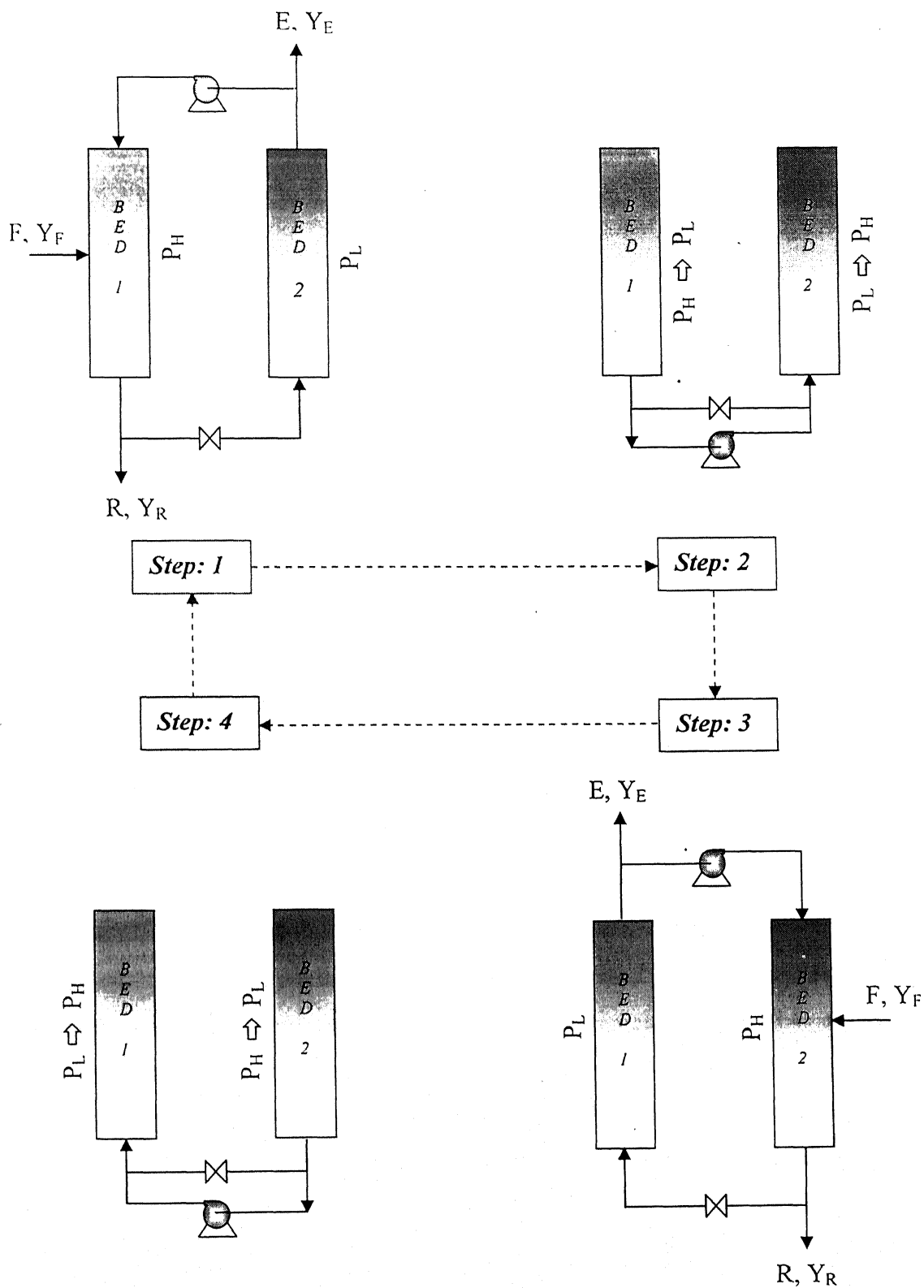


Fig.3.1 Sequence of steps in *Original duplex* and *MV-I duplex* PSA in a cycle

bed-2. A part of the outgoing stream from the top of bed-2, rich in heavy component is drawn as extract product. The remaining part is recycled to the top of bed-1 as extract recycle. The extract recycle is at low pressure,  $P_L$  so it has to be compressed to high pressure,  $P_H$  before recycling it into bed-1.

**Step 2:** This is pressure equalization and pressurization step. Table below shows the status of the beds.

	<i>Bed-1</i>	<i>Bed-2</i>
<b><i>Pressure</i></b>	$P_H \Leftrightarrow P_L$	$P_L \Leftrightarrow P_H$
<b><i>Status</i></b>	<i>Blowdown</i>	<i>Pressurization</i>

First, bottom end of both the beds are connected through a valve till pressure in the beds equalizes. Then, pressure in bed-1 is reduced to  $P_L$  and the gas coming out is used to pressurize bed-2 to  $P_H$  with the aid of a vacuum pump or compressor or both. It could be done from either ends of the beds viz. rich end (top of the beds enriched with heavy component) or lean end (bottom of the beds enriched with light component). In the next step, feed is switched to bed-2.

These two steps complete the first half cycle. The other half cycle is the mirror image of the first half cycle. Step-3 is the mirror image of step-1 and step-4 is the mirror image of step-2.

### 3.2 Modified version-I duplex PSA (MV-I duplex PSA)

*MV-I duplex PSA* process has the same steps as that of the Original duplex PSA with only modification in the time of extract withdrawal. In Original duplex PSA, a part of the outgoing stream from the bed undergoing purge is collected as extract product continuously throughout the step time whereas in MV-I duplex PSA, first part of the outgoing stream from the bed undergoing purge is collected as extract product and the remaining amount is recycled to the top of the bed undergoing feed step as extract recycle. The purity of both the end products in the MV-I duplex PSA gets enhanced over the Original duplex PSA.

**Pressure history in bed:** Pressure history in the beds in a cycle is the same for both the Original duplex and the MV-I duplex PSA. Figure 3.2 shows the pressure history in the beds in a cycle. In step 1 and step 3, pressure in the beds (undergoing feed and purge) does not change with time while in step 2 and step 4, pressure in the beds (undergoing equalization and pressurization) changes with time between  $P_H$  and  $P_L$ .

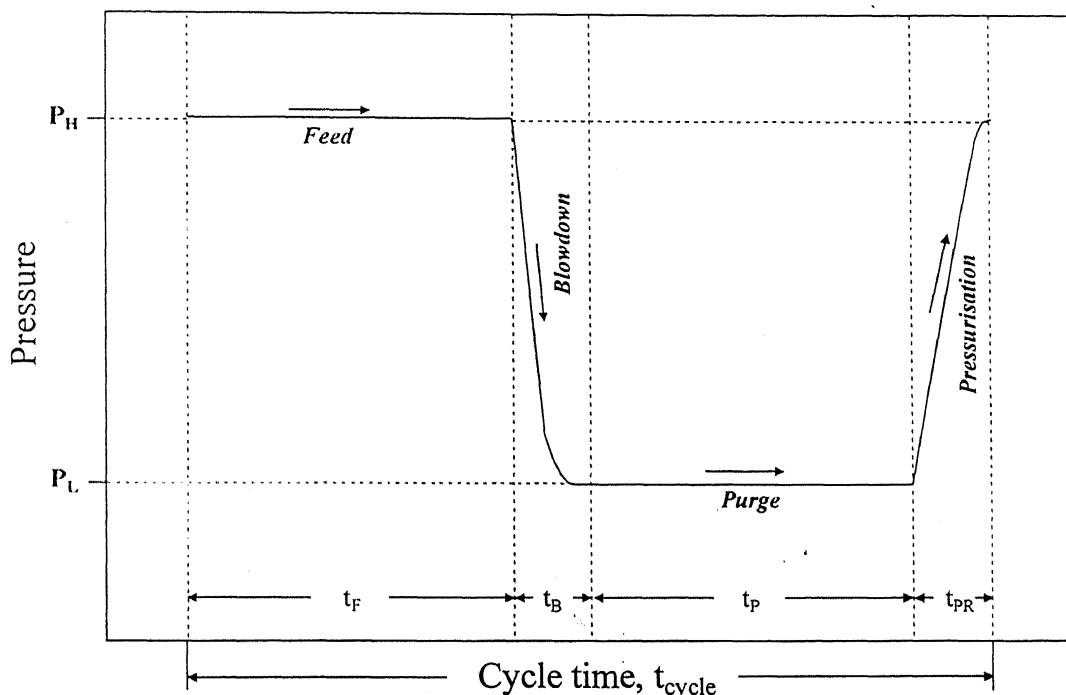


Fig3.2 Pressure history in the bed in a cycle in *original duplex* and *MV-I duplex PSA*

### 3.3 Modified version-II duplex PSA (MV-II duplex PSA)

MV-II duplex PSA process consists of six steps in a cycle. Figure 3.3 shows the steps involved. In the Original duplex PSA both the end products are drawn simultaneously in a step whereas in the MV-II duplex PSA, the end products are drawn in the two different steps.

**Step 1:** In this step, the feed is introduced into bed-1 and only raffinate product is drawn. Table below shows the status of the beds.

	<i>Bed-1</i>	<i>Bed-2</i>
<i>Pressure</i>	$P_H$	$P_L$
<i>Status</i>	<i>Feed</i>	<i>Purge</i>

Feed is introduced at an intermediate point along the length of bed-1. The heavy component gets adsorbed inside the bed. A part of the outgoing stream, rich in light component is drawn from the bottom as raffinate product. The remaining is recycled to the bottom of bed-2 as raffinate recycle. This will purge off the heavy component from bed-2. The total outgoing stream from the top of bed-2 rich in heavy component is recycled to the top of bed-1 as extract recycle. The extract recycle is at low pressure,  $P_L$  so it has to be compressed to high pressure,  $P_H$  before recycling it into bed-1.

**Step 2:** This is pressure equalization and pressurization step. Table below shows the status of the beds.

	<i>Bed-1</i>	<i>Bed-2</i>
<i>Pressure</i>	$P_H \Leftrightarrow P_I$	$P_L \Leftrightarrow P_H$
<i>Status</i>	<i>Intermediate-blowdown</i>	<i>Pressurization</i>

First, bottom end of both the beds are connected through a valve till pressure in the beds equalizes. Then, pressure in bed-1 is reduced to  $P_I$  and the amount coming out is used to pressurize bed-2 to  $P_H$  with the aid of vacuum pump or compressor or both. But this amount is not sufficient to pressurize bed-2 to  $P_H$  as  $P_L < P_I$  so, extra amount is required. The extra amount is taken from the raffinate product drawn from bottom of bed-1 during the step 2. By reducing the pressure in bed-1, the light component gets swept away from the bottom and the upper half portion becomes enriched with the heavy component.

**Step 3:** This is extract withdrawal step. Table below shows the status of the beds.

	<i>Bed-1</i>	<i>Bed-2</i>
<i>Pressure</i>	$P_I \Leftrightarrow P_L$	$P_H$
<i>Status</i>	<i>Final-blowdown</i>	<i>Frozen</i>

Pressure in bed-1 is lowered from top end with the aid of a vacuum pump. The outgoing stream, rich in heavy component is collected as extract product. Final-blowdown pressure,  $P_L$  in bed-1 is governed by the intermediate-blowdown pressure,  $P_I$  and the amount of extract to be withdrawn. During this step, bed-2 is assumed to be frozen at  $P_H$  as time step is very small. It is assumed that during frozen step, there is no change in gas



phase or solid phase concentration profile with time in bed as frozen step time is small. These three steps complete the first half cycle. The other half cycle is the mirror image of the first half cycle. Step 4 is the mirror image of step 1, step 5 is that of step 2 and step 6 is that of step 3.

**Pressure history in bed:** Figure 3.4 shows the Pressure history in the beds in a cycle. In step 1 and step 4, pressure in the beds (undergoing feed and purge) does not change with time while in step 2 and step 5, pressure in the beds (undergoing equalization and pressurization) changes with time. In step 4 and step 6, one bed remains at constant pressure (frozen) while pressure in other bed (undergoing extract withdrawal or final-blowdown) changes with time.

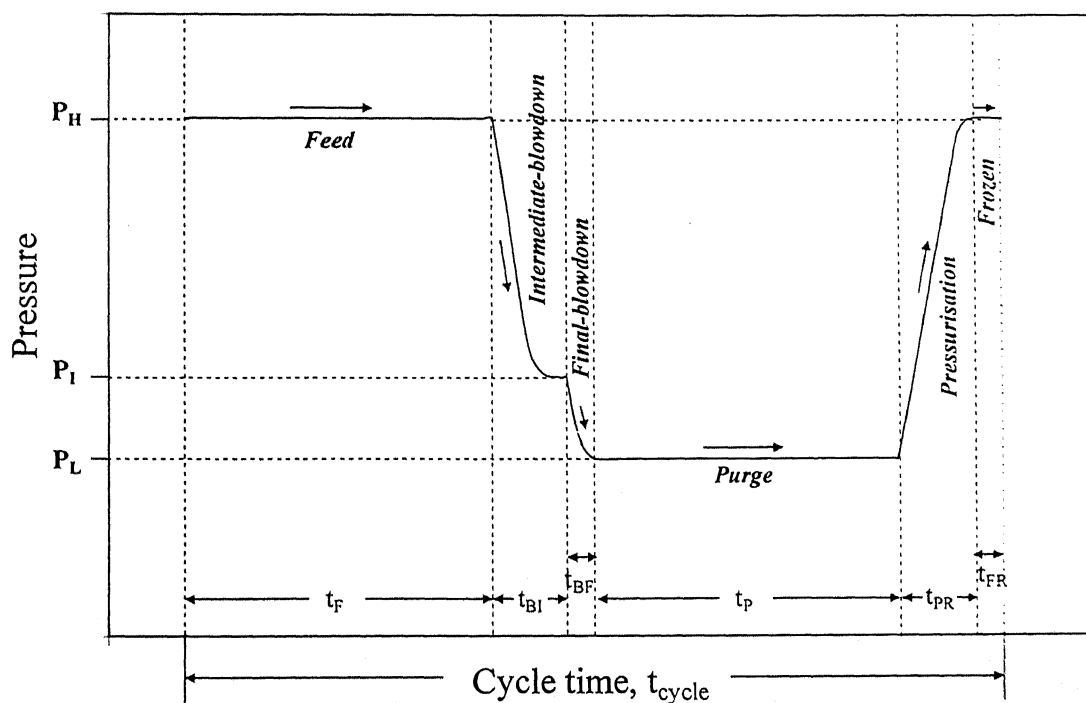


Fig.3.4 Pressure history in the bed in a cycle in *MV-II duplex PSA*



### 3.4 Duplex TSA

Based on the analogy with the *duplex PSA*, another process with temperature swing, *duplex TSA* has been proposed and the possibility of separation has been explored. The *duplex TSA* process consists of two steps in a cycle. Figure 3.5 shows the steps.

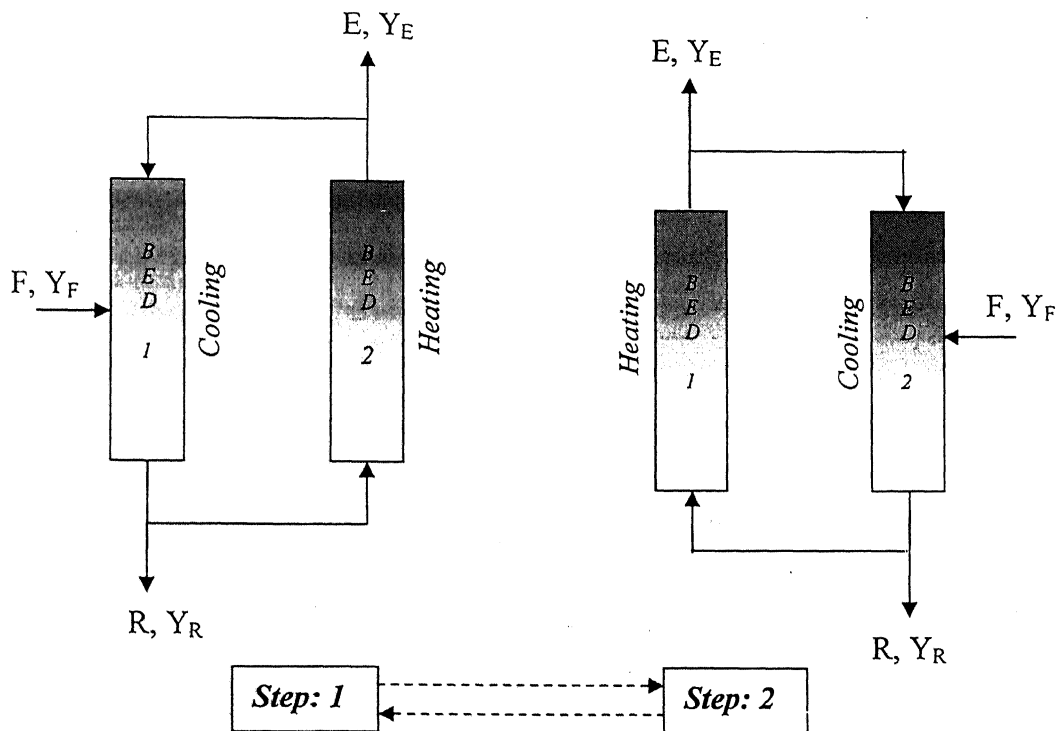


Fig.3.5 Sequence of steps in *duplex TSA* in a cycle

**Step 1:** In this step, the feed is introduced into bed-1 and both the end products are drawn simultaneously (raffinate from bottom of the bed-1 and extract from top of the bed-2). The operating pressure in both the beds are same. Table below shows the status of the beds.

	<i>Bed-1</i>	<i>Bed-2</i>
<i>Status</i>	<i>Cooling</i>	<i>Heating</i>

Feed is introduced at an intermediate point along the length of the bed-1. Bed-1 is undergoing cooling so the heavy component gets adsorbed inside the bed. A part of the

outgoing stream, rich in light component is drawn from the bottom as raffinate product. The remaining part is recycled to the bottom of bed-2 as raffinate recycle. As bed-2 is undergoing heating, heavy component will get desorbed and recycle stream will purge off the desorbed heavy component. A part of the outgoing stream, rich with heavy component from the top of bed-2 is drawn as extract product. The remaining part is recycled to the top of bed-1 as extract recycle.

Step-2 is the mirror image of step-1. In this step, feed is switched to bed-2. These two steps complete a cycle.

**Temperature history in bed:** Temperature profile inside the beds has been assumed to be linear (minimum at the top and maximum at the bottom). During any step, one bed will undergo cooling and other bed will undergo heating and in next step cooling and heating will get reversed. Temperature shift between the two ends of the beds has also been taken as linear. This is the ideal case, and has been taken to study the possible mechanism of separation which will help in developing a real *duplex TSA cycle*. Figure 3.6 and 3.7 shows the temperature shift in the beds undergoing cooling and heating respectively.

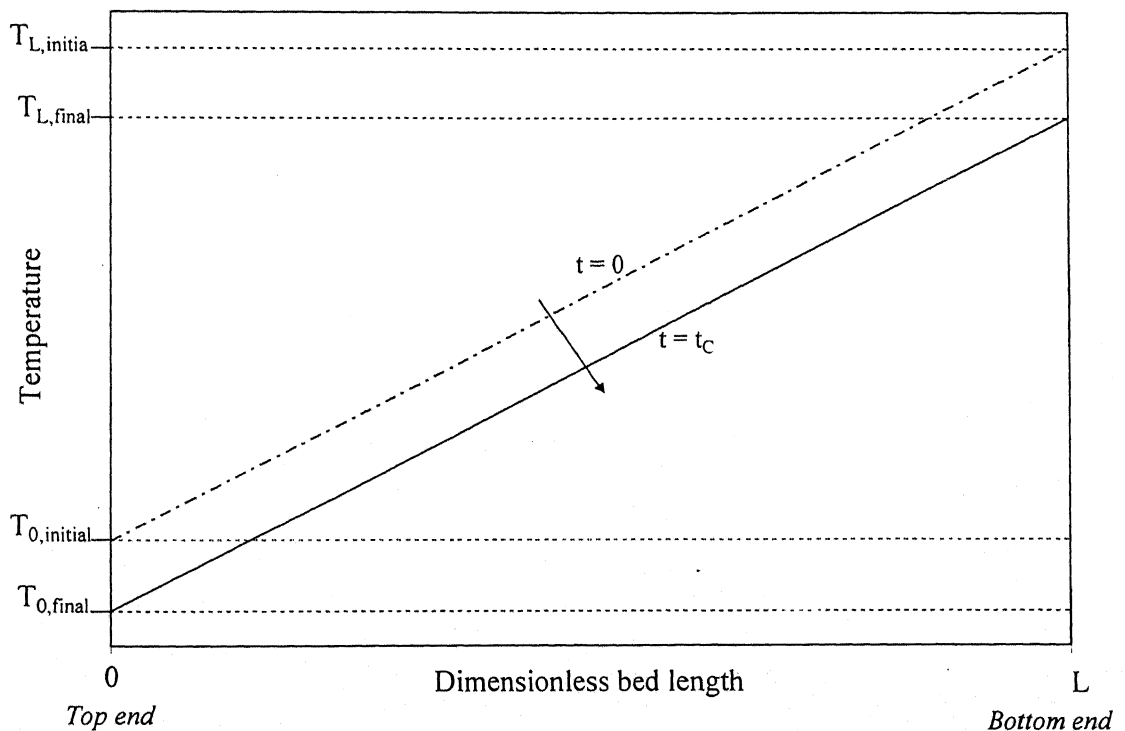


Fig.3.6 Temperature shift along the length of the bed undergoing cooling

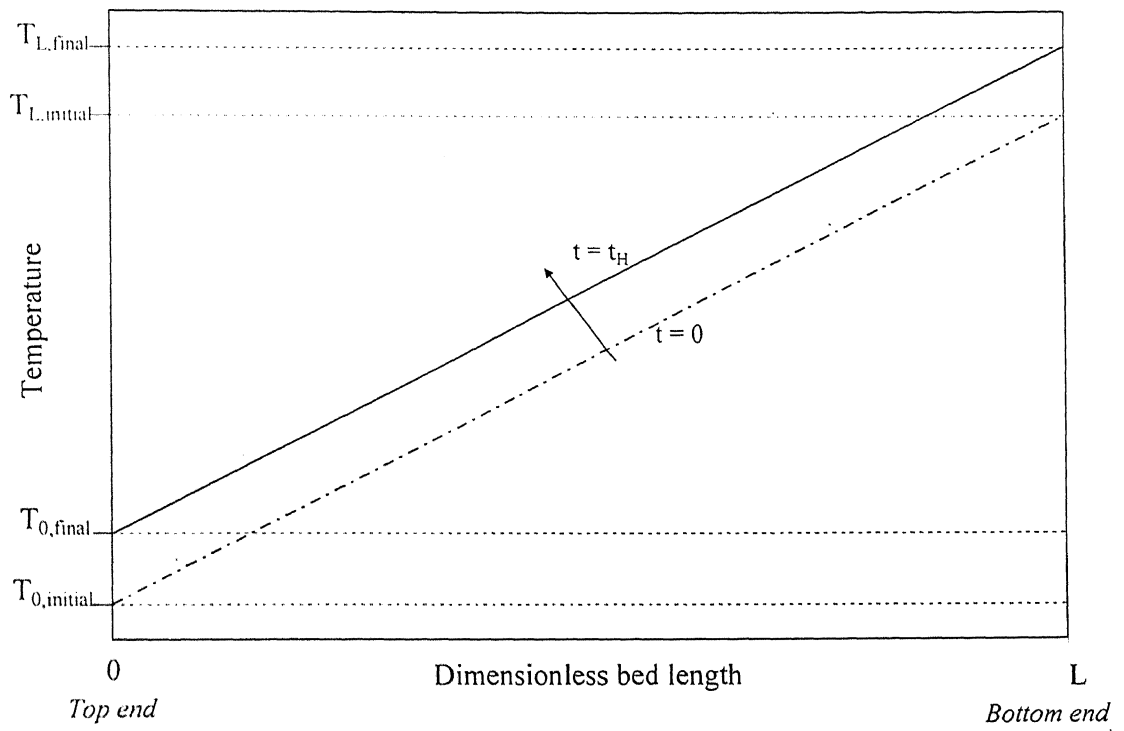


Fig.3.7 Temperature shift along the length of the bed undergoing heating

## Modeling and Simulation

This chapter presents the mathematical model and the method of simulation of the duplex PSA and the duplex TSA cycle.

### 4.1 Mathematical model

A gaseous mixture of  $N$  components is flowing through a fixed-bed of length  $L$  packed with adsorbent particles of identical size as shown in Figure 4.1. The flow is considered to be axial dispersed plug flow i.e. without gradients in the radial direction. The solid (adsorbent) and the fluid phases are considered to be separated by an interface. Mass and heat transfer between these two phases takes place through this interface. The governing partial differential equations are derived by making mass and heat balance in a differential element,  $\Delta z$  of the fixed-bed adsorber as shown below.

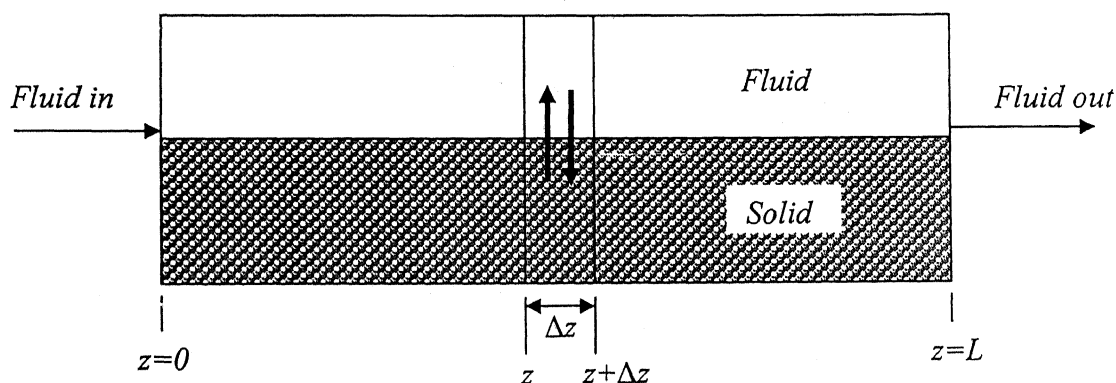


Fig 4.1 Differential element of a section of the adsorber

#### *Mass balance for the bulk fluid phase*

The mass balance of component  $i$  over the differential element,  $\Delta z$  for the gas phase is given as

$$\text{Input} = \text{Output} + \text{Accumulation}$$

$$\underbrace{\varepsilon A \left\{ -D_L \frac{\partial c_i}{\partial z} \right\}_z}_{\text{Dispersion}} + \underbrace{\varepsilon A (v_f c_i) \Big|_z}_{\text{Convection}} = \varepsilon A \underbrace{\left\{ -D_L \frac{\partial c_i}{\partial z} \right\}_{z+\Delta z}}_{\text{Dispersion}} + \varepsilon A \underbrace{(v_f c_i) \Big|_{z+\Delta z}}_{\text{Convection}} + \underbrace{\varepsilon A \frac{\partial c_i}{\partial t} \Delta z + A(1-\varepsilon) \frac{\partial q_i}{\partial t} \Delta z}_{\text{Accumulation}}$$

(4.1)

where,

- $c_i$  - gas phase molar concentration of component  $i$ , ( $\text{mol}/\text{m}^3$ )
- $v_f$  - interstitial fluid velocity, ( $\text{m}/\text{s}$ )
- $A$  - cross sectional area of the adsorber, ( $\text{m}^2$ )
- $\varepsilon$  - bed voidage
- $q_i$  - solid phase molar concentration of component  $i$ , ( $\text{mol}/\text{m}^3$ )
- $t$  - time, ( $\text{s}$ )
- $\frac{\partial q_i}{\partial t}$  - molar rate of interfacial transfer of component  $i$ , ( $\text{mol}/\text{m}^3 \cdot \text{s}$ )
- $D_L$  - axial dispersion coefficient, ( $\text{m}^2/\text{s}$ )

Equation (4.1) can be rearranged to,

$$\varepsilon A \left[ \left( -D_L \frac{\partial c_i}{\partial z} + v_f c_i \right) \Big|_{z+\Delta z} - \left( -D_L \frac{\partial c_i}{\partial z} + v_f c_i \right) \Big|_z \right] + \varepsilon A \frac{\partial c_i}{\partial t} \Delta z + A(1-\varepsilon) \frac{\partial q_i}{\partial t} \Delta z = 0$$

(4.2)

On dividing Equation (4.2) by  $\varepsilon A \Delta z$ , we get

$$\frac{\partial c_i}{\partial t} + \frac{\partial}{\partial z} (v_f c_i) - \frac{\partial}{\partial z} \left( D_L \frac{\partial c_i}{\partial z} \right) + \frac{(1-\varepsilon)}{\varepsilon} \frac{\partial q_i}{\partial t} = 0$$

(4.3)

Assuming the gas obeys ideal gas law,  $c_i$  can be expressed as

$$c_i = \frac{P}{RT_g}$$

(4.4)

where,

$c_t$  - total gas phase molar concentration ( $mol/m^3$ )

$P$  - pressure ( $atm$ )

$R$  - universal gas constant ( $atm\cdot m^3/gmol\cdot K$ )

$T_g$  - gas phase temperature ( $K$ )

The gas phase concentration of component  $i$  is given by

$$c_i = y_i c_t \quad (4.5)$$

where,  $y_i$  is the mole fraction of component  $i$  in the gas phase.

On substituting the Equation (4.5) in Equation (4.3), we get

$$\frac{\partial}{\partial t}(C_i y_i) + \frac{\partial}{\partial z}(v_f C_i y_i) - \frac{\partial}{\partial z}\left(D_L \frac{\partial C_i y_i}{\partial z}\right) + \frac{(1-\varepsilon)}{\varepsilon} \frac{\partial q_i}{\partial t} = 0 \quad (4.6)$$

The pressure effect on axial dispersion coefficient can be expressed as

$$D_L = \frac{D_{Lo}}{P} \quad (4.7)$$

where  $D_{Lo}$  is the axial dispersion coefficient at reference pressure (1 atm).

The interstitial fluid velocity,  $v_f$  is calculated by the Blake-Kozeny equation.

$$\begin{aligned} v_f &= -\frac{d_p^2 \varepsilon^2}{150\mu(1-\varepsilon)^2} \frac{\partial P}{\partial z} \\ &= -K \frac{\partial P}{\partial z} \end{aligned} \quad (4.8)$$

where,

$$K = \frac{d_p^2 \varepsilon^2}{150\mu(1-\varepsilon)^2}$$

$d_p$  - particle diameter, (m)

On substituting Equation (4.5), (4.7) and (4.8) in Equation (4.6), we get

$$\frac{\partial}{\partial t} \left( \frac{Py_i}{RT_g} \right) + \frac{\partial}{\partial z} \left[ -K \frac{\partial P}{\partial z} \left( \frac{Py_i}{RT_g} \right) \right] - \frac{\partial}{\partial z} \left[ \frac{D_{l,o}}{P} \frac{\partial}{\partial z} \left( \frac{Py_i}{RT_g} \right) \right] + \frac{(1-\varepsilon)}{\varepsilon} \frac{\partial q_i}{\partial t} = 0 \quad (4.9)$$

On simplifying Equation (4.9), we get

$$\begin{aligned} \frac{\partial y_i}{\partial t} = \frac{D_{l,o}}{P} \left[ \frac{\partial^2 y_i}{\partial z^2} + \frac{y_i}{P} \frac{\partial^2 P}{\partial z^2} + \frac{1}{P} \frac{\partial y_i}{\partial z} \frac{\partial P}{\partial z} - \frac{y_i}{P^2} \left( \frac{\partial P}{\partial z} \right)^2 - \frac{y_i}{T_g} \frac{\partial^2 T_g}{\partial z^2} - \frac{2}{T_g} \frac{\partial y_i}{\partial z} \frac{\partial T_g}{\partial z} - \frac{y_i}{PT_g} \frac{\partial P}{\partial z} \frac{\partial T_g}{\partial z} + \frac{2y_i}{T_g^2} \left( \frac{\partial T_g}{\partial z} \right)^2 \right] \\ + K \left[ y_i \frac{\partial^2 P}{\partial z^2} + \frac{\partial y_i}{\partial z} \frac{\partial P}{\partial z} + \frac{y_i}{P} \left( \frac{\partial P}{\partial z} \right)^2 - \frac{y_i}{T_g} \frac{\partial P}{\partial z} \frac{\partial T_g}{\partial z} \right] - \frac{y_i}{P} \left( \frac{\partial P}{\partial t} \right) + \frac{y_i}{T_g} \left( \frac{\partial T_g}{\partial t} \right) - \frac{RT_g}{P} \frac{(1-\varepsilon)}{\varepsilon} \frac{\partial q_i}{\partial t} \end{aligned}$$

for  $i = 1$  to  $N-1$  (4.10)

On summing up Equation (4.10) over all components  $\left( \sum_{i=1}^N y_i = 1 \right)$  and rearranging, we get

$$\begin{aligned} \frac{\partial P}{\partial t} = \frac{D_{l,o}}{P} \left[ \frac{\partial^2 P}{\partial z^2} - \frac{1}{P} \left( \frac{\partial P}{\partial z} \right)^2 - \frac{P}{T_g} \frac{\partial^2 T_g}{\partial z^2} - \frac{1}{T_g} \frac{\partial P}{\partial z} \frac{\partial T_g}{\partial z} + \frac{2P}{T_g^2} \left( \frac{\partial T_g}{\partial z} \right)^2 \right] \\ + K \left[ P \frac{\partial^2 P}{\partial z^2} + \left( \frac{\partial P}{\partial z} \right)^2 - \frac{P}{T_g} \frac{\partial P}{\partial z} \frac{\partial T_g}{\partial z} \right] + \frac{P}{T_g} \left( \frac{\partial T_g}{\partial t} \right) - RT_g \frac{(1-\varepsilon)}{\varepsilon} \sum_{i=1}^N \frac{\partial q_i}{\partial t} \end{aligned} \quad (4.11)$$

**Further simplification of  $\frac{\partial y_i}{\partial t}$  &  $\frac{\partial P}{\partial t}$**

Equation (4.10) can be rearranged as,

$$\begin{aligned} \frac{\partial y_i}{\partial t} = \left( K + \frac{D_{l,o}}{P^2} \right) \left[ y_i \frac{\partial^2 P}{\partial z^2} + \frac{\partial y_i}{\partial z} \frac{\partial P}{\partial z} - \frac{y_i}{T_g} \frac{\partial P}{\partial z} \frac{\partial T_g}{\partial z} \right] + \left( K - \frac{D_{l,o}}{P^2} \right) \left[ \frac{y_i}{P} \left( \frac{\partial P}{\partial z} \right)^2 \right] \\ + \frac{D_{l,o}}{P} \left[ \frac{\partial^2 y_i}{\partial z^2} - \frac{y_i}{T_g} \frac{\partial^2 T_g}{\partial z^2} - \frac{2}{T_g} \frac{\partial y_i}{\partial z} \frac{\partial T_g}{\partial z} + \frac{2y_i}{T_g^2} \left( \frac{\partial T_g}{\partial z} \right)^2 \right] - \frac{y_i}{P} \left( \frac{\partial P}{\partial t} \right) + \frac{y_i}{T_g} \left( \frac{\partial T_g}{\partial t} \right) - \frac{RT_g}{P} \frac{(1-\varepsilon)}{\varepsilon} \frac{\partial q_i}{\partial t} \end{aligned} \quad (4.12)$$

$$\text{If } K \gg \frac{D_{l,o}}{P^2} \Rightarrow \left( K \pm \frac{D_{l,o}}{P^2} \right) \approx K$$

Equation (4.12) simplifies further to,

$$\begin{aligned} \frac{\partial y_i}{\partial t} = \frac{D_{Lo}}{P} & \left[ \frac{\partial^2 y_i}{\partial z^2} - \frac{y_i}{T_g} \frac{\partial^2 T_g}{\partial z^2} - \frac{2}{T_g} \frac{\partial y_i}{\partial z} \frac{\partial T_g}{\partial z} + \frac{2y_i}{T_g^2} \left( \frac{\partial T_g}{\partial z} \right)^2 \right] \\ & + K \left[ y_i \frac{\partial^2 P}{\partial z^2} + \frac{\partial y_i}{\partial z} \frac{\partial P}{\partial z} - \frac{y_i}{T_g} \frac{\partial P}{\partial z} \frac{\partial T_g}{\partial z} + \frac{y_i}{P} \left( \frac{\partial P}{\partial z} \right)^2 \right] - \frac{y_i}{P} \left( \frac{\partial P}{\partial t} \right) + \frac{y_i}{T_g} \left( \frac{\partial T_g}{\partial t} \right) - \frac{RT_g}{P} \frac{(1-\varepsilon)}{\varepsilon} \frac{\partial q_i}{\partial t} \end{aligned} \quad (4.13)$$

On summing up Equation (4.13) over all components  $\left( \sum_{i=1}^N y_i = 1 \right)$  and rearranging, we get

$$\begin{aligned} \frac{\partial P}{\partial t} = D_{Lo} & \left[ \frac{2}{T_g^2} \left( \frac{\partial T_g}{\partial z} \right)^2 - \frac{1}{T_g} \frac{\partial^2 T_g}{\partial z^2} \right] + K \left[ P \frac{\partial^2 P}{\partial z^2} + \left( \frac{\partial P}{\partial z} \right)^2 - \frac{P}{T_g} \frac{\partial P}{\partial z} \frac{\partial T_g}{\partial z} \right] + \frac{P}{T_g} \left( \frac{\partial T_g}{\partial t} \right) \\ & - RT_g \frac{(1-\varepsilon)}{\varepsilon} \sum_{i=1}^N \frac{\partial q_i}{\partial t} \end{aligned} \quad (4.14)$$

By putting Equation (4.14) into Equation (4.13),  $\frac{\partial y_i}{\partial t}$  further reduces to

$$\begin{aligned} \frac{\partial y_i}{\partial t} = \frac{D_{Lo}}{P} & \left( \frac{\partial^2 y_i}{\partial z^2} - \frac{2}{T_g} \frac{\partial y_i}{\partial z} \frac{\partial T_g}{\partial z} \right) + K \frac{\partial y_i}{\partial z} \frac{\partial P}{\partial z} + \frac{RT_g}{P} \frac{(1-\varepsilon)}{\varepsilon} \left( y_i \sum_{i=1}^N \frac{\partial q_i}{\partial t} - \frac{\partial q_i}{\partial t} \right) \\ & \text{for } i = 1 \text{ to } N-1 \end{aligned} \quad (4.15)$$

For the isothermal process,

$$T_g = \text{constant} \quad \Rightarrow \quad \frac{\partial T_g}{\partial z} = 0 ; \quad \frac{\partial^2 T_g}{\partial z^2} = 0, \text{ so Equation (4.14) and (4.15) will reduce to}$$

$$\frac{\partial P}{\partial t} = K \left[ P \frac{\partial^2 P}{\partial z^2} + \left( \frac{\partial P}{\partial z} \right)^2 \right] - RT_g \frac{(1-\varepsilon)}{\varepsilon} \sum_{i=1}^N \frac{\partial q_i}{\partial t} \quad (4.16)$$

$$\frac{\partial y_i}{\partial t} = \frac{D_{Lo}}{P} \left( \frac{\partial^2 y_i}{\partial z^2} \right) + K \frac{\partial y_i}{\partial z} \frac{\partial P}{\partial z} + \frac{RT_g}{P} \frac{(1-\varepsilon)}{\varepsilon} \left( y_i \sum_{i=1}^N \frac{\partial q_i}{\partial t} - \frac{\partial q_i}{\partial t} \right) \quad \text{for } i = 1 \text{ to } N-1 \quad (4.17)$$



### Mass balance for the solid phase

The rate of interfacial mass transfer between the solid and the fluid phase is represented by the Glueckauf's linear driving force (LDF) model.

$$\frac{\partial q_i}{\partial t} = k_i (q_i^* - q_i) \quad \text{for } i = 1 \text{ to } N \quad (4.18)$$

where,

$k_i$  - linear driving force(LDF) mass transfer coefficient, ( $s^{-1}$ )

$q_i^*$  - solid phase molar concentration in equilibrium with  $c_i$ , ( $mol/m^3$ )

### Heat balance for the bulk fluid phase

Considering the process is adiabatic, the heat balance over the differential element,  $\Delta z$  shown in the Figure 4.1 for the gas phase is given by

$$\text{Input} = \text{Output} + \text{Accumulation}$$

$$\underbrace{\varepsilon A \left\{ -K_{e,ax} \frac{\partial T_g}{\partial z} \right\}_z}_{\text{Conduction}} + \underbrace{\left\{ (\rho_g C_{pg} v_f T_g) \right\}_z}_{\text{Convection}} = \underbrace{\varepsilon A \left\{ -K_{e,ax} \frac{\partial T_g}{\partial z} \right\}_{z+\Delta z}}_{\text{Conduction}} + \underbrace{\left\{ (\rho_g C_{pg} v_f T_g) \right\}_{z+\Delta z}}_{\text{Convection}} + \underbrace{h_p a_s (T_g - T_s) A \Delta z}_{\text{Interfacial transfer}} + \underbrace{\frac{\partial}{\partial t} [A \varepsilon \rho_g C_{pg} T_g] \Delta z}_{\text{Accumulation}} \quad (4.19)$$

One assumption has been made that the velocity,  $v_f$  of the fluid is constant in the small differential element  $\Delta z$  and will vary from the element to element along the length of the bed.

On dividing Equation (4.19) by  $\varepsilon A \Delta z$  and rearranging, we get

$$\frac{\partial T_g}{\partial t} = \frac{K_{e,ax}}{\rho_g C_{pg}} \frac{\partial^2 T_g}{\partial z^2} - v_f \frac{\partial T_g}{\partial z} - \frac{h_p a_s}{\varepsilon \rho_g C_{pg}} (T_g - T_s) \quad (4.20)$$

The velocity is calculated by the Blake-Kozeny Equation (4.8). On putting Equation (4.8) into Equation (4.20), we get

$$\frac{\partial T_g}{\partial t} = \alpha \frac{\partial^2 T_g}{\partial z^2} + K \frac{\partial P}{\partial z} \frac{\partial T_g}{\partial z} - \frac{h_p a_s}{\varepsilon \rho_g C_{pg}} (T_g - T_s) \quad (4.21)$$

where,

$K_{e,ax}$  - effective axial thermal conductivity of gas,  $(W / mK)$

$\rho_g$  - density of gas,  $(kg / m^3)$

$C_{pg}$  - specific heat of gas,  $(J / kgK)$

$\alpha$  -  $\frac{K_{e,ax}}{\rho_g C_{pg}}$ , effective axial thermal diffusivity of gas,  $(m^2/s)$

$h_p$  - particle heat transfer coefficient,  $(W/m^2K)$

$\rho_s$  - density of solid,  $(kg / m^3)$

$C_{ps}$  - specific heat of solid,  $(J / kgK)$

$T_s$  - solid phase temperature,  $(K)$

### ***Heat balance for the solid phase***

Considering the process is adiabatic, the heat balance over the differential element,  $\Delta z$  shown in the Figure 4.1 for the solid phase is given by

$$\text{Input} = \text{Output} + \text{Accumulation}$$

$$\underbrace{\sum_{i=1}^N (-\Delta H)_i \frac{\partial q_i}{\partial t} (1-\varepsilon) A \Delta z}_{\text{Heat of adsorption}} + \underbrace{h_p a_s (T_g - T_s) A \Delta z}_{\text{Interfacial transfer}} = \underbrace{\frac{\partial}{\partial t} [A(1-\varepsilon) \rho_s C_{ps} T_s] \Delta z}_{\text{Accumulation}} \quad (4.22)$$

where,

$$a_s = \frac{6(1-\varepsilon)}{d_p} \quad ; \text{ specific surface area of the adsorbent particle, } (m^{-1})$$

$\Delta H$  - heat of adsorption,  $(J/mol)$

On dividing Equation (4.22) by  $A(1-\varepsilon)\Delta z$  and rearranging, we get

$$\frac{\partial T_s}{\partial t} = \frac{1}{\rho_s C_{ps}} \sum_{i=1}^N (-\Delta H)_i \frac{\partial q_i}{\partial t} + \frac{h_p a_s}{\rho_s C_{ps} (1-\varepsilon)} (T_g - T_s) \quad (4.23)$$

The duplex PSA cycle has been simulated at isothermal condition whereas the duplex TSA cycle has been simulated at non-isothermal condition.

The governing partial differential equations (PDE's) derived above for duplex PSA and duplex TSA are being summarized below.

#### ***Governing PDE's for duplex PSA***

$$\frac{\partial P}{\partial t} = K \left[ P \frac{\partial^2 P}{\partial z^2} + \left( \frac{\partial P}{\partial z} \right)^2 \right] - RT_g \frac{(1-\varepsilon)}{\varepsilon} \sum_{i=1}^N \frac{\partial q_i}{\partial t} \quad (4.16)$$

$$\frac{\partial y_i}{\partial t} = \frac{D_{i,o}}{P} \left( \frac{\partial^2 y_i}{\partial z^2} \right) + K \frac{\partial y_i}{\partial z} \frac{\partial P}{\partial z} + \frac{RT_g}{P} \frac{(1-\varepsilon)}{\varepsilon} \left( y_i \sum_{i=1}^N \frac{\partial q_i}{\partial t} - \frac{\partial q_i}{\partial t} \right) \quad \text{for } i=1 \text{ to } N-1 \quad (4.17)$$

$$\frac{\partial q_i}{\partial t} = k_i (q_i^* - q_i) \quad \text{for } i=1 \text{ to } N \quad (4.18)$$

## Governing PDE's for duplex TSA

$$\begin{aligned} \frac{\partial P}{\partial t} = & D_{Lo} \left[ \frac{2}{T_g^2} \left( \frac{\partial T_g}{\partial z} \right)^2 - \frac{1}{T_g} \frac{\partial^2 T_g}{\partial z^2} \right] + K \left[ P \frac{\partial^2 P}{\partial z^2} + \left( \frac{\partial P}{\partial z} \right)^2 - \frac{P}{T_g} \frac{\partial P}{\partial z} \frac{\partial T_g}{\partial z} \right] + \frac{P}{T_g} \left( \frac{\partial T_g}{\partial t} \right) \\ & - RT_g \frac{(1-\varepsilon)}{\varepsilon} \sum_{i=1}^N \frac{\partial q_i}{\partial t} \end{aligned} \quad (4.14)$$

$$\begin{aligned} \frac{\partial y_i}{\partial t} = & \frac{D_{Lo}}{P} \left( \frac{\partial^2 y_i}{\partial z^2} - \frac{2}{T_g} \frac{\partial y_i}{\partial z} \frac{\partial T_g}{\partial z} \right) + K \frac{\partial y_i}{\partial z} \frac{\partial P}{\partial z} + \frac{RT_g}{P} \frac{(1-\varepsilon)}{\varepsilon} \left( y_i \sum_{i=1}^N \frac{\partial q_i}{\partial t} - \frac{\partial q_i}{\partial t} \right) \\ & \text{for } i = 1 \text{ to } N-1 \end{aligned} \quad (4.15)$$

$$\frac{\partial q_i}{\partial t} = k_i (q_i^* - q_i) \quad \text{for } i = 1 \text{ to } N \quad (4.18)$$

$$\frac{\partial T_g}{\partial t} = \alpha \frac{\partial^2 T_g}{\partial z^2} + K \frac{\partial P}{\partial z} \frac{\partial T_g}{\partial z} - \frac{h_p a_s}{\varepsilon \rho_g C_{pg}} (T_g - T_s) \quad (4.21)$$

$$\frac{\partial T_s}{\partial t} = \frac{1}{\rho_s C_{ps}} \sum_{i=1}^N (-\Delta H)_i \frac{\partial q_i}{\partial t} + \frac{h_p a_s}{\rho_s C_{ps} (1-\varepsilon)} (T_g - T_s) \quad (4.23)$$

## 4.2 Initial and boundary conditions

The partial differential Equations [(4.14), (4.15), (4.16), (4.17) and (4.21)] are first order with respect to time and second order with respect to length. It requires initial condition and two boundary conditions whereas Equations [(4.18) and (4.23)] are first order with respect to time and requires only initial condition to solve it numerically. The initial and boundary conditions for different steps of duplex PSA and duplex TSA are given below.

### 4.2.1 Original duplex and MV-I duplex PSA

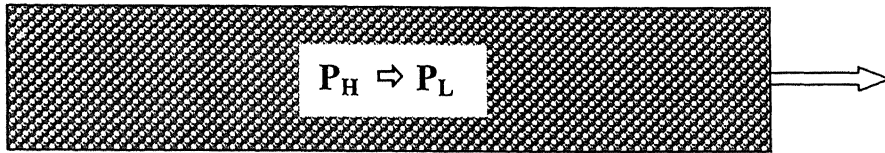
The Original duplex PSA and the MV-I duplex PSA cycle employs four steps viz. blowdown, purge, pressurization and feed step. The initial and boundary conditions for each step are given below.

#### ➤ Blowdown step

I.C's: at  $t = 0$

$$y_i(z, 0) = y_{i, ini} ; \quad P(z, 0) = P_H$$

$$q_i(z, 0) = q_i^*(y_i, P, T_g)$$



$$\left. \frac{\partial y}{\partial z} \right|_{z=0} = 0$$

$$\left. \frac{\partial y}{\partial z} \right|_{z=L} = 0$$

$$\left. \frac{\partial P}{\partial z} \right|_{z=0} = 0$$

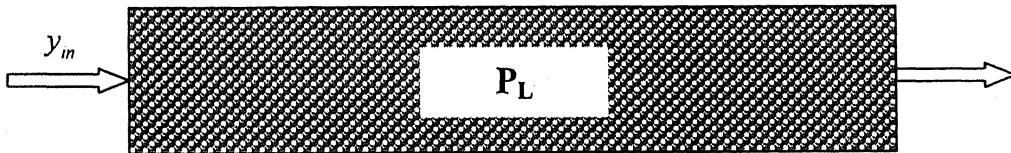
$$\left. \frac{\partial P}{\partial z} \right|_{z=L} = -\frac{v_f}{K}$$

#### ➤ Purge step

I.C's: at  $t = 0$

$$y_i(z, 0) = y_i(z, t_B) ; \quad P(z, 0) = P(z, t_B)$$

$$q_i(z, 0) = q_i(z, t_B)$$



$$\left. \frac{\partial y}{\partial z} \right|_{z=0} = -\frac{v_f}{D_L} (y_{in} - y|_{z=0})$$

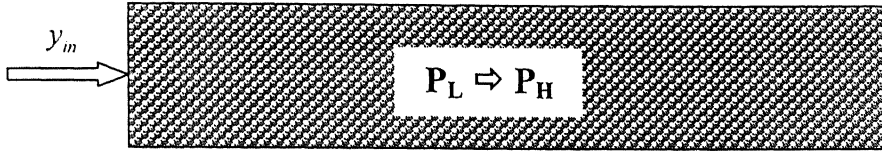
$$\left. \frac{\partial y}{\partial z} \right|_{z=L} = 0$$

$$\left. \frac{\partial P}{\partial z} \right|_{z=0} = -\frac{v_f}{K}$$

$$\left. \frac{\partial P}{\partial t} \right|_{z=L} = 0$$

➤ **Pressurization step**

I.C's: at  $t=0$   
 $y_i(z, 0) = y_i(z, t_P); \quad P(z, 0) = P(z, t_P)$   
 $q_i(z, 0) = q_i(z, t_P)$

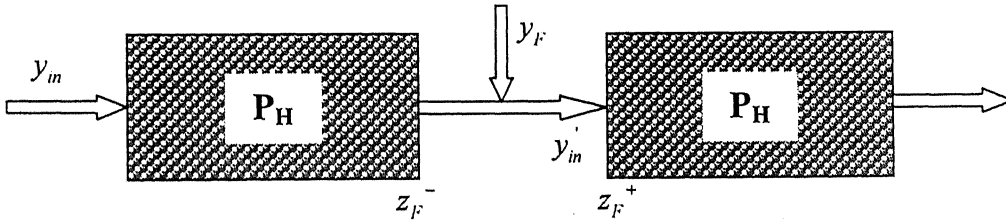


$$\left. \frac{\partial y}{\partial z} \right|_{z=0} = -\frac{v_f}{D_L} (y_{in} - y|_{z=0}) \qquad \left. \frac{\partial y}{\partial z} \right|_{z=L} = 0$$

$$\left. \frac{\partial P}{\partial z} \right|_{z=0} = -\frac{v_f}{K} \qquad \left. \frac{\partial P}{\partial z} \right|_{z=L} = 0$$

➤ **Feed step**

I.C's: at  $t=0$   
 $y_i(z, 0) = y_i(z, t_{PR}); \quad P(z, 0) = P(z, t_{PR})$   
 $q_i(z, 0) = q_i(z, t_{PR})$



$$\left. \frac{\partial y}{\partial z} \right|_{z=0} = -\frac{v_f}{D_L} (y_{in} - y|_{z=0}) \qquad \left. \frac{\partial y}{\partial z} \right|_{z=L} = 0$$

$$\left. \frac{\partial P}{\partial z} \right|_{z=0} = -\frac{v_f}{K} \qquad \left. \frac{\partial P}{\partial t} \right|_{z=L} = 0$$

$z_F^-$  and  $z_F^+$  represents the bed position just before and after the feed inlet position respectively. Boundary conditions at these two grids are given below. Expression for composition of the mixed stream,  $y_{in}'$  has been given in Appendix-A.

at  $z_{f^-}$

$$\left. \frac{\partial y}{\partial z} \right|_{z=z_{f^-}} = 0$$

$$\left. \frac{\partial P}{\partial t} \right|_{z=z_{f^-}} = 0$$

at  $z_{f^+}$

$$\left. \frac{\partial y}{\partial z} \right|_{z=z_{f^+}} = -\frac{v_f}{D_L} (y_{in} - y|_{z=z_{f^+}})$$

$$\left. \frac{\partial P}{\partial z} \right|_{z=z_{f^+}} = -\frac{v_f}{K}$$

#### 4.2.2 MV-II duplex PSA

The MV-II duplex PSA cycle employs six steps viz. intermediate-blowdown, final-blowdown, purge, pressurization, frozen and feed step

There are two blowdown steps viz. intermediate-blowdown and final-blowdown step. The boundary conditions for the intermediate-blowdown and the final-blowdown step are same as that of the blowdown step in the Original duplex PSA. Other steps like purge, pressurization and feed steps have the same boundary conditions as that of the Original duplex.

#### 4.2.3 Duplex TSA

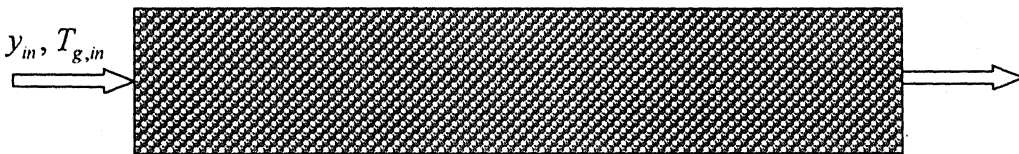
The duplex TSA cycle employs two steps viz. heating and cooling step. The initial and boundary conditions for each step are given below.

##### ➤ Heating step

I.C's: at  $t=0$

$$y_i(z, 0) = y_{i,ini}; \quad T_g(z, 0) = T_{g,ini}$$

$$T_s(z, 0) = T_{s,ini}; \quad q_i(z, 0) = q_i^*(y_b, P, T_g)$$



$$\left. \frac{\partial y}{\partial z} \right|_{z=0} = -\frac{v_f}{D_L} (y_{in} - y|_{z=0})$$

$$\left. \frac{\partial P}{\partial z} \right|_{z=0} = -\frac{v_f}{K}$$

$$\left. \frac{\partial y}{\partial z} \right|_{z=L} = 0$$

$$\left. \frac{\partial P}{\partial t} \right|_{z=L} = 0$$

$$\left. \frac{\partial T_g}{\partial z} \right|_{z=0} = -\frac{v_f}{\alpha} (T_{g,in} - T_g|_{z=0})$$

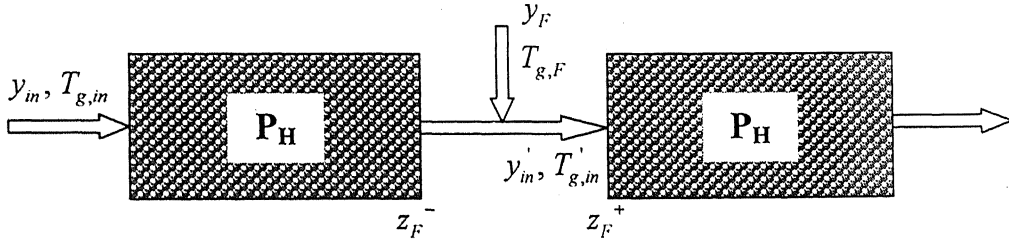
$$\left. \frac{\partial T_g}{\partial z} \right|_{z=l} = 0$$

➤ **Cooling (feed) step**

I.C's: at  $t=0$

$$y_i(z, 0) = y_i(z, t_h); \quad T_g(z, 0) = T_g(z, t_h)$$

$$T_s(z, 0) = T_s(z, t_h); \quad q_i(z, 0) = q_i(z, t_h)$$



$$\left. \frac{\partial y}{\partial z} \right|_{z=0} = -\frac{v_f}{D_L} (y_{in} - y|_{z=0})$$

$$\left. \frac{\partial y}{\partial z} \right|_{z=l} = 0$$

$$\left. \frac{\partial P}{\partial z} \right|_{z=0} = -\frac{v_f}{K}$$

$$\left. \frac{\partial P}{\partial t} \right|_{z=l} = 0$$

$$\left. \frac{\partial T_g}{\partial z} \right|_{z=0} = -\frac{v_f}{\alpha} (T_{g,in} - T_g|_{z=0})$$

$$\left. \frac{\partial T_g}{\partial z} \right|_{z=l} = 0$$

$z_F^-$  and  $z_F^+$  represents the bed position just before and after the feed inlet position respectively. Boundary conditions at these two grids are given below. Expression for composition and temperature of the mixed stream,  $y_{in}'$  and  $T_{g,in}'$  is given in Appendix-A.

at  $z_F^-$

$$\left. \frac{\partial y}{\partial z} \right|_{z=z_F^-} = 0$$

$$\left. \frac{\partial P}{\partial t} \right|_{z=z_F^-} = 0$$

$$\left. \frac{\partial T_g}{\partial z} \right|_{z=z_F^-} = 0$$

at  $z_F^+$

$$\left. \frac{\partial y}{\partial z} \right|_{z=z_F^+} = -\frac{v_f}{D_L} (y_{in}' - y|_{z=z_F^+})$$

$$\left. \frac{\partial P}{\partial z} \right|_{z=z_F^+} = -\frac{v_f}{K}$$

$$\left. \frac{\partial T_g}{\partial z} \right|_{z=z_F^+} = -\frac{v_f}{\alpha} (T_{g,in}' - T_g|_{z=z_F^+})$$



### 4.3 Parameters estimation

The estimation of parameters used in the mathematical model of the duplex PSA and the duplex TSA is described below.

#### *Adsorption equilibrium isotherm*

The equilibrium solid phase concentration has been represented by the extended-Langmuir isotherm

$$\frac{q_i^*}{q_{s,i}} = \frac{b_i c_i}{1 + \sum_{i=1}^N b_i c_i} \quad \text{for } i = 1 \text{ to } N \quad (4.24)$$

where,

$q_{s,i}$  - saturation constant of component  $i$ , ( $\text{mol/m}^3$ )

$b_i$  - Langmuir constant of component  $i$ , ( $\text{mol/m}^3$ )<sup>-1</sup>

temperature dependency of  $q_{s,i}$  and  $b_i$  (Cho et al., 1995)

$$q_{s,i} = q_{so,i} \frac{\exp(k_1 T_g)}{\exp(k_2 T_g)}$$

$$b_i = b_{o,i} \exp(k_2 T)$$

where

$k_1, k_2$  - temperature parameters, (K)

$T_g$  - gas phase temperature, (K)

#### *Interfacial mass transfer coefficient*

The interfacial mass transfer coefficient has been estimated by the Glueckauf model.

$$k_i = \frac{15 \varepsilon_p D_e c_{if}}{R_p^2 q_{if}^*} \quad (4.25)$$

where,

$k_i$  - linear driving force mass transfer coefficient, ( $\text{s}^{-1}$ )

$\varepsilon_p$  - particle porosity

$D_e$  - effective diffusivity, ( $\text{m}^2/\text{s}$ )

$R_p$  - particle radius, (m)

$c_{if}$  - feed concentration, (mol/m<sup>3</sup>)

$q_{if}^*$  - solid phase molar concentration in equilibrium with feed concentration of component  $i$ , (mol/m<sup>3</sup>)

The validity of the LDF model however is limited to  $\frac{D_e t_c}{R_p^2} > 0.1$  but it can also provide

an adequate description of the diffusion behaviour for even  $\frac{D_e t_c}{R_p^2} < 0.1$ , provided that the

LDF constant is adjusted as a function of  $\frac{D_e t_c}{R_p^2}$  (Alpay and Scott, 1992).

where  $t_c$  is half cycle time, (s) for a cyclic process.

### ***Axial dispersion coefficient***

The axial dispersion coefficient has been estimated from the correlation given by Wen and Fan (1975)

$$D_{LO} = 0.75D_M + \frac{0.5d_p v_f}{1 + 9.5 \left( \frac{D_M}{d_p v_f} \right)} \quad (4.26)$$

where  $D_M$  is molecular diffusivity, (m<sup>2</sup>/s)

### ***Particle heat transfer coefficient***

The particle heat transfer coefficient has been estimated from the correlation given by Wakao and Kaguei, (1982)

$$\varepsilon \frac{h_p}{C_{pg} G_g} \left( \frac{\mu C_{pg}}{K_g} \right)^{\frac{2}{3}} = \frac{2.876}{\text{Re}_p} + \frac{0.3023}{\text{Re}_p^{0.35}} \quad (4.27)$$

where,

$h_p$  = particle heat transfer coefficient, (W / m<sup>2</sup> K)

$G_g = \rho_g v_f$ ; mass velocity of fluid, (Kg/m<sup>2</sup>s)

$$Re_p = \frac{\rho_g v_f d_p}{\mu}; \text{ particle Reynolds number}$$

### **Effective axial thermal conductivity of gas**

The effective axial thermal conductivity for the gas flowing through a packed bed has been estimated from the correlation given by Wakao and Kaguei, (1982)

$$\frac{K_{e,ax}}{K_g} = \frac{K_e^o}{K_g} + 0.5(Pr)(Re_p) \quad (4.28)$$

where,

$K_{e,ax}$  - effective axial thermal conductivity of gas

$K_g$  - thermal conductivity of gas

$K_e^o$  - effective thermal conductivity for quiescent bed

$Pr$  - Prandtl number

$Re_p$  - particle Reynolds number

$K_e^o$  for a bed of spherical particle is given by

$$\frac{K_e^o}{K_g} = \left( \frac{K_s}{K_g} \right)^m \quad (4.29)$$

$$m = 0.280 - 0.757 \log_{10} \varepsilon - 0.057 \log_{10} \left( \frac{K_s}{K_g} \right)$$

where,

$K_s$  - thermal conductivity of solid

$\varepsilon$  - bed voidage

### **Energy equation**

Energy required for the compression or evacuation of a gas stream in a open system is given by (Smith and Van Ness, 1996)

$$W(isentropic) = \frac{\gamma nRT_g}{\gamma - 1} \left[ \left( \frac{P_2}{P_1} \right)^{\frac{\gamma-1}{\gamma}} - 1 \right] \quad (4.30)$$

where,

$$\gamma = C_p / C_v = \begin{array}{l} 1.67 \text{ (monoatomic gas)} \\ 1.40 \text{ (diatomic gas)} \\ 1.30 \text{ (polyatomic gas)} \end{array}$$

$n$  - moles of gas to be compressed or evacuated from pressure  $P_1$  to  $P_2$

$\gamma = 1.4$  has been taken in energy calculation.

### Valve equation

The valve equation is based on a simple pipe flow and equivalent length corresponding to the pressure drop through a valve

$$\frac{\Delta P}{\rho_g} = \frac{4 f L_e v_f^2}{2 D g_c} \quad (4.31)$$

On rearranging the above equation, we get

$$v_f = C (\Delta P)^{0.5}$$

where

$$C = \left( \frac{D g_c}{2 f L_e \rho} \right)^{0.5}$$

$f$  - fanning friction factor

$\rho_g$  - density of gas, (kg/m<sup>3</sup>)

$L_e$  - equivalent length of pipe, (m)

$D$  - diameter of the pipe, (m)

In the blowdown and the pressurization step, velocity at the opening of the bed should be such that the bed reaches the desired pressure in the given step time. For this, the above equation has been modified as

$$v_f = k C (\Delta P)^{0.5}$$

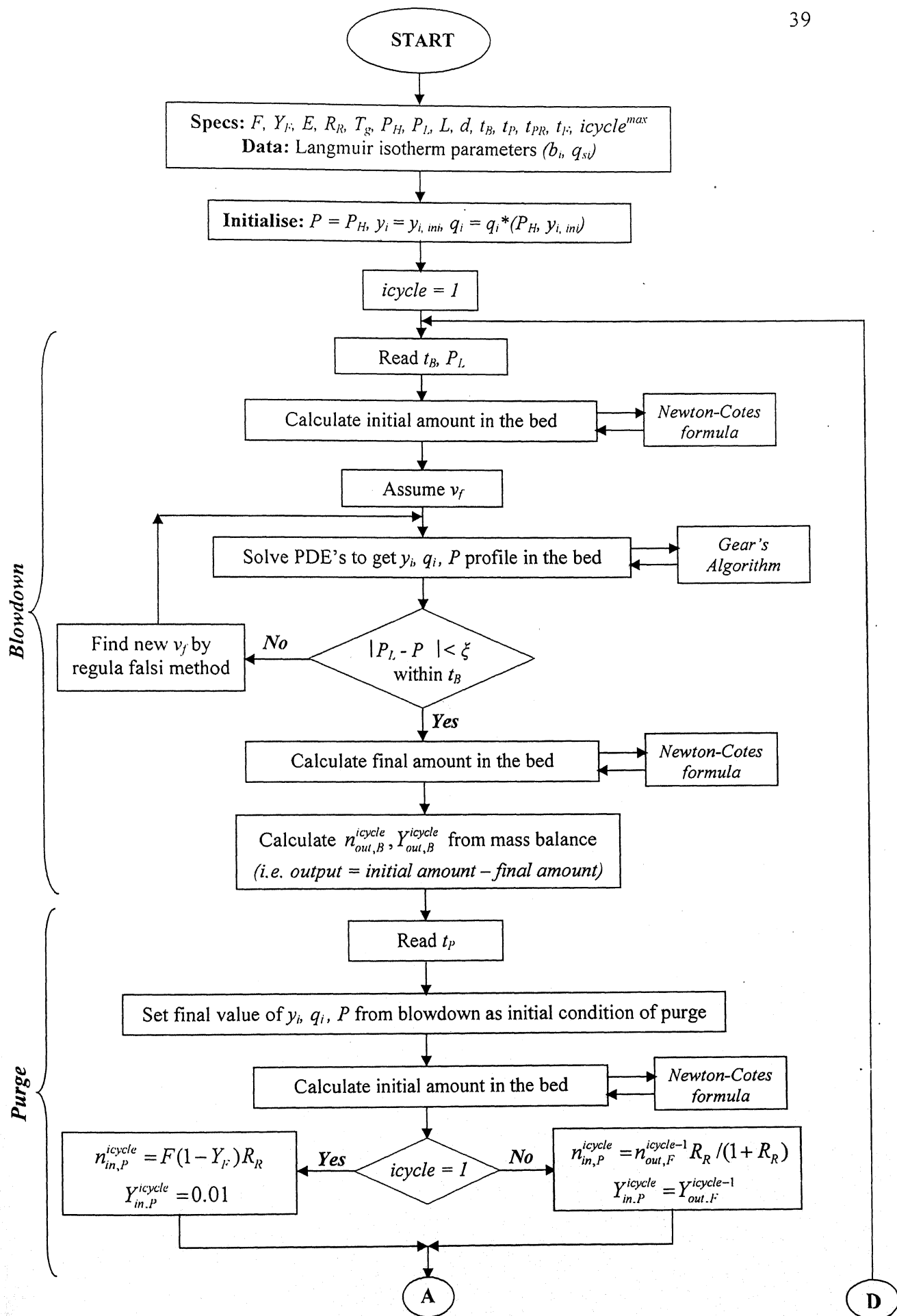
The  $k$  is found by the regula-falsi method.

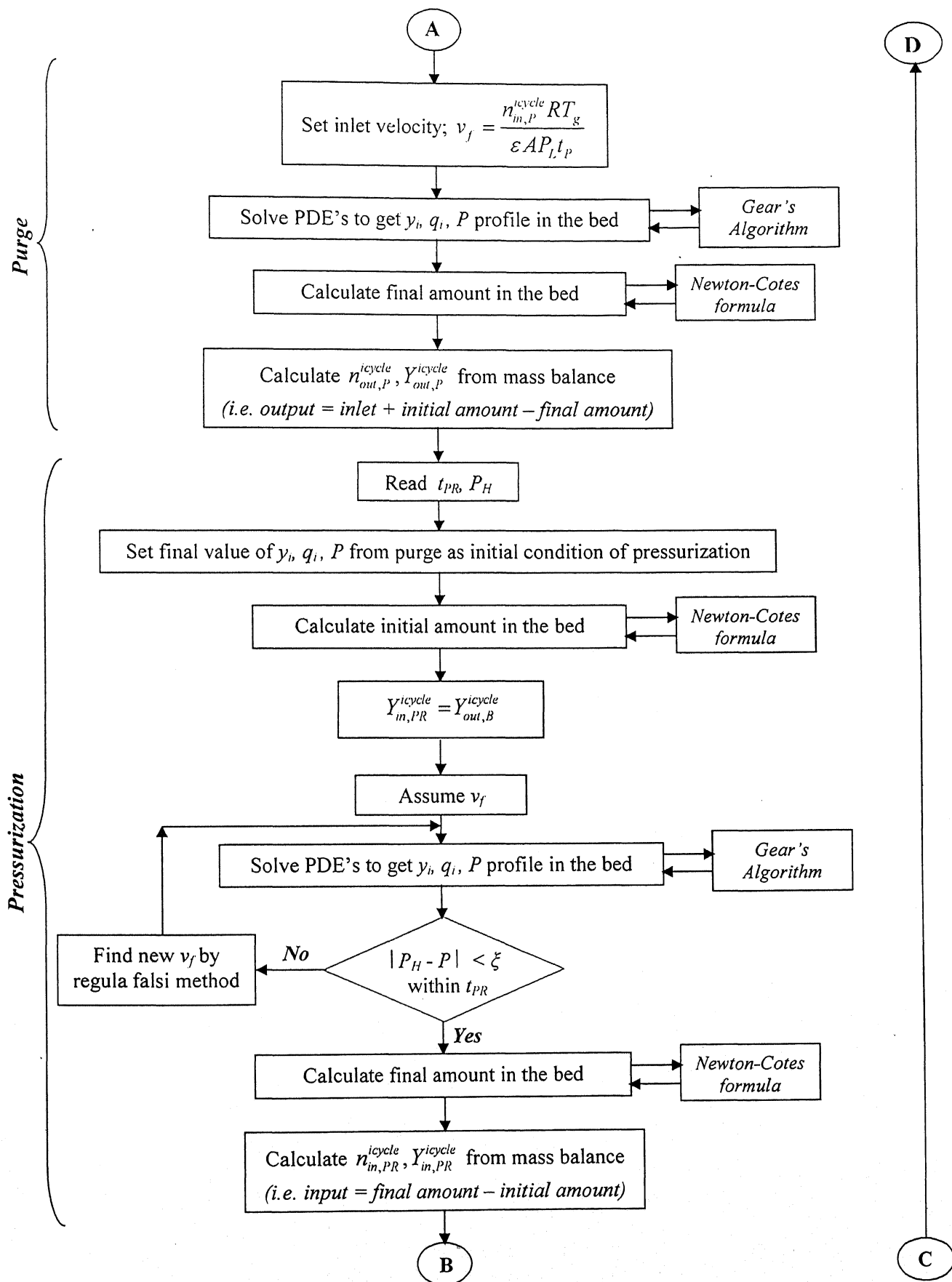
#### 4.4 Method of solution

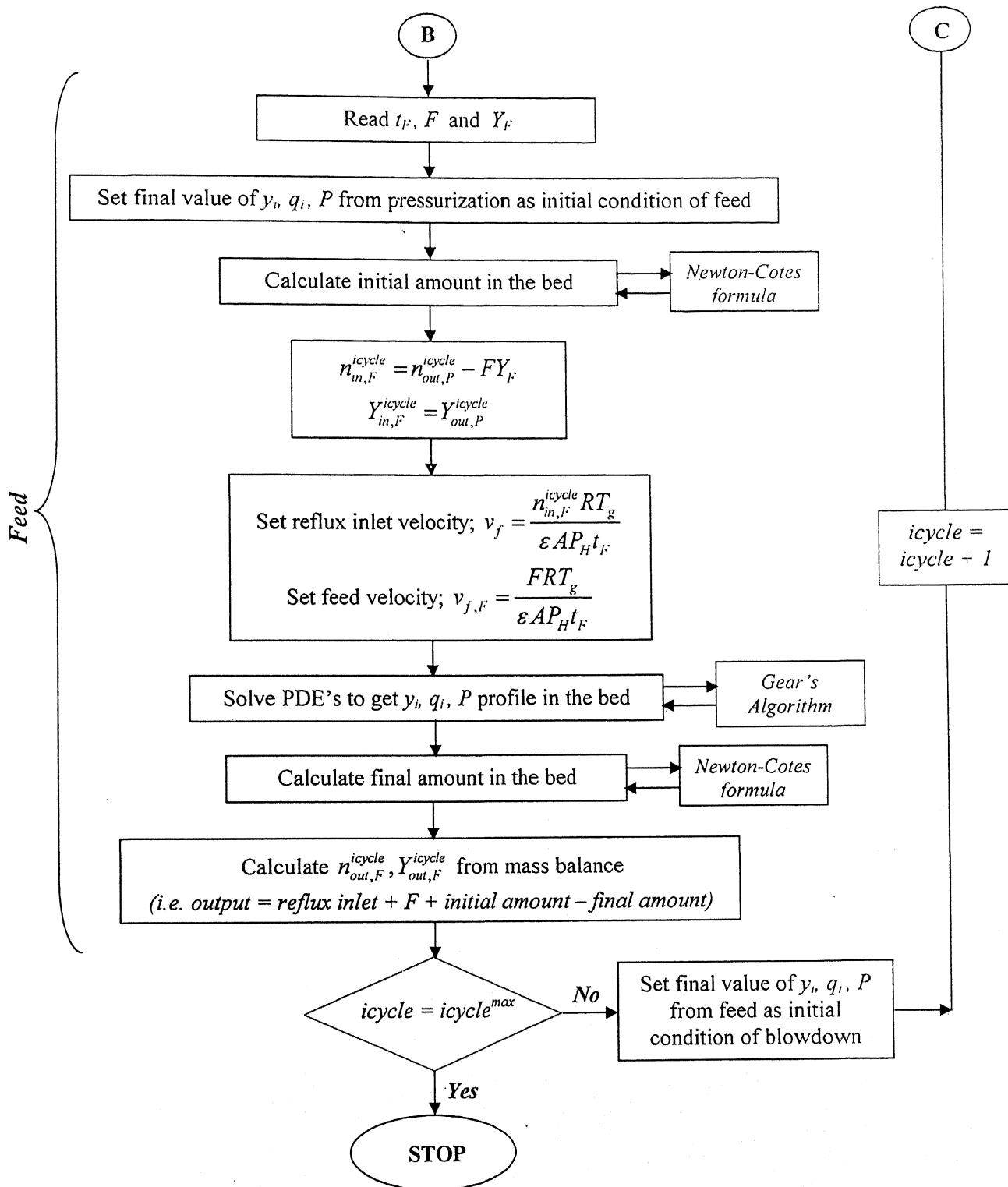
The governing partial differential equations [(4.19), (4.20) and (4.21)] for the duplex PSA and [(4.22), (4.23), (4.24), (4.25) and (4.26)] for the duplex TSA have been simultaneously solved along with their initial and boundary conditions. To solve them numerically, the PDE's were discretized in space domain using central difference scheme of the finite difference method (FDM). Thus the PDE's were converted into a set of ordinary differential equations. The discretized form of the PDE's for both the duplex PSA and the duplex TSA is given in Appendix-A. Since the equation is stiff in nature, it has been solved using an ODE solver, namely DDASPG subroutine in the IMSL library of FORTRAN-PowerStation which is based on the Gear's method.

The simulation code has been written in FORTRAN and executed on a Pentium-4 PC with 1GB RAM. CPU time was found to depend mainly upon the number of grids used in discretization of the PDE's. CPU time taken for one cycle with 53, 105, 157 and 205 grids are 5, 17, 38 and 77 s respectively. The cyclic steady state was reached between 150 to 200 cycles depending on the operating parameters.

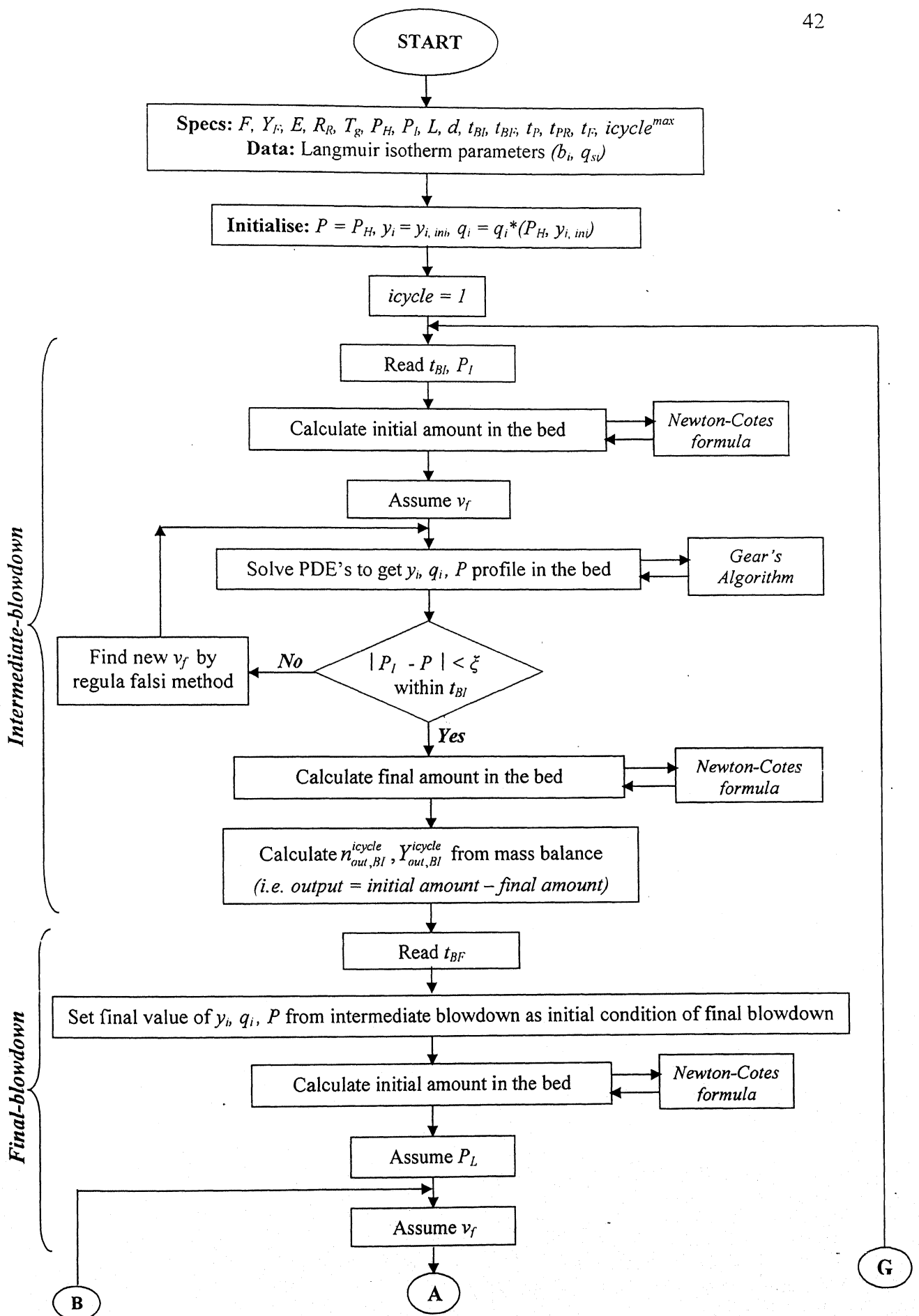
Flow charts for simulation of the Original duplex PSA and the MV-I duplex PSA and the MV-II duplex PSA cycle is given below in Figure (4.2) and (4.3).

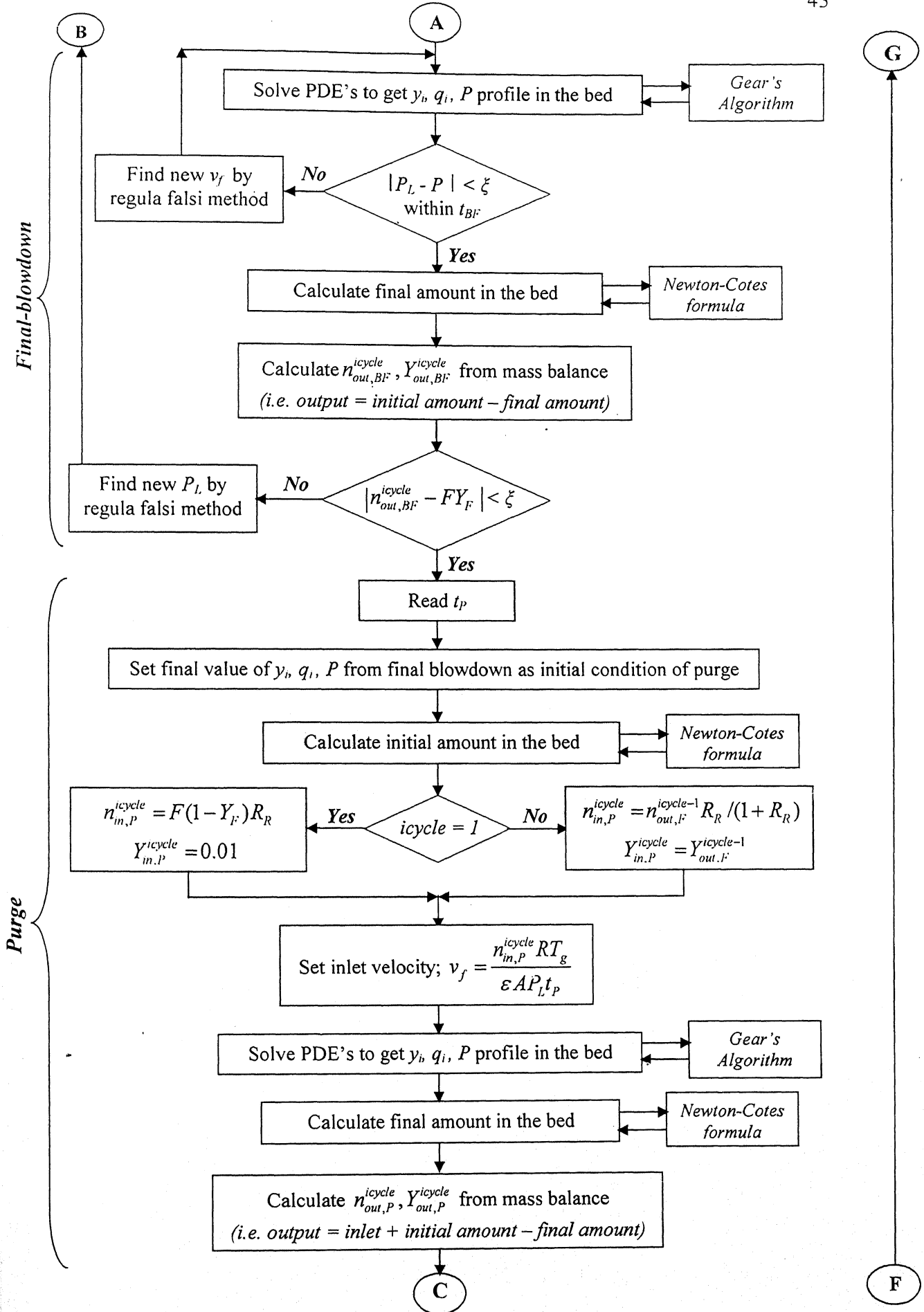


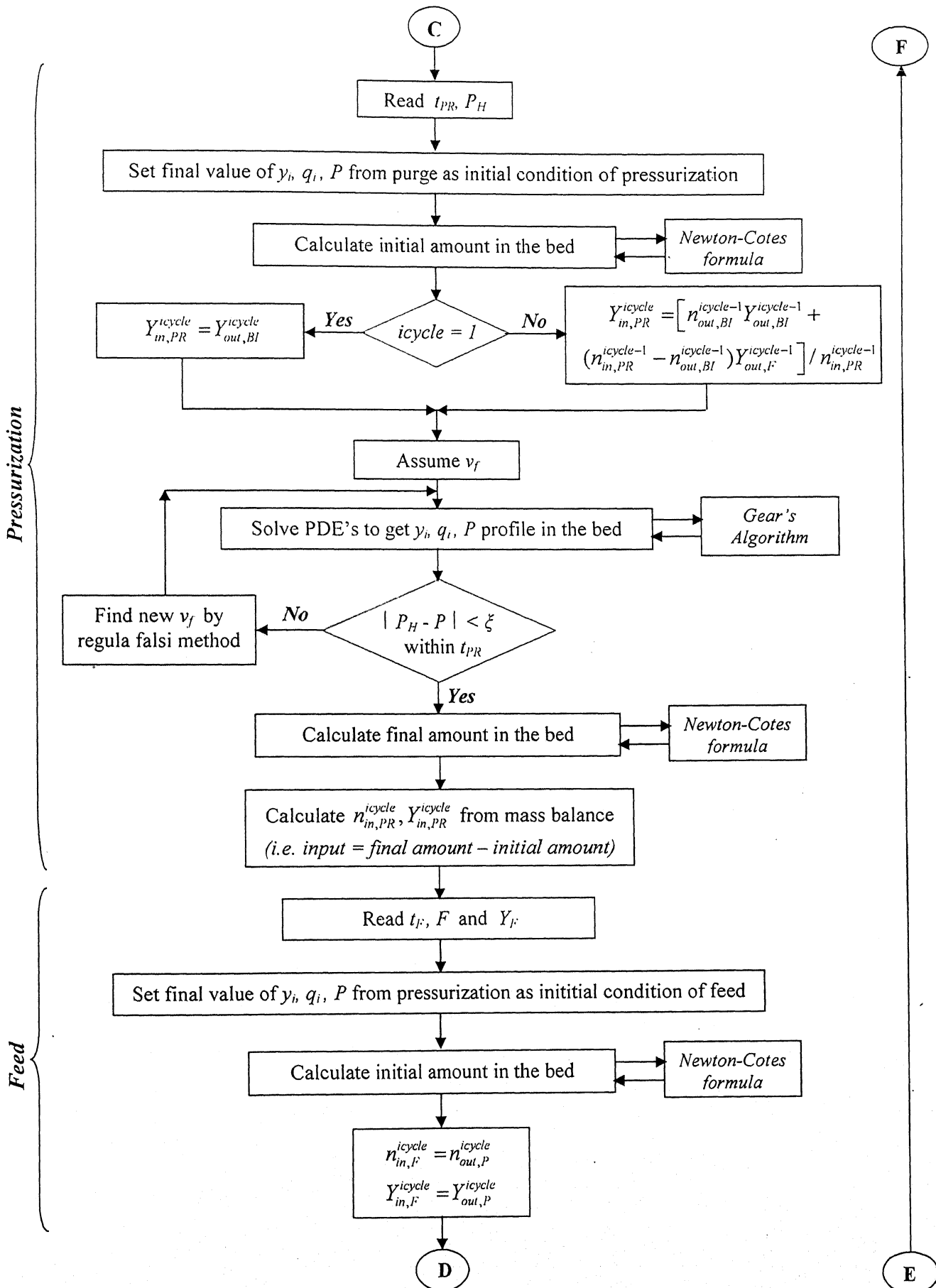


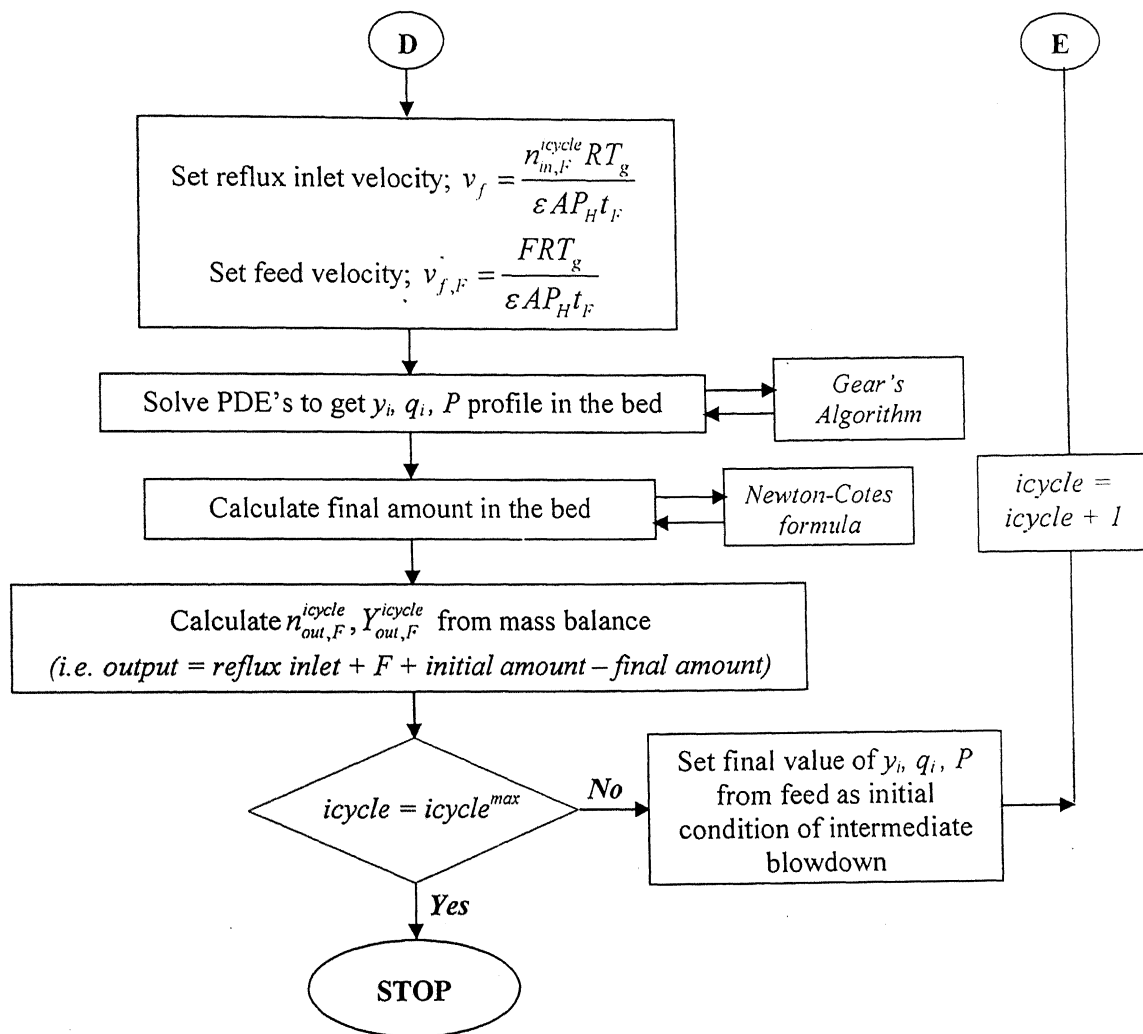












### Results and Discussion

This chapter presents the results of the simulation studies of the Original duplex PSA, the MV-I duplex PSA, the MV-II duplex PSA and the duplex TSA.

The following set of systems has been used to assess the comparative performance of the three duplex PSA cycle.

- Systems with one component as non-adsorbing.
  - Carbon dioxide and nitrogen over Zeolite 13X (nitrogen is non-adsorbing).
  - Methane and hydrogen over Activated carbon (hydrogen is non-adsorbing).
- System where both the components are adsorbing.
  - Nitrogen and oxygen over Zeolite 5A

The possibility of separation in the duplex TSA cycle has been presented based on the analogy with the duplex PSA.

The product purity, recovery, productivity and energy requirement has been used as measures to assess the process performance. These are defined as:

$$\text{Product purity (\%)} = \frac{\text{moles of desired component in product}}{\text{Total moles of product}} \times 100$$

$$\text{Recovery (\%)} = \frac{\text{moles of desired component in product}}{\text{moles of desired component in feed}} \times 100$$

$$\text{Productivity} = \frac{\text{moles of desired component in product}}{(\text{weight of adsorbent}) (\text{time})}$$

*Energy requirement has been calculated for:*

- *Compression of a flowing stream from the low pressure bed to the high pressure bed*
- *Pressurizing a bed from low to high pressure and*
- *Evacuating a bed from high to low pressure.*

## 5.1 Fractionation of carbon dioxide-nitrogen (CO<sub>2</sub>-N<sub>2</sub>) mixture

Carbon dioxide is one of the major green house gases causing global warming. The flue gases discharged by power plants and industries contribute to more than 70% of total CO<sub>2</sub> emitted into the atmosphere. Therefore it is important to capture CO<sub>2</sub> from flue gases to maintain eco-balance of the earth. Currently, absorption of CO<sub>2</sub> using various solvents is being practiced commercially. The energy required for the solvent regeneration is significantly high. Adsorptive and membrane separations are the potential alternatives to the existing absorption processes. We have assessed the performance of the duplex PSA for recovery of CO<sub>2</sub> from the flue gas. In the present work, we have taken flue gas as a binary mixture of CO<sub>2</sub> and N<sub>2</sub>. As N<sub>2</sub> adsorbed inside the bed is very small compared to that of the CO<sub>2</sub>, we have considered N<sub>2</sub> as non-adsorbing component. The parameters used in simulation are listed in Table 5.1.

Table 5.1 Parameters used in simulation of fractionation of carbon dioxide-nitrogen mixture

---

1. Molar feed composition	:	20% CO <sub>2</sub> , 80% N <sub>2</sub>
2. Feed position	:	middle of the bed
3. Adsorbent	:	Zeolite 13X
4. Particle diameter, <i>cm</i>	:	0.0707
5. Bed voidage	:	0.4
6. Bulk density, <i>kg/m<sup>3</sup></i>	:	590
7. Bed length, <i>cm</i>	:	100
8. Bed diameter, <i>cm</i>	:	2.5
9. Langmuir constant for CO <sub>2</sub> ( <i>b</i> ), <i>m<sup>3</sup>/mol</i>	:	0.4405
10. Saturation constant for CO <sub>2</sub> ( <i>q<sub>s</sub></i> ), <i>mol/m<sup>3</sup></i>	:	3411.0
11. LDF constant for CO <sub>2</sub> , <i>s<sup>-1</sup></i>	:	0.808
12. Operating temperature, <i>K</i>	:	298.15
13. Cycle time, <i>s</i> (Original and MV-I duplex)	:	50
Feed ( <i>t<sub>F</sub></i> ), <i>s</i>	:	20
Blowdown ( <i>t<sub>B</sub></i> ), <i>s</i>	:	5
Purge ( <i>t<sub>P</sub></i> ), <i>s</i>	:	20
Pressurization ( <i>t<sub>PR</sub></i> ), <i>s</i>	:	5

---

14. Cycle time, s (MV-II duplex)	:	54
Feed ( $t_F$ ), s	:	20
Intermediate-blowdown ( $t_{BI}$ ), s	:	5
Final-blowdown ( $t_{BF}$ ), s	:	2
Purge ( $t_P$ ), s	:	20
Pressurization ( $t_{PR}$ ), s	:	5
Frozen ( $t_{FR}$ ), s	:	2

---

The equilibrium data for carbon dioxide-nitrogen mixture over Zeolite 13X reported by Hirose et al. (1996) has been used. Figure 5.1 shows the adsorption isotherm of carbon dioxide on Zeolite 13X for different pressure at 298.15 K.

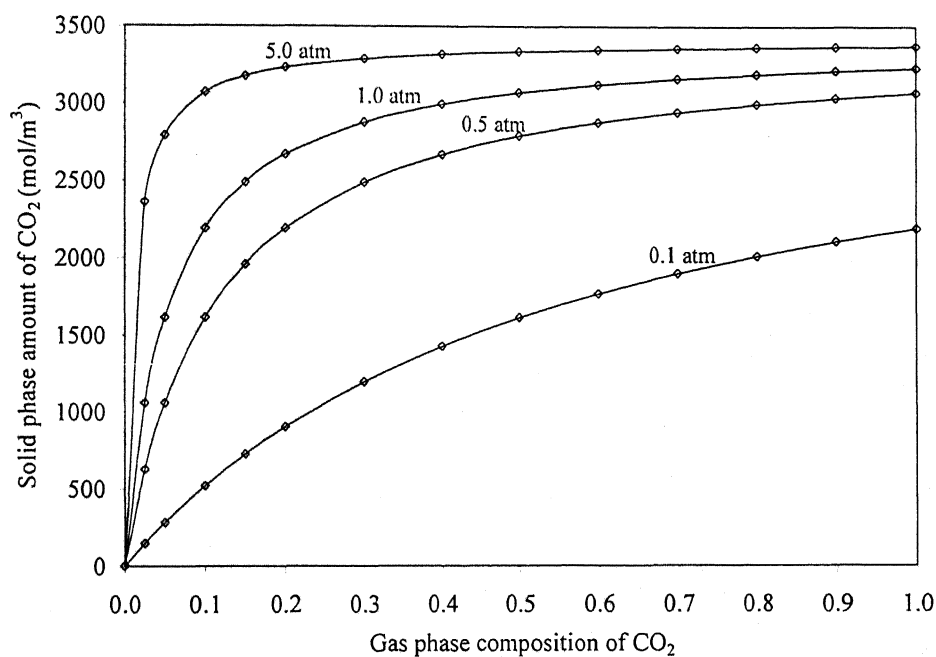


Fig.5.1 Adsorption isotherm of carbon dioxide on Zeolite 13X at 298.15 K

Simulation results of the Original duplex, MV-I duplex and MV-II duplex PSA is given below.

### 5.1.1 Original duplex PSA

In Original duplex PSA, the equalization and pressurization step can be operated in two modes. It could be done either from the CO<sub>2</sub> rich end (mode-I) or the N<sub>2</sub> rich end (mode-II). Figure 5.2 shows two different modes of equalization and pressurization.

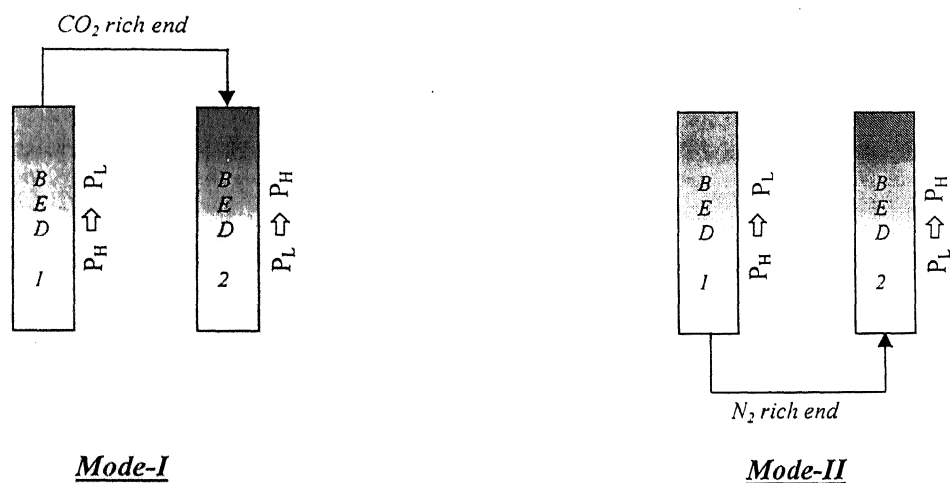


Fig.5.2 Two modes of equalization and pressurization

The performance of both the modes has been compared. Figure 5.3 and 5.4 shows the mass balance sheet for the mode-I and the mode-II respectively.

The product purity is about the same in both the modes. But, the energy requirement in the mode-I is about 1.5 times more than that in the mode-II. This is because of the amount of gas to be compressed or evacuated is more in the mode-I than that in the mode-II. The amount of extract recycle to be compressed is about same in both the modes but the amount coming out from the bed undergoing blowdown in mode-I is about 7 times more than the amount coming out in mode-II resulting in more energy requirement. In mode-II, most of the CO<sub>2</sub> gets locked inside and only a small amount of CO<sub>2</sub> comes out from the bed. We call it as 'locking in blowdown' and is explained below.

**Locking in blowdown:** The amount adsorbed inside the bed is governed by its partial pressure in the gas phase. To understand the locking of CO<sub>2</sub>, we have examined and



compared the partial pressure and solid phase profile of  $\text{CO}_2$  in the bed undergoing blowdown for both the modes of equalization and pressurization.

Figure 5.5 (a) shows the partial pressure and solid phase concentration profile of  $\text{CO}_2$  in the bed undergoing blowdown step from  $\text{CO}_2$  rich end (mode-I). The initial and final partial pressure profile of  $\text{CO}_2$  in the first half of the bed is almost same and there is significant change only in the second half. The same trend can be seen for the solid phase profile. The change in solid phase profile in second half of the bed is significant so a large amount of  $\text{CO}_2$  comes out from the bed.

Whereas, on evacuating the bed from the  $\text{N}_2$  rich end, a small amount of  $\text{CO}_2$  comes out because of the locking effect. Figure 5.5 (b) shows the partial pressure and solid phase concentration profile of  $\text{CO}_2$  in the bed undergoing blowdown from  $\text{N}_2$  rich end (mode-II). It is clear from the solid phase concentration profile that the  $\text{CO}_2$  gets desorbed and then again adsorbed in the first half of the bed according to the partial pressure profile while, in the second half of the bed, there is no significant change in the profiles. The overall effect is that, a small amount of  $\text{CO}_2$  comes out from the bed or most of the  $\text{CO}_2$  gets locked inside the bed.

Bed length (cm) = 100  
 Bed diameter(cm) = 2.5  
 Feed (mmol/half cycle) = 100  
 Half cycle time (s) = 20 + 5  
 $P_H$  (atm) = 1.0  
 $P_L$  (atm) = 0.3  
 $T$  (K) = 298.15  
 $R_E$  = 2.17

System : CO<sub>2</sub>-N<sub>2</sub>  
 Adsorbent : Zeolite 13X

	CO <sub>2</sub>	N <sub>2</sub>
Purity (%)	78.69	94.84
Recovery (%)	78.7	94.8
Productivity (mol/kg-h)	3.9	18.9
Energy requirement (kJ/mol of feed)	3.7	

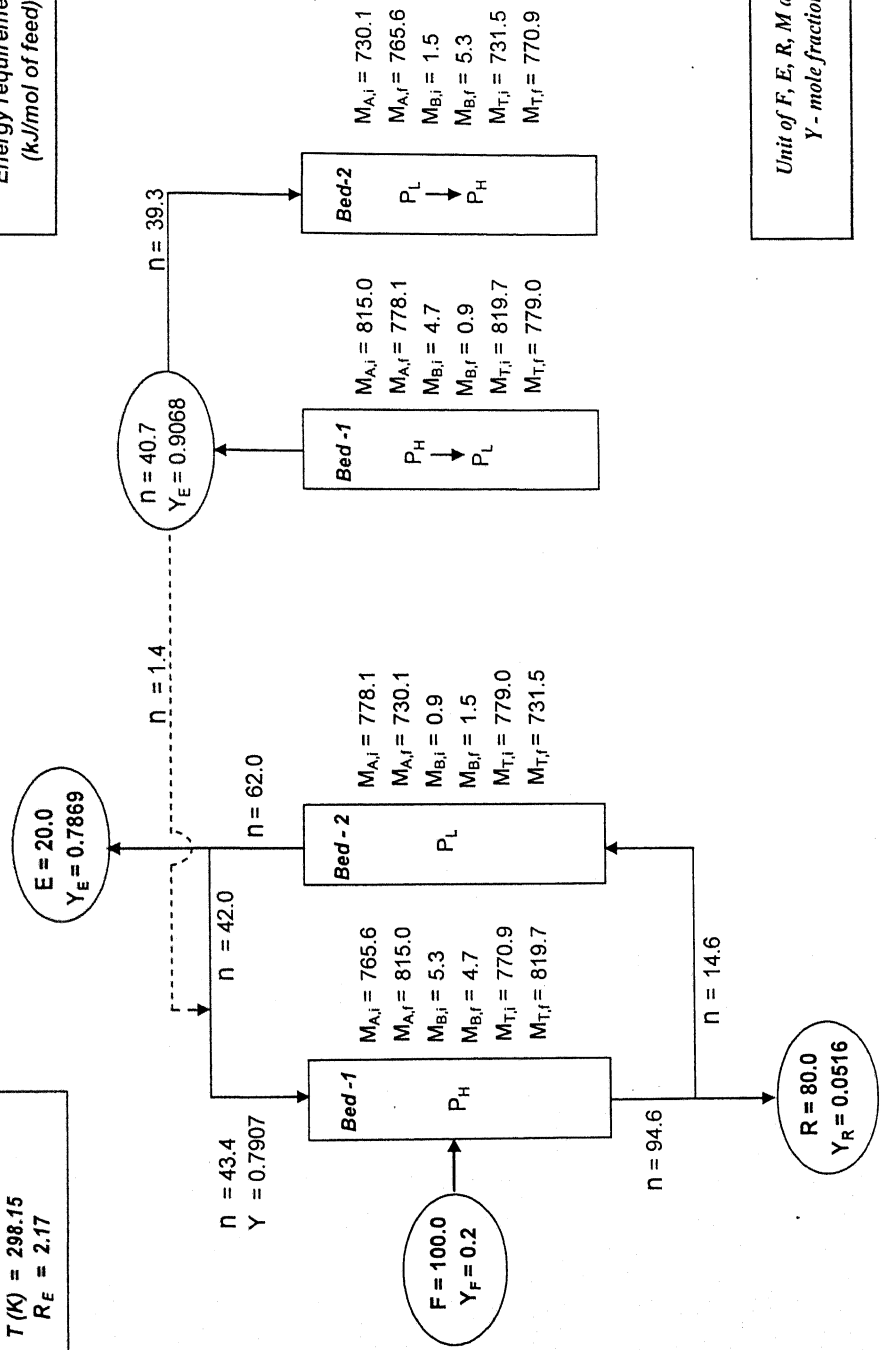


Fig.5.3 Mass balance sheet of Original duplex PSA with equalization and pressurization from CO<sub>2</sub> rich end (mode-I)

	CO <sub>2</sub>	N <sub>2</sub>
Purity (%)	77.03	94.16
Recovery (%)	77.0	94.2
Productivity (mol/kg-h)	3.8	18.8
Energy requirement (kJ/mol of feed)	2.4	

System : CO<sub>2</sub> - N<sub>2</sub>  
Adsorbent : Zeolite 13X

Bed length (cm) = 100  
Bed diameter (cm) = 2.5  
Feed (mmol/half cycle) = 100  
Half cycle time (s) = 20 + 5  
 $P_H$  (atm) = 1.0  
 $P_L$  (atm) = 0.3  
 $T$  (K) = 298.15  
 $R_R$  = 0.2

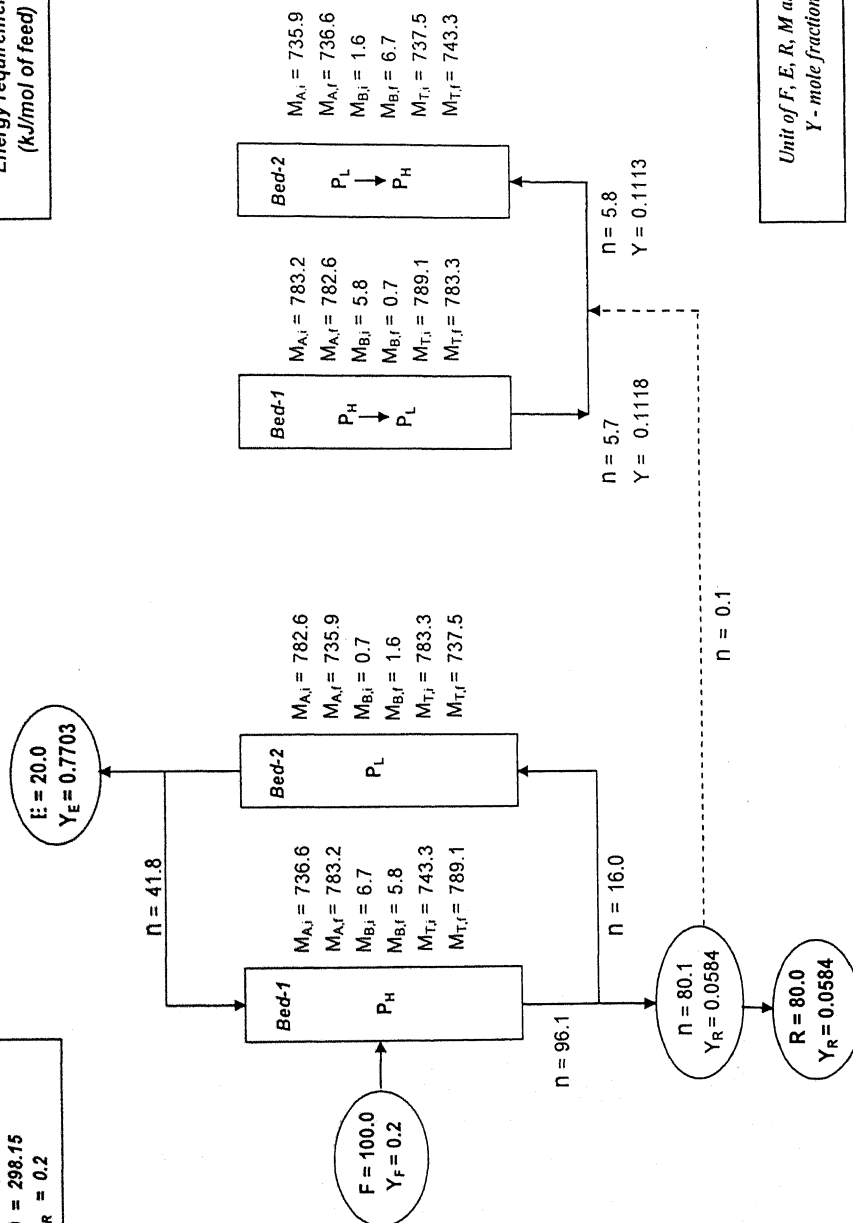


Fig.5.4 Mass balance sheet of Original duplex PSA with equalization and pressurization from N<sub>2</sub> rich end (mode-II)

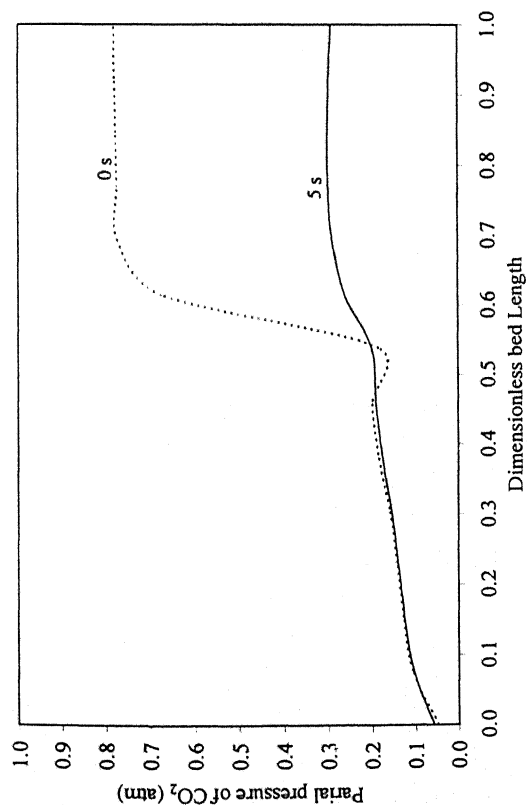


Fig.5.5 (a) Partial pressure and solid phase concentration profile of  $\text{CO}_2$  in the bed undergoing blowdown step from  $\text{CO}_2$  rich end

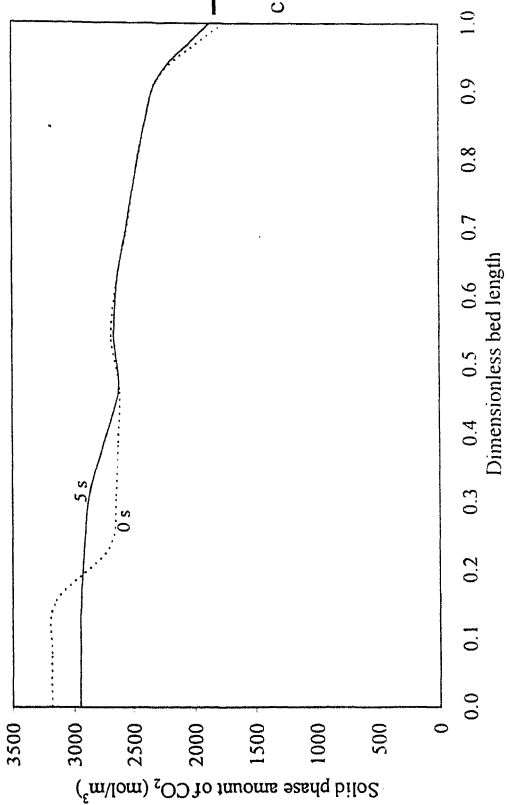
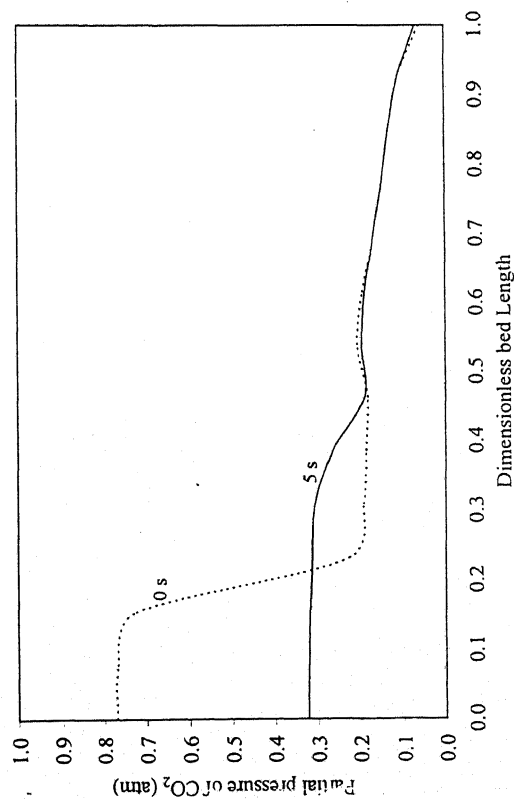
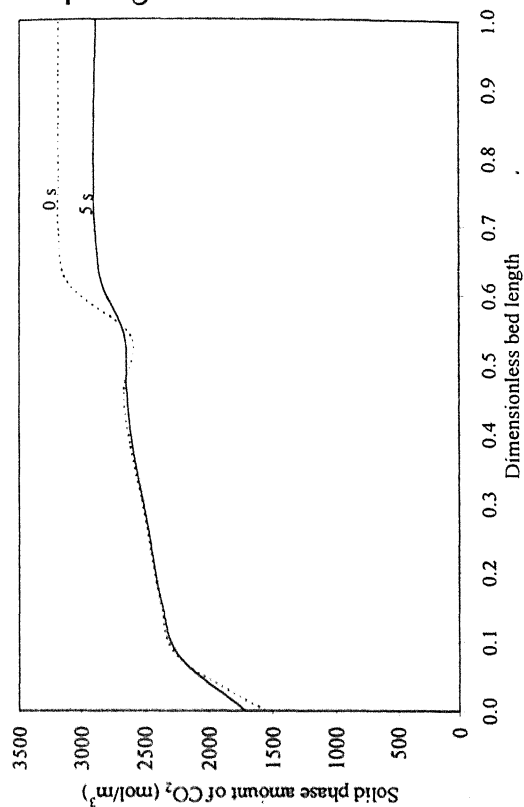


Fig.5.5 (b) Partial pressure and solid phase concentration profile of  $\text{CO}_2$  in the bed undergoing blowdown step from  $\text{N}_2$  rich

It can be seen that, the product purity is about the same for both the modes but energy requirement is less in the mode-II. Hence, operating duplex PSA in mode-II is more effective than mode-I from energy consideration. So now onwards, we have considered the equalization and pressurization of the beds to be done from the  $N_2$  rich end.

Figures 5.6 (a, b, c, d, e, f, g, h) show the change in the gas and the solid phase concentration with time in the bed undergoing feed, blowdown, purge and pressurization (equalization and pressurization from  $N_2$  rich end) for the mass balance sheet given in Figure 5.4. In all the profiles, dimensionless bed length, '0' represents the end of the bed where the stream is entering. The direction of incoming and outgoing streams from the beds has been represented by arrow ( $\rightarrow$ ) sign.

**Feed:** Figures 5.6 (a) and 5.6 (b) show the gas and the solid phase concentration profiles of the feed step. There are two inlet streams. The extract recycle, rich in  $\text{CO}_2$  is fed to the top end and the feed is introduced in the middle of the bed. The  $\text{CO}_2$  gets adsorbed and the raffinate product, rich in  $\text{N}_2$  is drawn from the bottom. At the feed position, sudden change in the bed profiles can be observed as feed mixes with a stream of different composition. The  $\text{CO}_2$  present in the extract recycle gets adsorbed only in the initial portion of the bed and the latter portion up to the feed position seems to be unused. The bed profiles can be stretched by increasing the amount of the recycle but then product purity will go down.

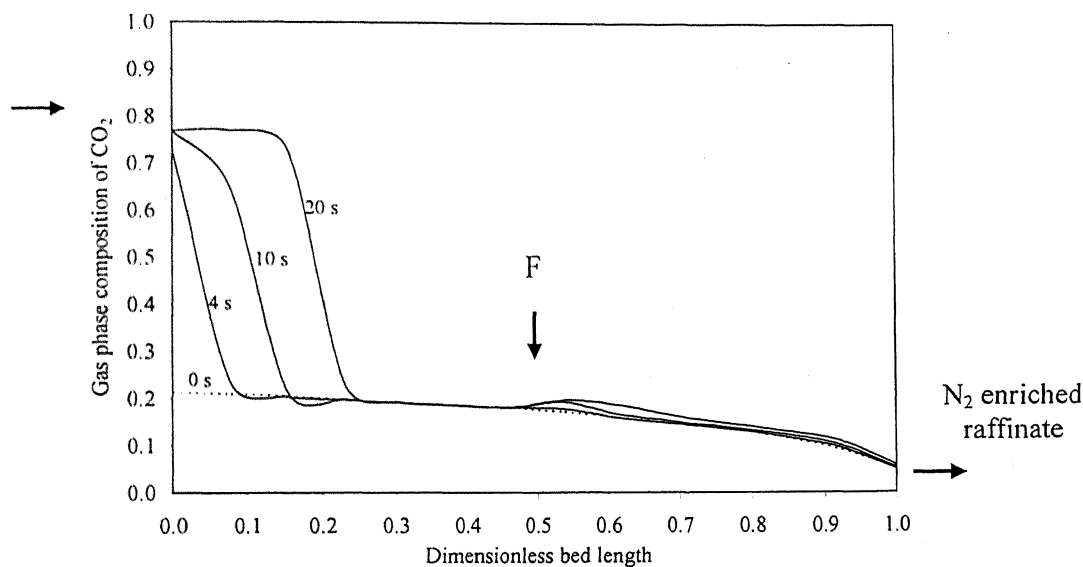


Fig.5.6 (a) Gas phase concentration profile in the bed undergoing feed step (Original duplex)

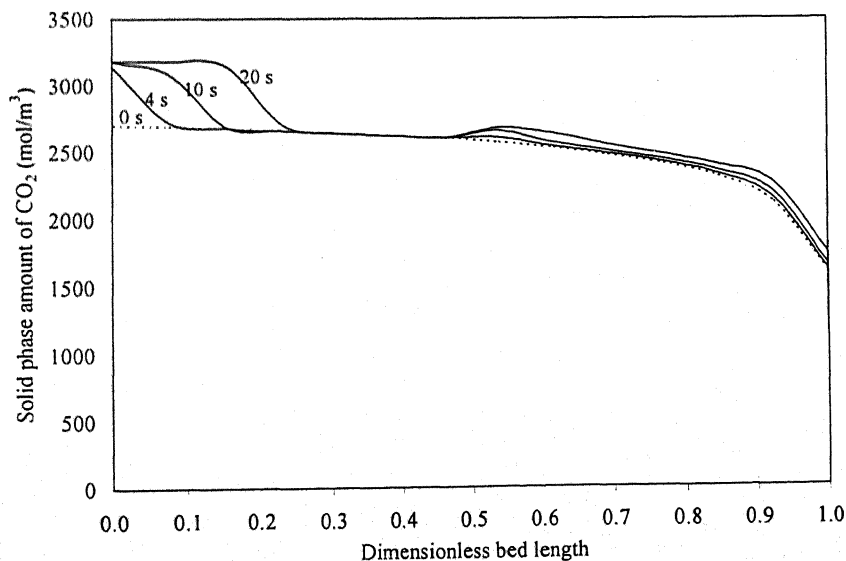


Fig. 5.6 (b) Solid phase concentration profile in the bed undergoing feed step (Original duplex)

**Blowdown:** Figures 5.6 (c) and 5.6 (d) show the gas and the solid phase concentration profiles of the blowdown step. As the pressure reduces from  $P_H$  (1 atm) to  $P_L$  (0.3 atm),  $\text{CO}_2$  gets desorbed from the solid and the gas composition of  $\text{CO}_2$  increases. It can be seen that in the first half of the bed,  $\text{CO}_2$  gets locked inside and most of the  $\text{CO}_2$  comes out from the other half of the bed. The overall effect is that a very small amount of  $\text{CO}_2$  (0.64 mmol) comes out from the bed and the outgoing stream is enriched with  $\text{N}_2$ .

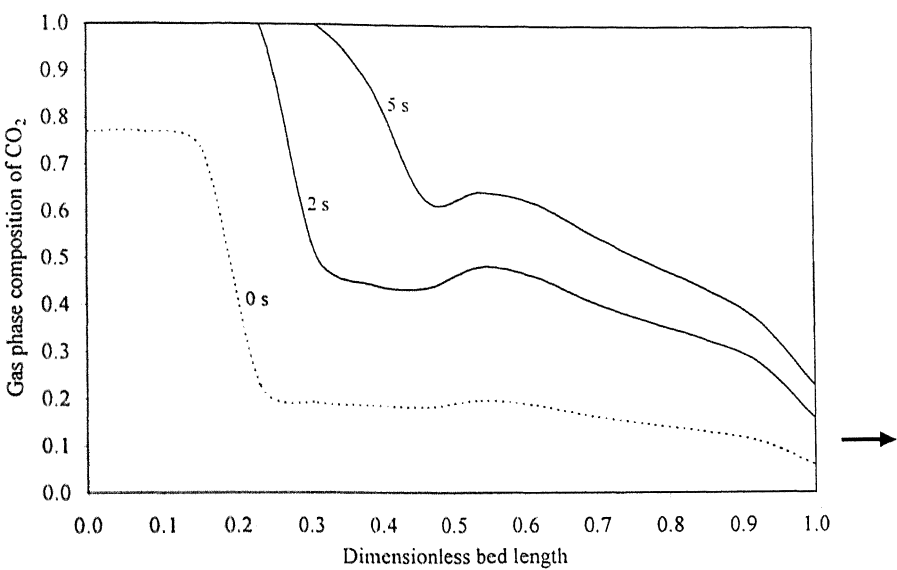


Fig.5.6 (c) Gas phase concentration profile in the bed undergoing blowdown step (Original duplex)

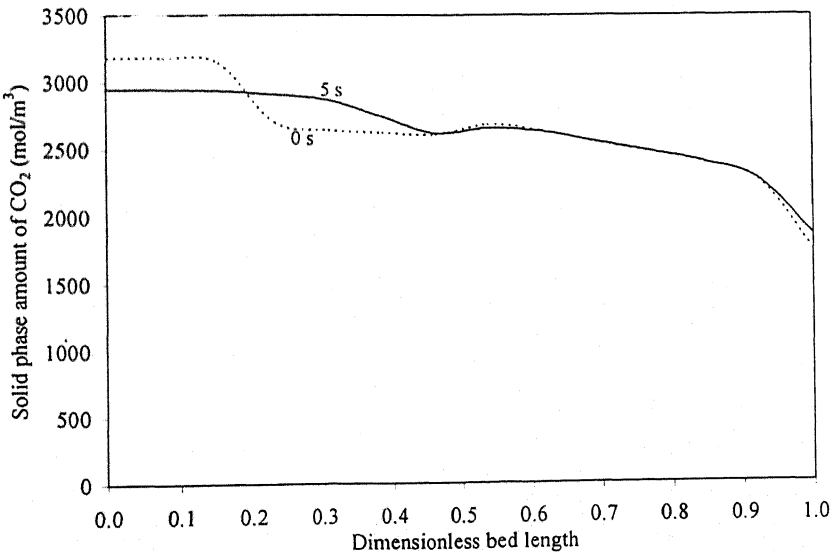


Fig. 5.6 (d) Gas phase concentration profile in the bed undergoing blowdown step (Original duplex)

**Purge:** Figures 5.6 (e) and 5.6 (f) show the gas and the solid phase concentration profiles of the purge step. As the raffinate recycle stream rich in  $N_2$  enters the bed, the gas phase composition of  $CO_2$  decreases. This results in the decrease in the partial pressure of  $CO_2$  as total pressure is constant (0.3 atm). So, the  $CO_2$  gets desorbed and purged off from the bed. A part of the outgoing stream, rich in  $CO_2$  is collected as extract product.

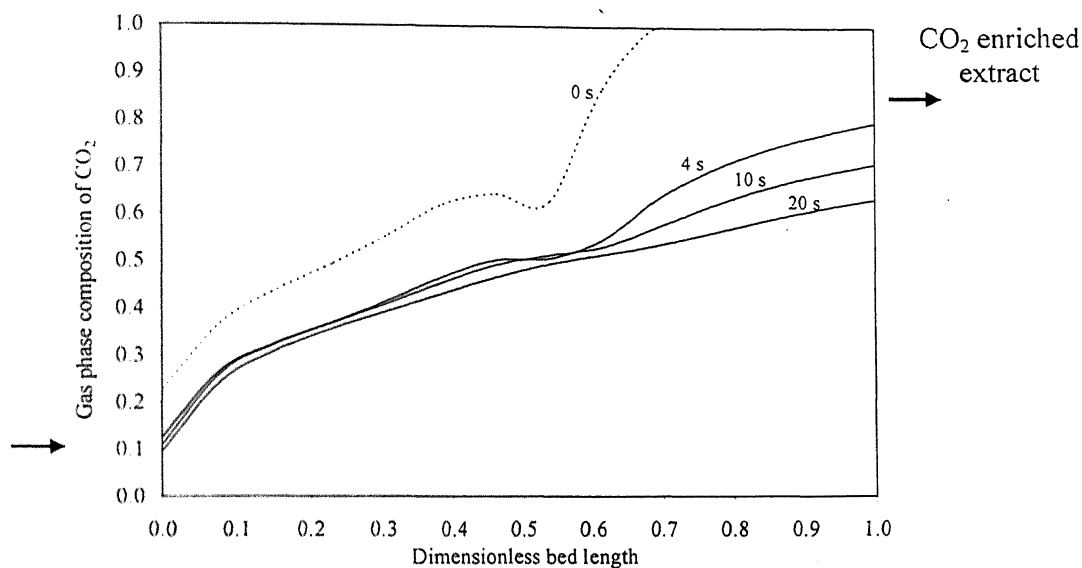


Fig.5.6 (e) Gas phase concentration profile in the bed undergoing purge step (Original duplex)

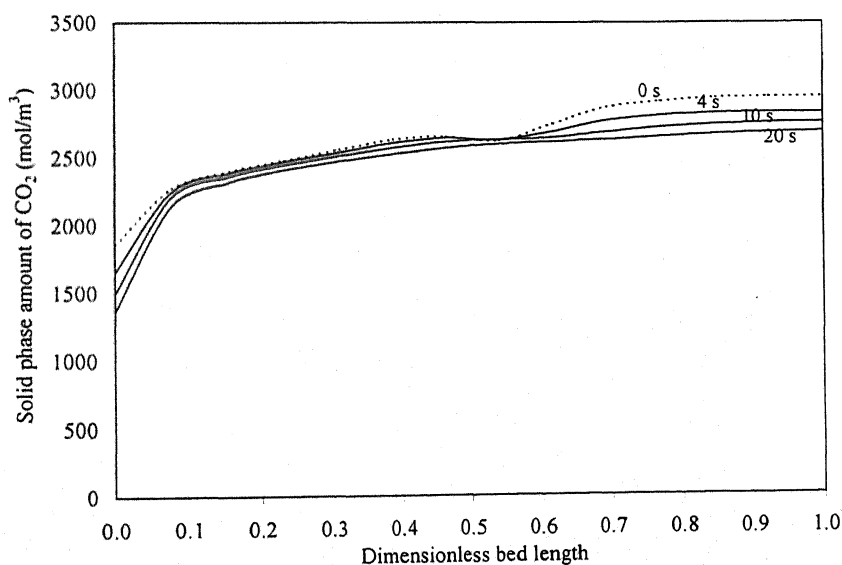


Fig.5.6 (f) Solid phase concentration profile in the bed undergoing purge step (Original duplex)



**Pressurization:** Figures 5.6 (g) and 5.6 (h) show the gas and the solid phase concentration profiles of the pressurization step. The bed is pressurized from  $P_L$  (0.3 atm) to  $P_H$  (1 atm) with the gas coming out (5.7 mmol) from the bed undergoing blowdown. But, the amount of gas required to pressurize the bed is 5.8 mmol. The extra amount (0.1 mmol) is taken from the outgoing stream of the bed undergoing feed step. It can be seen from the bed profiles that the composition of  $\text{CO}_2$  in the gas phase decreases but the change in the solid phase amount is marginal and only in the initial portion of the bed. This is because the inlet stream is rich in  $\text{N}_2$  and most of the  $\text{CO}_2$  present gets adsorbed on just entering the bed.

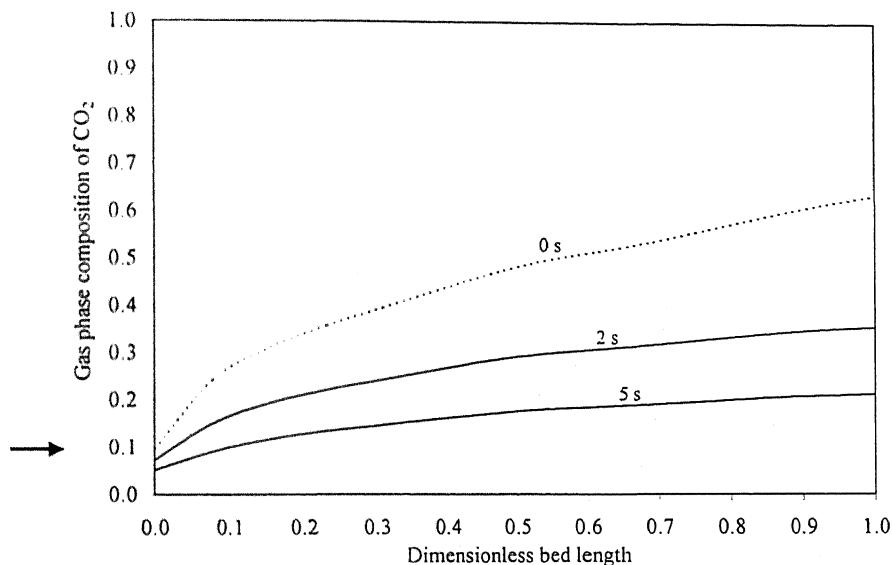


Fig.5.6 (g) Gas phase concentration profile in the bed undergoing pressurization step (Original duplex)

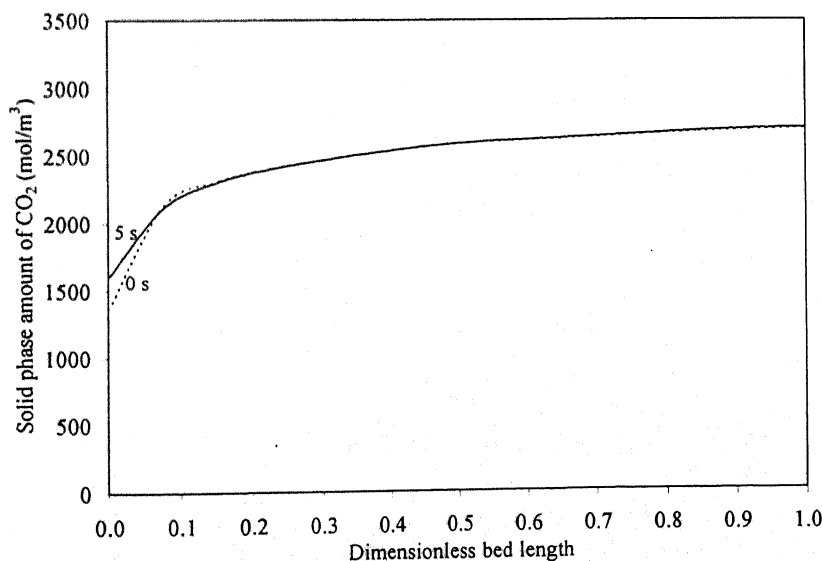


Fig.5.6 (h) Solid phase concentration profile in the bed undergoing pressurization step (Original duplex)

### 5.1.2 Parametric study of Original duplex PSA

The effect of feed, raffinate recycle ratio and desorption pressure on the performance of Original duplex PSA has been presented below.

#### *Effect of raffinate recycle ratio, $R_R$*

Figure 5.7 shows the effect of raffinate recycle ratio on the product purity and energy requirement at two different values of feed rate. At a low value of  $R_R$  (0.1), product purity is small. This is because the amount of gas recycled is not sufficient enough to purge off the  $\text{CO}_2$  from the bed undergoing purge. On further increasing the amount of gas recycled, product purity gets improved and reached an optimum at  $R_R$  value of 0.2. Further increase in  $R_R$  resulted in the decrease of product purity. The continuous decrease in purity is because of the non adsorbing nature of the  $\text{N}_2$ . The bed (purge) in which the raffinate recycle enters is at low pressure 0.3 atm and at this pressure the void space inside the bed can hold only 2.6 mmol of the gas. So, most of the  $\text{N}_2$  present in the recycle stream will come out from the bed resulting in poor performance of the Original duplex. It can be seen from Figure 5.7 that even at two different values of feed, the optimum purity is reached at  $R_R$  value of 0.2.

On increasing the amount of raffinate recycle, the amount of gas circulating between the beds increases so the energy required to compress the extract recycle stream coming out from the low pressure bed also increases.

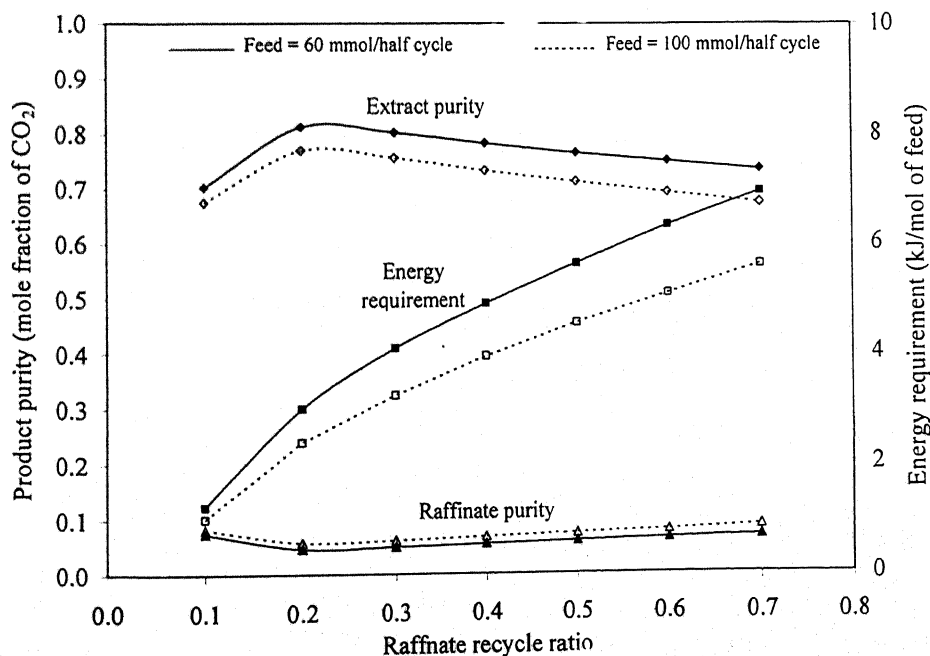


Fig.5.7 Effect of raffinate recycle ratio;  $P_H=1\text{atm}$ ,  $P_L=0.3\text{atm}$

### Effect of feed, $F$

Figure 5.8 shows the effect of feed on the product purity and the energy requirement. As the amount of feed increases, the amount of raffinate recycle stream (rich in  $N_2$ ) increases for a fixed value of raffinate recycle ratio. As explained above, most of the  $N_2$  present in recycle stream will come out from the bed affecting the extract purity.

As feed increases, the energy requirement per unit mole of feed decreases. This is because of the decrease in relative amount of the extract recycle (i.e.  $R_E/F$ ) to be compressed from  $P_L$  (0.3 atm) to  $P_H$  (1 atm).

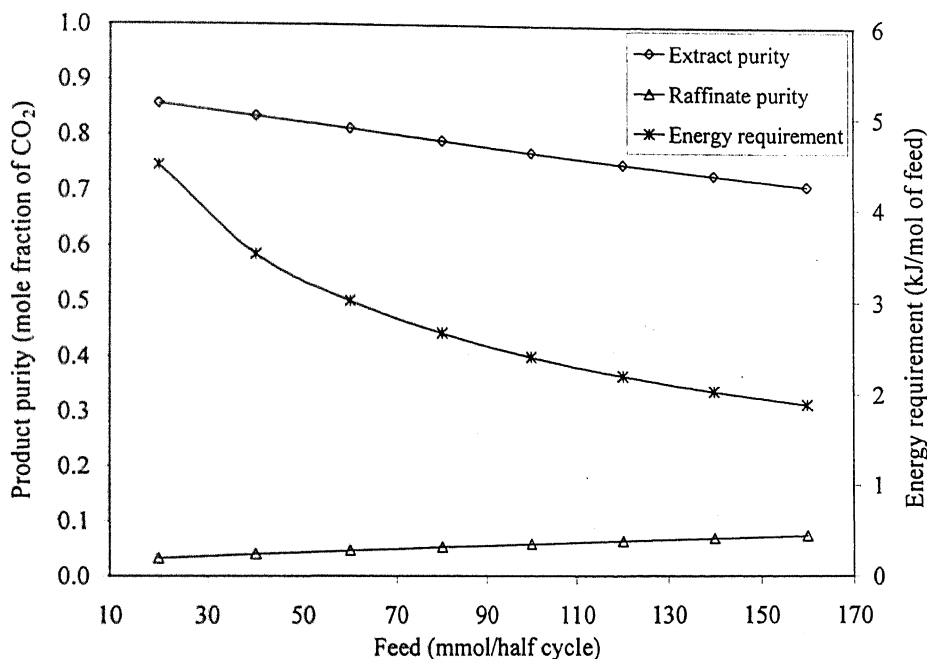


Fig.5.8 Effect of feed;  $P_H=1$  atm,  $P_L=0.3$  atm,  $R_R=0.2$

### Effect of desorption pressure, $P_L$

Figure 5.9 shows the effect of desorption pressure on the product purity and the energy requirement. At large value of desorption pressure (0.9 atm), purity of both the end products is poor. This is because at this pressure,  $CO_2$  is strongly adsorbed inside the bed and the raffinate recycle is not able to properly purge off the adsorbed  $CO_2$ . Product purity increases on decreasing the desorption pressure and reaches an optimum value at about  $P_L$  value of 0.3 atm. On further decreasing the desorption pressure, concentration front of  $CO_2$  in the bed undergoing blowdown breaks through and more amount of  $CO_2$

starts coming out. As this stream is used for pressurization, the  $\text{CO}_2$  present gets adsorbed around the end of the bed from where  $\text{N}_2$  rich raffinate product will be drawn in the next step. Because of this, a slight drop in the product purity can be observed.

As  $P_L$  decreases, the energy requirement increases because of increase in the pressure ratio ( $P_H/P_L$ ).

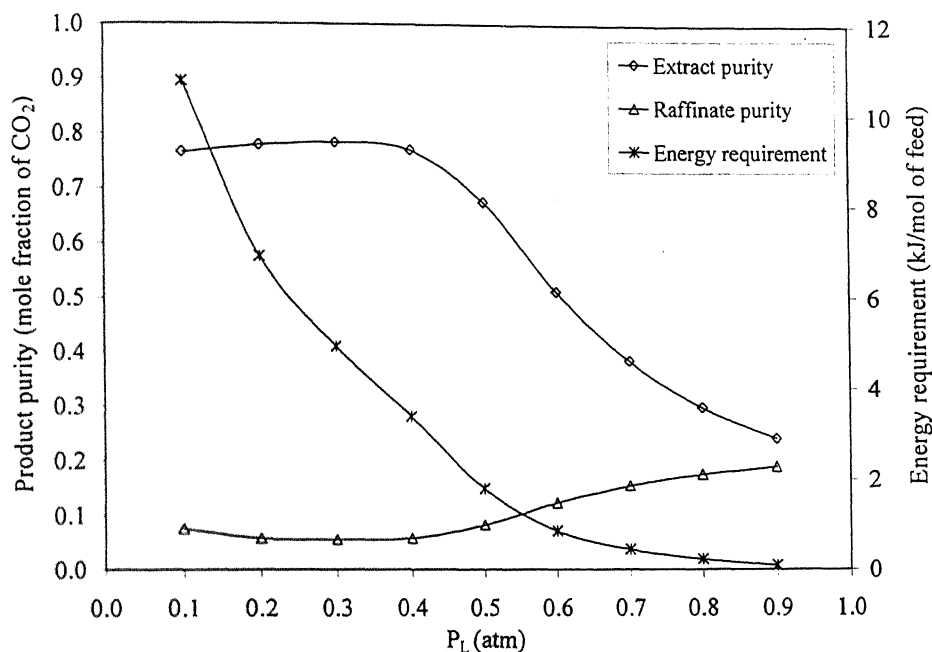


Fig.5.9 Effect of desorption pressure;  $F=60\text{mmol/half cycle}$ ,  $P_H=1\text{ atm}$ ,  $R_R=0.4$

From the above parametric study it can be concluded that the product purity in Original duplex is limited by the raffinate recycle gas (rich in non adsorbing  $\text{N}_2$ ). To overcome the recycle limitation, we modified the time of extract withdrawal in Original duplex. The basis of the modification is explained below.

### 5.1.3 MV-I duplex PSA

In Original duplex, a part of the outgoing stream from the bed undergoing purge is collected as extract product (rich in  $\text{CO}_2$ ) continuously throughout the step time (20 s). Figure 5.10 shows the variation in the mole fraction of  $\text{CO}_2$  and corresponding

cumulative amount drawn with time in outgoing stream from the bed undergoing purge. It can be seen that the initial amount coming out is pure CO<sub>2</sub> and then, the CO<sub>2</sub> composition starts decreasing and drops to 70% after 20 s. This is because of the N<sub>2</sub> present in the gas (raffinate recycle) entering the bed starts coming out continuously with time.

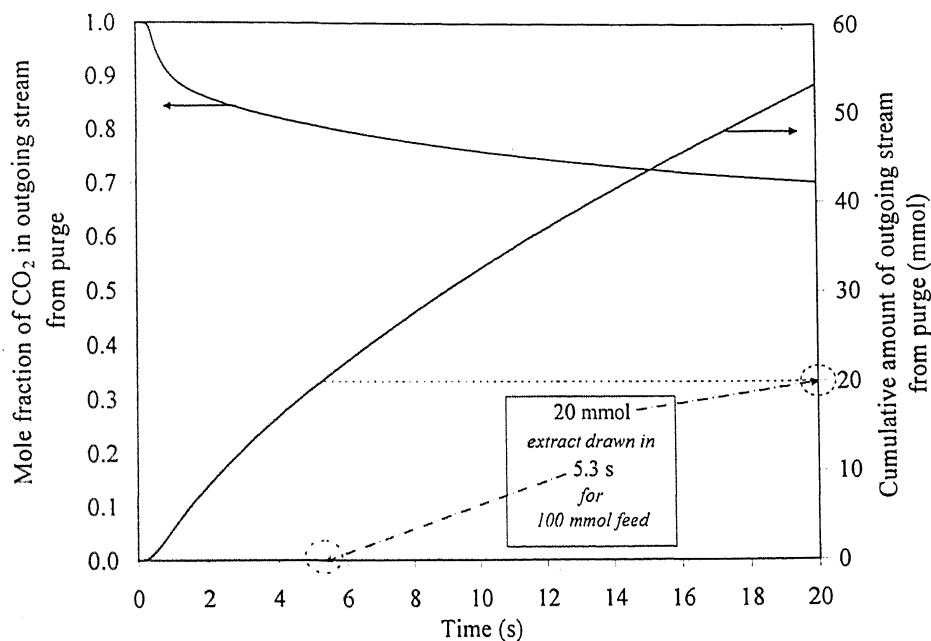


Fig.5.10 Variation in mole fraction of CO<sub>2</sub> and cumulative amount with time in outgoing stream from purge;  $F=100\text{mmol/half cycle}$ ,  $P_H=1\text{atm}$ ,  $P_L=0.3\text{atm}$ ,  $R_R=0.2$

So there is a scope to improve the product purity by modifying the time of extract withdrawal. The first part of the outgoing stream from the bed undergoing purge is collected as extract product and the remaining amount is recycled as extract recycle to the top of the bed undergoing feed step. By doing so, the purity of both the end products gets enhanced over the purities obtained with the Original duplex PSA.

Figure 5.11 shows the mass balance sheet of the MV-I duplex with operating parameters same as that of the Original duplex (Figure 5.4).

	CO <sub>2</sub>	N <sub>2</sub>
Purity (%)	80.61	95.07
Recovery (%)	80.6	95.1
Productivity (mol/kg-h)	4.0	18.9
Energy requirement (kJ/mol of feed)	2.2	

System : CO<sub>2</sub> - N<sub>2</sub>  
Adsorbent : Zeolite 13X

Bed length (cm) = 100  
Bed diameter (cm) = 2.5  
Feed (mmol/half cycle) = 100  
Half cycle time (s) = 20 + 5  
P<sub>H</sub> (atm) = 1.0  
P<sub>L</sub> (atm) = 0.3  
T (K) = 298.15  
R<sub>R</sub> = 0.2

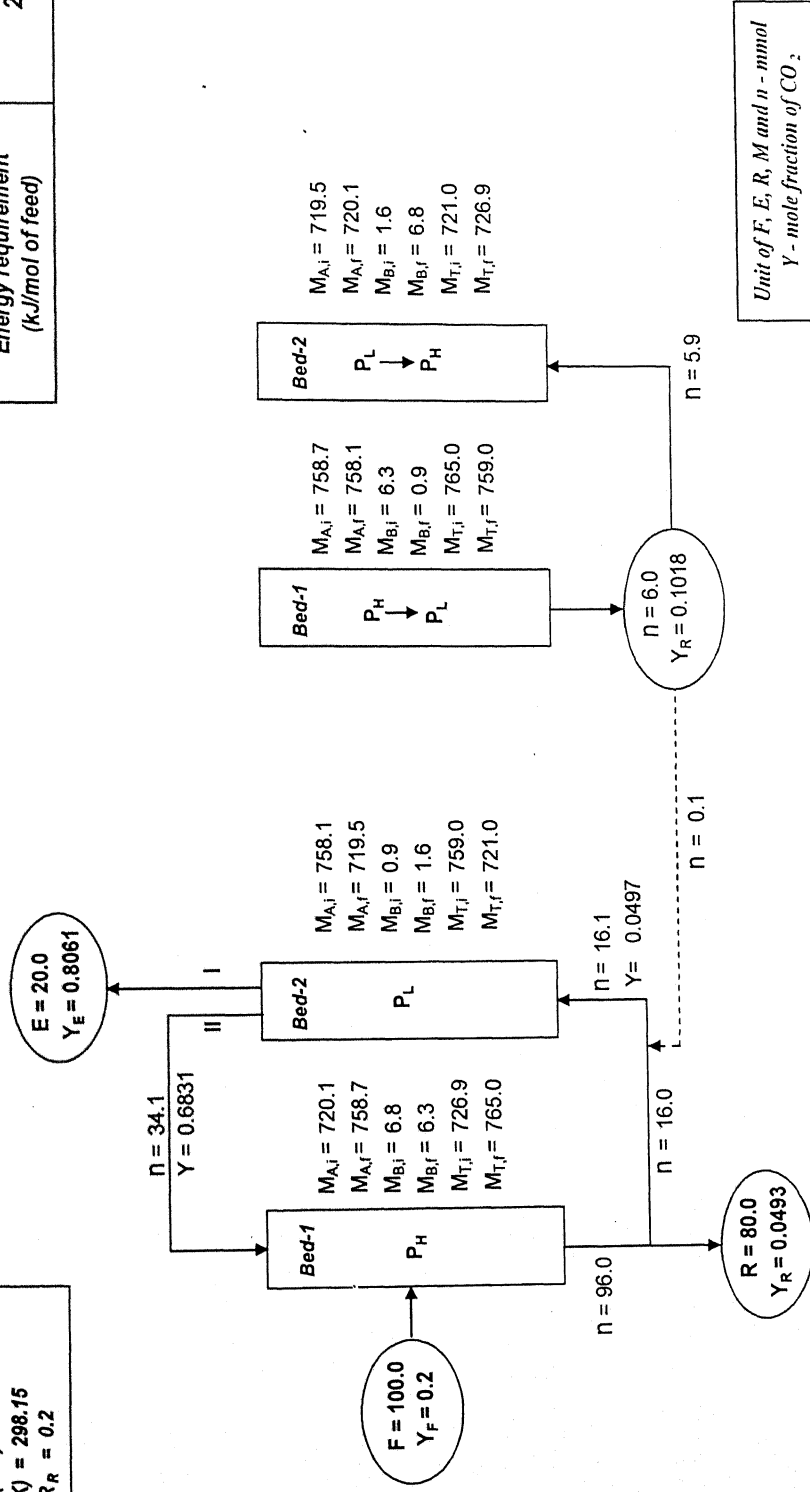


Fig.5.11 Mass balance sheet of MV-I duplex PSA

It can be seen that composition of  $\text{CO}_2$  in the rich gas (extract) improved from 77% to 81% and that of  $\text{N}_2$  in lean gas (raffinate) from 94% to 95%.

However, the trend in the gas and the solid phase concentration profile in the bed is the same as that of the Original duplex.

The comparative performance of the MV-I duplex and the Original duplex PSA is given below.

#### 5.1.4 Comparison of MV-I duplex and Original duplex PSA

Figure 5.12, 5.13 and 5.14 shows the comparative performance of the MV-I duplex and the Original duplex PSA with change in raffinate recycle ratio, feed and desorption pressure respectively. It can be seen that in all cases, performance of MV-I duplex improved over Original duplex.

Figure 5.12 and 5.14 shows that at low value of raffinate recycle ratio (0.1) or large value of desorption pressure ( $>0.5$ ) there is no improvement in product purity because  $\text{CO}_2$  is not properly purged off.

##### *Effect of raffinate recycle ratio*

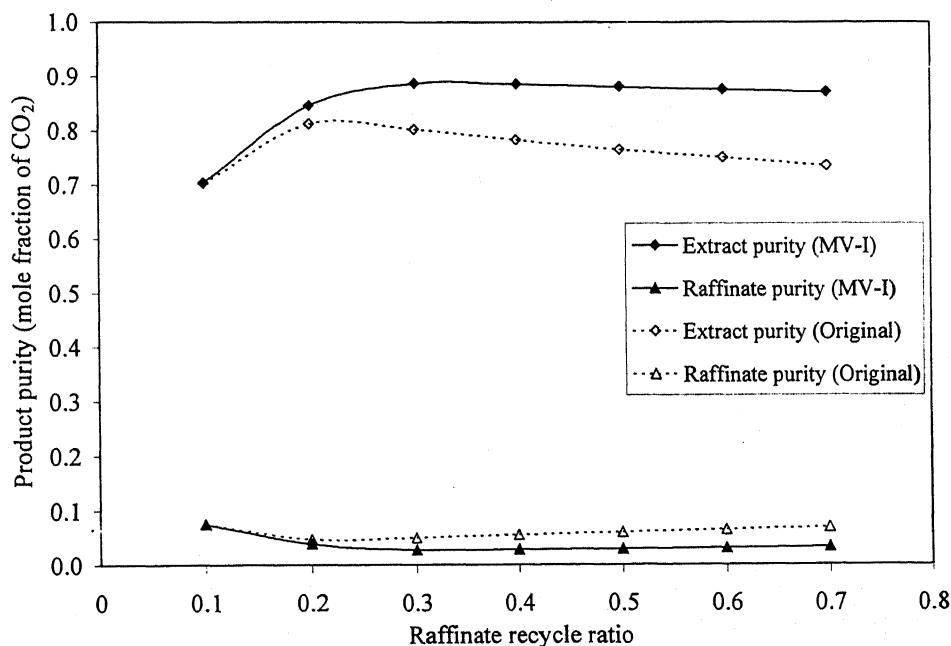


Fig.5.12 Effect of raffinate recycle ratio;  $F=60\text{mmol/half cycle}$ ,  $P_H=1\text{atm}$ ,  $P_L=0.3\text{atm}$

### Effect of feed

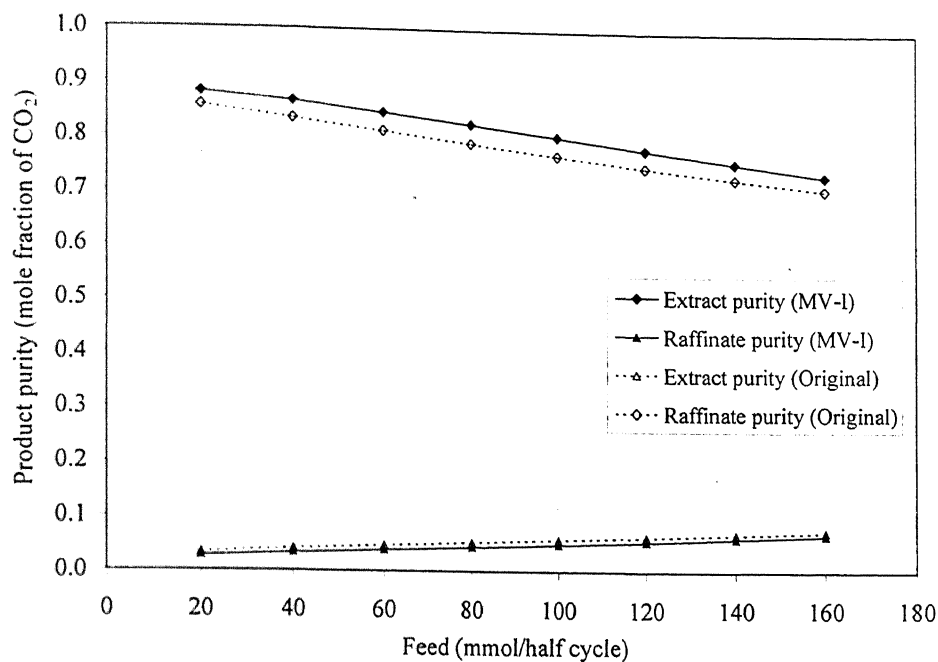


Fig.5.13 Effect of feed;  $P_H=1\text{atm}$ ,  $P_L=0.3\text{atm}$ ,  $R_R=0.2$

### Effect of desorption pressure

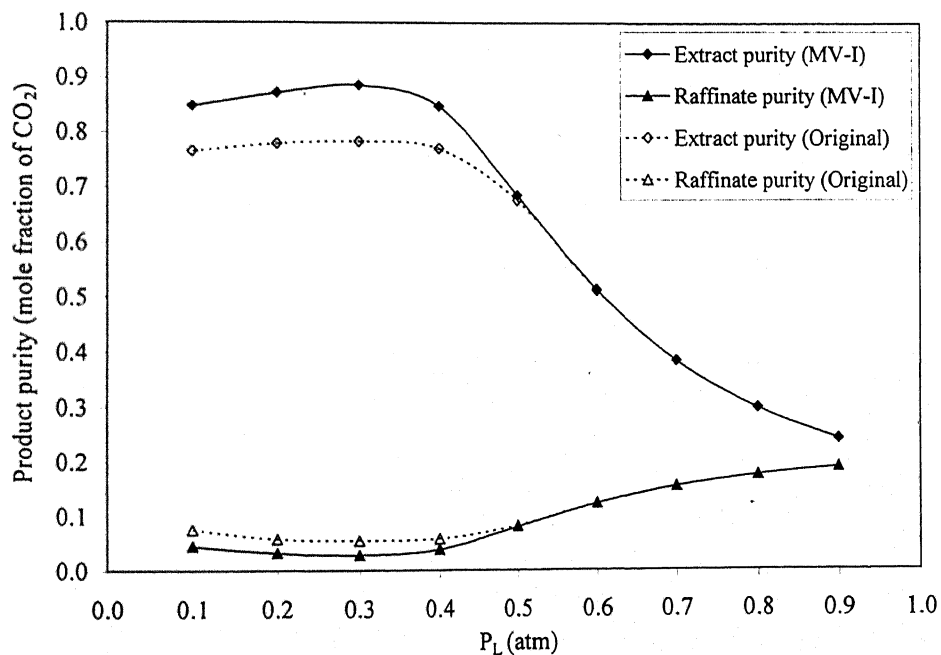


Fig.5.14 Effect of desorption pressure;  $F=60\text{mmol/half cycle}$ ,  $P_H=1\text{atm}$ ,  $R_R=0.4$



Though there is a marginal improvement in product purity in MV-I duplex over Original duplex, it gives an insight to further modify the Original duplex cycle for clean separation of  $\text{CO}_2\text{-N}_2$ .

### 5.1.5 MV-II duplex PSA

From the parametric study of Original and MV-I duplex PSA, it can be concluded that the product purity is limited by the recycle stream circulating between the beds. The extract product cannot be enriched to 99+%  $\text{CO}_2$  when the extract is drawn from the outgoing stream of the bed undergoing purge step. To overcome this, the extract withdrawal step in MV-II duplex has been modified and it dramatically improved the product purities.

It can be seen that during equalization and pressurization step, most of the  $\text{N}_2$  present in the bed undergoing blowdown gets swept away from the bottom and the upper half portion becomes enriched with pure  $\text{CO}_2$ . On further evacuating the bed from top end, pure  $\text{CO}_2$  as extract will come out.

Figure 5.15 shows the mass balance sheet of MV-II duplex for 100 mmol/half cycle of feed. The adsorption pressure,  $P_H$  has been fixed as 1 atm and intermediate-blowdown pressure,  $P_I$  as 0.5 atm. The final-blowdown pressure,  $P_L$  (0.34 atm) is governed by the intermediate-blowdown pressure and the amount of extract (20 mmol) to be drawn. During equalization and pressurization, the amount coming out from bed-1 undergoing intermediate-blowdown is not sufficient to pressurize bed-2 to  $P_H$  as  $P_L < P_I$  and an extra amount of 1.4 mmol is required. The extra amount is taken from the raffinate product drawn from bottom of bed-1 undergoing feed step. The purity of extract in MV-II duplex improved drastically from 77% to 99.5% with 99.7% recovery and that of raffinate from 94% to 99.9% with 99.9% recovery.

Figures 5.16 (a, b, c, d, e, f, g, h, i, j) show the change in the gas and the solid phase concentration with time in the bed undergoing feed, intermediate-blowdown, final-blowdown, purge and pressurization step for the mass balance sheet given in Figure 5.15. In all the profiles, dimensionless bed length, '0' represents that end of the bed where the stream is entering. The direction of incoming and outgoing streams from the beds has been represented by arrow ( $\longrightarrow$ ) sign.



**Feed:** Figures 5.16 (a) and 5.16 (b) show the gas and the solid phase concentration profiles of the feed step. There are two inlet streams. The total gas (rich in  $\text{CO}_2$ ) coming out from the bed undergoing purge is fed to the top as extract recycle, and feed is introduced in the middle of the bed. The  $\text{CO}_2$  gets adsorbed and the raffinate product (rich in  $\text{N}_2$ ) is drawn from the bottom. At the feed position, sudden change in the bed profiles can be observed as the feed mixes with a stream of different composition. The bed profiles are stretched throughout the length as the amount of extract recycle (164 mmol) is quite large compared to that in the Original duplex (42 mmol).

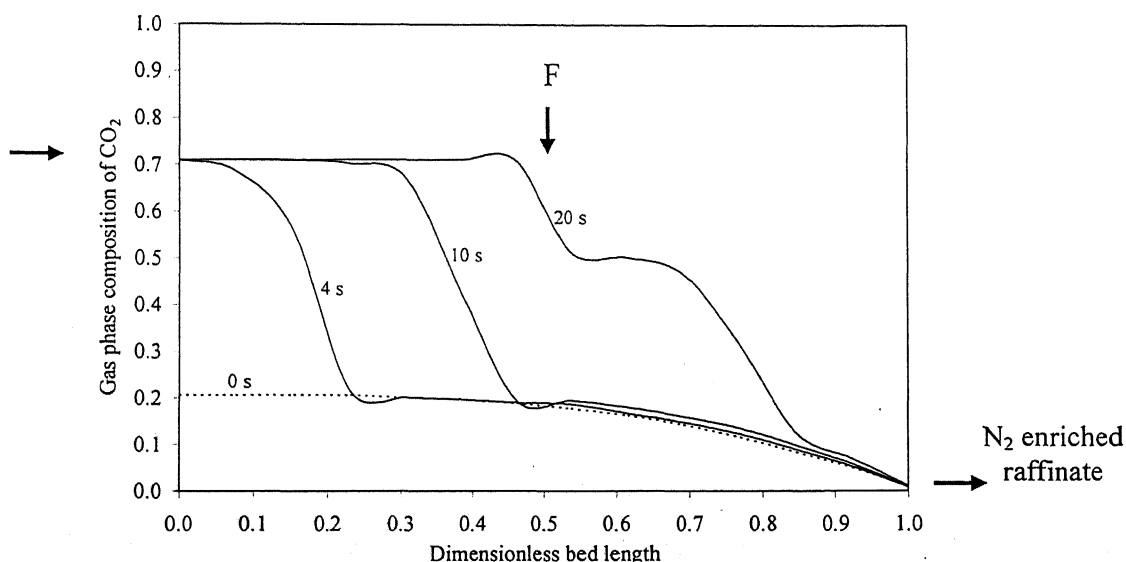


Fig.5.16 (a) Gas phase concentration profile in the bed undergoing feed step (MV-II duplex)

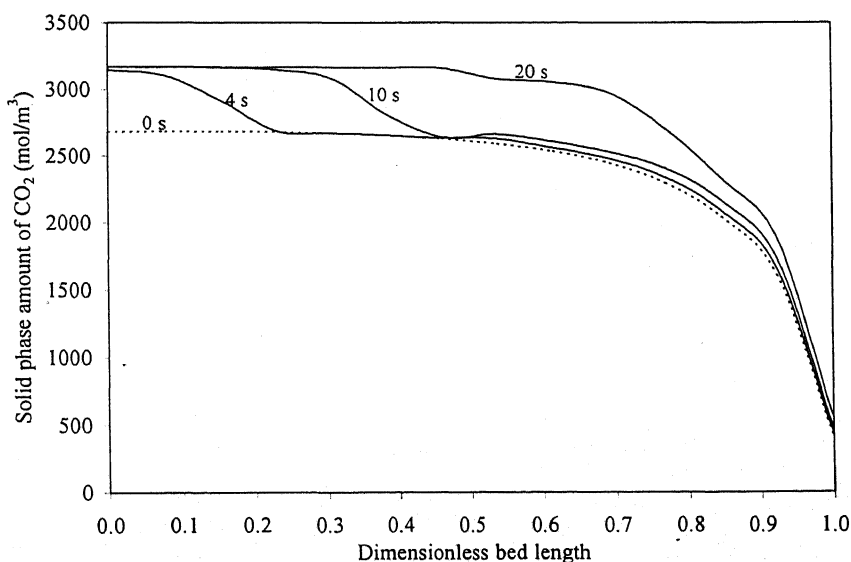


Fig.5.16 (b) Solid phase concentration profile in the bed undergoing feed step (MV-II duplex)

**Intermediate-blowdown:** Figures 5.16 (c) and 5.16 (d) show the gas and the solid phase concentration profiles of the intermediate-blowdown step. As the pressure reduces from  $P_H$  (1 atm) to  $P_I$  (0.5 atm), the  $\text{CO}_2$  gets desorbed from the solid and the gas composition of  $\text{CO}_2$  increases. A little amount of  $\text{CO}_2$  (0.25 mmol) comes out from the bed because of the locking effect. The  $\text{N}_2$  present in first half of the bed gets swept away and becomes enriched with pure  $\text{CO}_2$ .

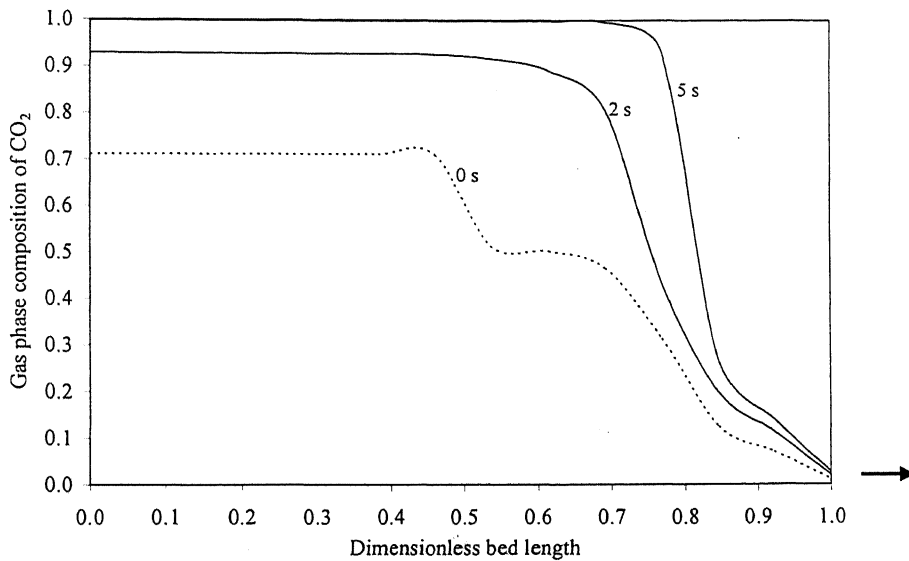


Fig.5.16 (c) Gas phase concentration profile in the bed undergoing intermediate-blowdown step (MV-II duplex)

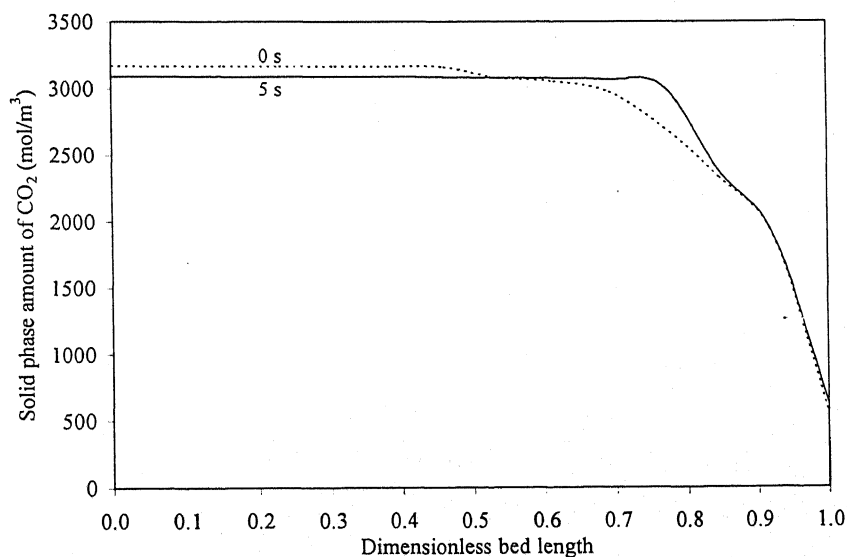


Fig.5.16 (d) Solid phase concentration profile in the bed undergoing intermediate-blowdown step (MV-II duplex)

**Final-blowdown:** Figures 5.16 (e) and 5.16 (f) show the gas and the solid phase concentration profiles of the final-blowdown step. It can be seen from the bed profiles that initially, upper half portion of the bed is enriched with pure CO<sub>2</sub>. On evacuating the bed from top, the outgoing gas (extract product) is enriched with 99.48% CO<sub>2</sub>. To draw 20 mmol extract product, bed has to be evacuated from P<sub>I</sub> (0.5 atm) to P<sub>L</sub> (0.34 atm).

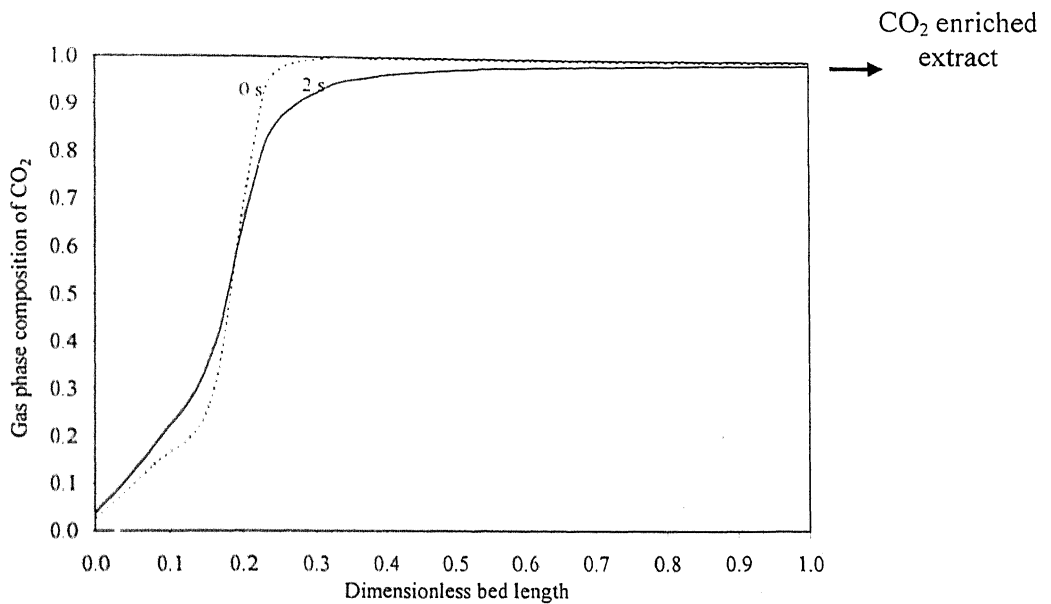


Fig.5.16 (e) Gas phase concentration profile in the bed undergoing final-blowdown step (MV-II duplex)

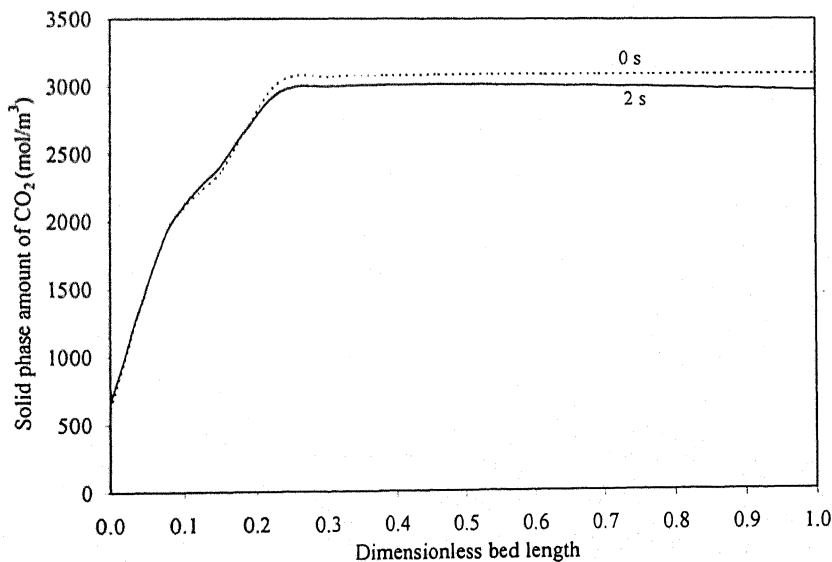


Fig.5.16 (f) Solid phase concentration profile in the bed undergoing final-blowdown step (MV-II duplex)

**Purge:** Figures 5.16 (g) and 5.16 (h) show the gas and the solid phase concentration profiles of the purge step. The bed undergoing purge is at final-desorption pressure (0.34 atm). As the raffinate recycle stream rich in  $N_2$  enters the bed, the gas phase composition of  $CO_2$  decreases. This results in the decrease in the partial pressure of  $CO_2$  as total pressure is constant. So, the  $CO_2$  gets desorbed and purged off from the bed.

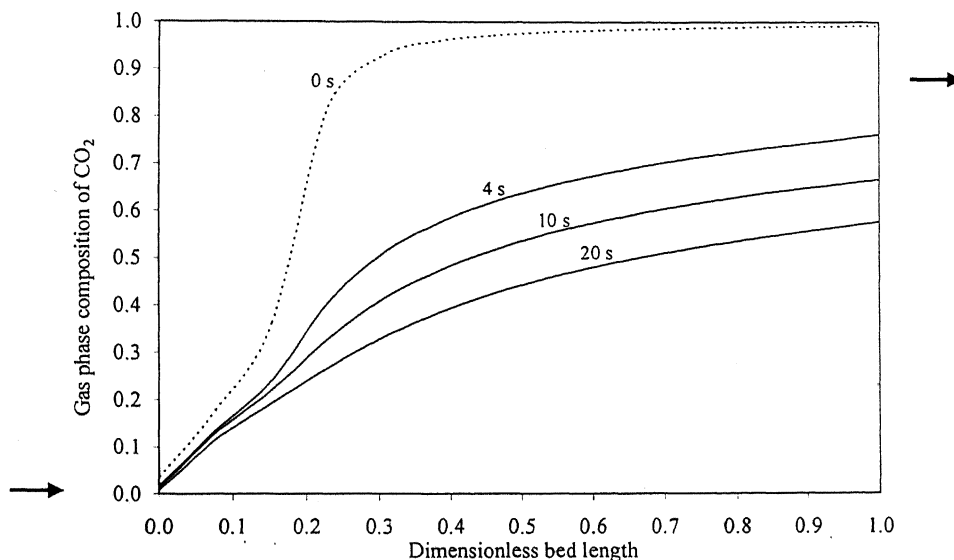


Fig.5.16 (g) Gas phase concentration profile in the bed undergoing purge step (MV-II duplex)

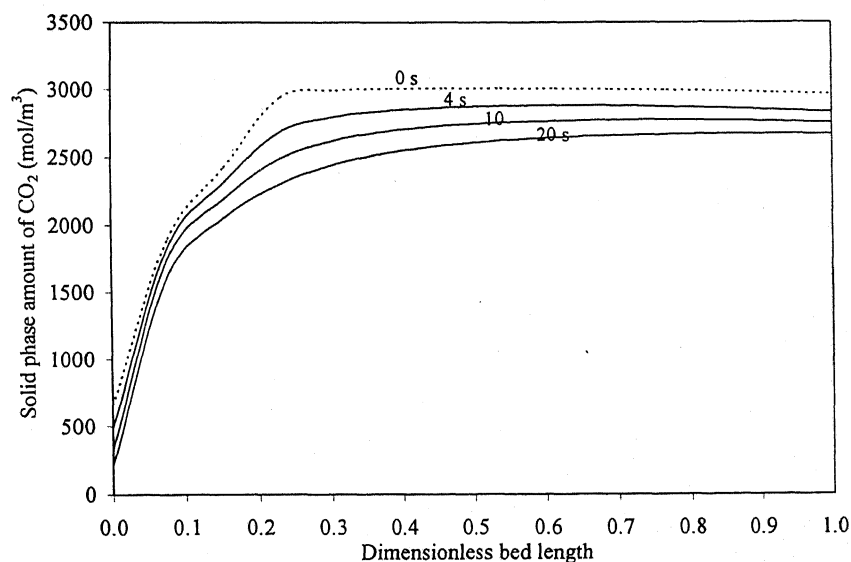


Fig.5.16 (h) Solid phase concentration profile in the bed undergoing purge step (MV-II duplex)

**Pressurization:** Figures 5.16 (i) and 5.16 (j) show the gas and the solid phase concentration profiles of the pressurization step. The bed is pressurized from  $P_1$  (0.34 atm) to  $P_H$  (1 atm). It can be seen from the bed profiles that the composition of  $\text{CO}_2$  in the gas phase decreases but the change in the solid phase amount is marginal and only in the initial portion of the bed. This is because the inlet stream is rich in 95%  $\text{N}_2$  which is non-adsorbing.

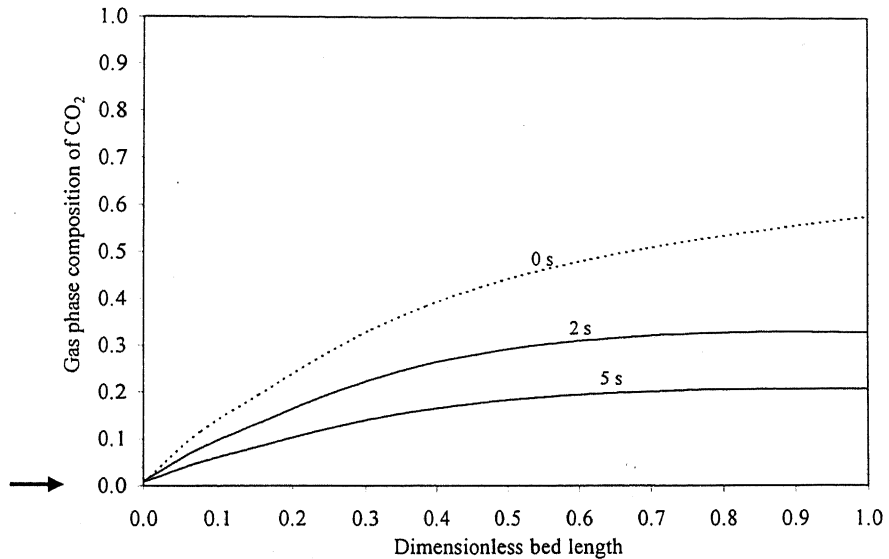


Fig.5.16 (i) Gas phase concentration profile in the bed undergoing pressurization step (MV-II duplex)

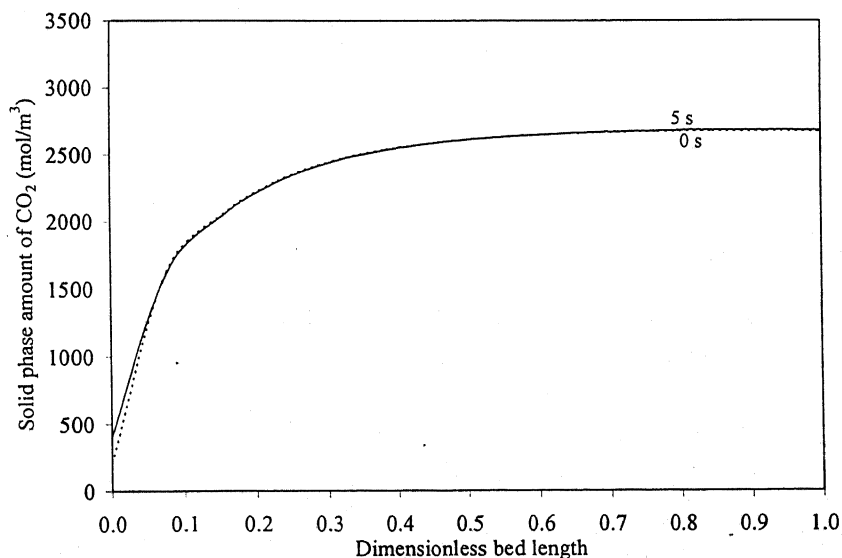


Fig.5.16 (j) Solid phase concentration profile in the bed undergoing pressurization step (MV-II duplex)

### 5.1.6 Parametric study of MV-II duplex PSA

The effect of feed, raffinate recycle ratio and desorption pressure on the performance of MV-II duplex PSA has been studied.

#### *Effect of raffinate recycle ratio, $R_R$*

Figure 5.17 shows the effect of raffinate recycle ratio on the product purity and the energy requirement. At low value of  $R_R$  (0.2), product purity is small. On increasing the recycle ratio, product purity gets improved. There is no change in product purity between recycle ratio 0.4 to 1.4 and thereafter that it starts decreasing.

On increasing the raffinate recycle ratio, the amount of gas circulating between the beds increases so the energy requirement also increases.

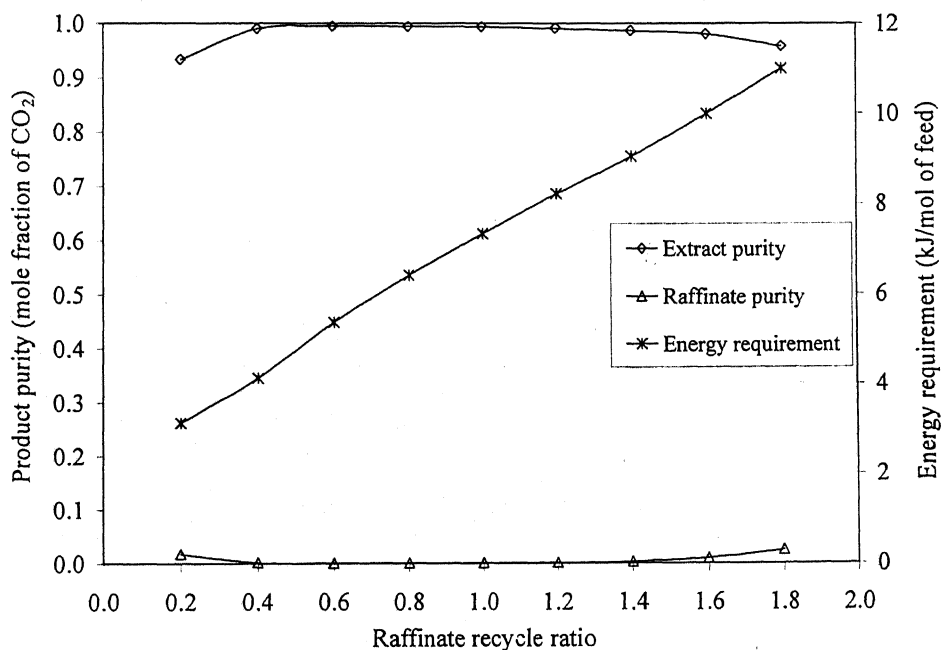


Fig.5.17 Effect of raffinate recycle ratio;  $F=100\text{mmol/half cycle}$ ,  $P_H=1\text{atm}$ ,  $P_I=0.5\text{atm}$

The reason for the purity trends can be understood by looking at the bed profiles of the intermediate-blowdown step at different recycle ratios. It gives the details of how much  $\text{N}_2$  is left inside the bed at the end of this step. Since the bed after intermediate-blowdown step goes for withdrawal of  $\text{CO}_2$  rich extract (final-blowdown step), the  $\text{N}_2$  present inside the bed may come out with the  $\text{CO}_2$  effecting its purity. Figures 5.18 (a), (b) and (c) show the gas phase concentration profiles in the bed undergoing intermediate-blowdown



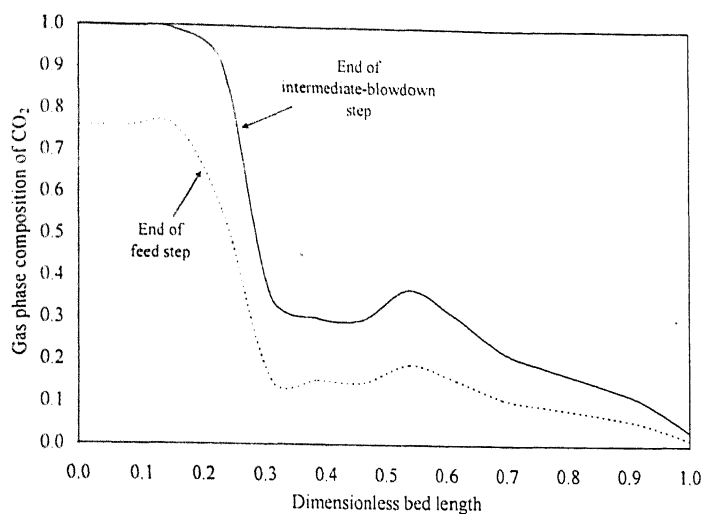


Fig.5.18 (a) Gas phase concentration profile ( $R_R = 0.2$ )

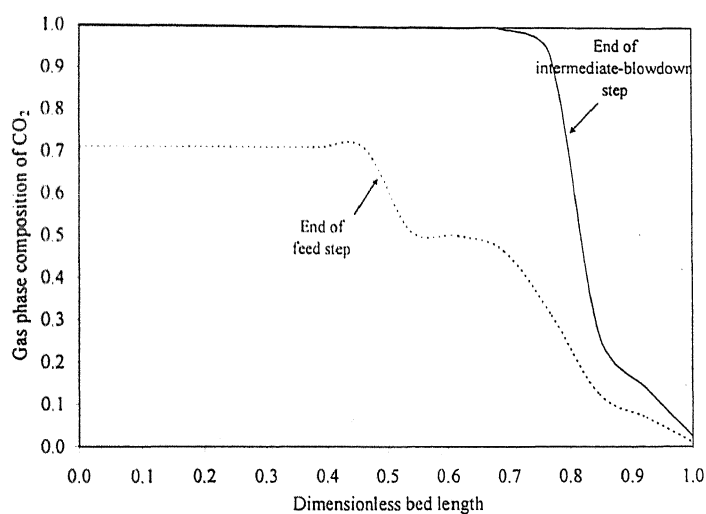


Fig.5.18 (b) Gas phase concentration profile ( $R_R = 0.6$ )

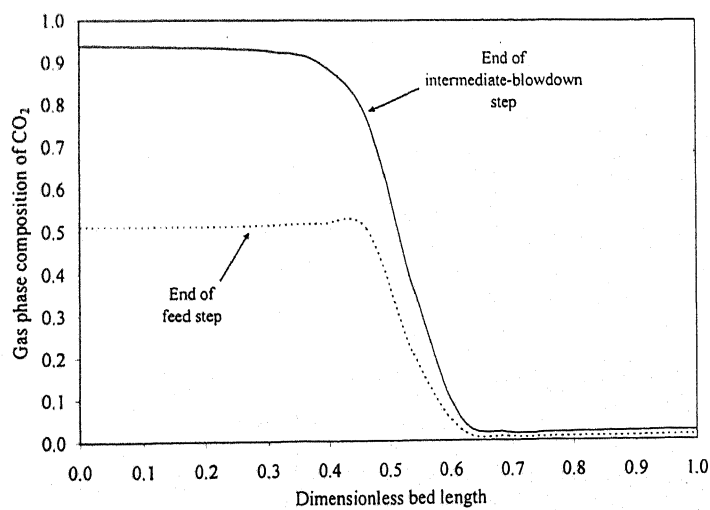


Fig.5.18 (c) Gas phase concentration profile ( $R_R = 1.8$ )

for a recycle ratio of 0.2, 0.6 and 1.8 respectively. It can be seen that at a  $R_R$  value of 0.2, the  $\text{CO}_2$  in extract recycle entering from top of the bed is not sufficient and they get adsorbed only in the initial part. Most part of the bed at the end of feed step is filled with  $\text{N}_2$ . The  $\text{N}_2$  present in the bed is not properly swept away even after evacuating the bed (during intermediate-blowdown). As the bed after intermediate-blowdown goes for extract withdrawal, the  $\text{N}_2$  left in the initial portion of the bed comes out with  $\text{CO}_2$  effecting its purity. Whereas, at raffinate recycle ratio of 0.6, the first half portion of the bed after intermediate-blowdown gets enriched with pure  $\text{CO}_2$  and on evacuating the bed, extract (rich in  $\text{CO}_2$ ) with 99.5% purity comes out.

The drop in product purity at  $R_R$  value of 1.8 can be explained in the same way from the corresponding bed profile shown in Figure 5.18 (c).

### Effect of feed, $F$

Figure 5.19 shows the effect of feed on the product purity and the energy requirement.

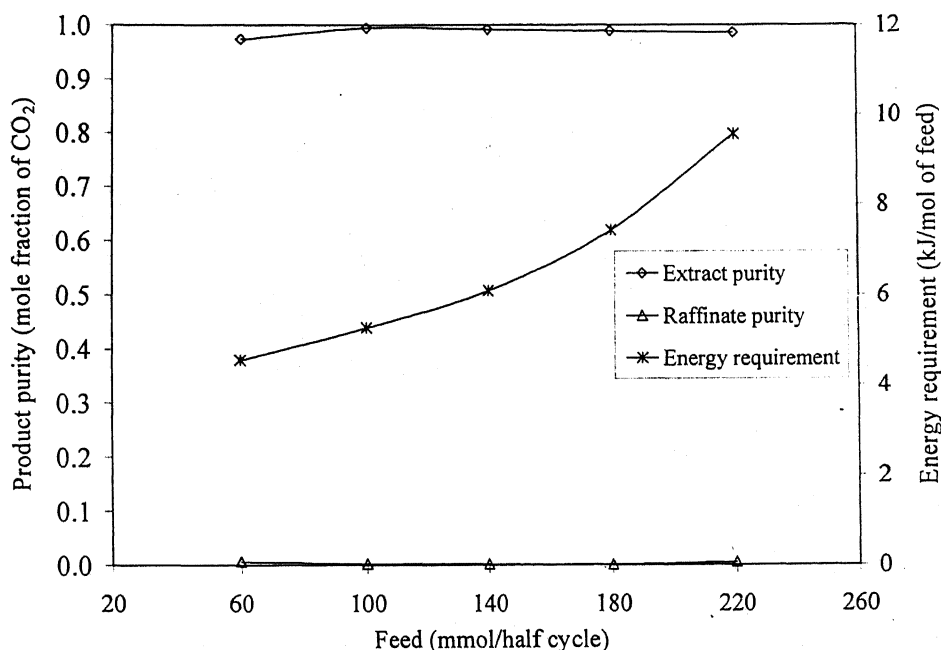


Fig.5.19 Effect of feed;  $P_H=1\text{atm}$ ,  $P_I=0.5\text{atm}$ ,  $R_R=0.6$

At a feed rate of 60 mmol/half cycle, the extract purity is 97% and that of raffinate is 99%. On increasing the feed, the purity increases and reaches an optimum (extract purity

- 99.5% and raffinate purity - 99.7%) at a feed rate of 100 mmol/half cycle. On further increasing the feed rate, a slight drop in product purity is observed. The reason can be explained in same way as that of the raffinate recycle ratio effect because increasing the feed is equivalent to increasing the amount of recycle stream.

The energy requirement increases with feed rate because of the decrease in  $P_L$  required to draw the corresponding amount of the extract ( $F \cdot X_F$ ).

### *Effect of intermediate-desorption pressure, $P_I$*

Figure 5.20 shows the effect of intermediate-desorption pressure on the product purity and the energy requirement. At large value of  $P_I$  ( $> 0.4$  atm), purity of both the end products are poor. This is because during equalization and pressurization step, desorption pressure ( $P_I$ ) is not sufficient to sweep off the  $N_2$  present in the bed undergoing intermediate-blowdown. The  $N_2$  left inside the bed will come out when extract (rich in  $CO_2$ ) will be drawn. Other reason is that at large value of  $P_I$ , the corresponding pressure ( $P_L$ ) in the bed undergoing purge is also large and the raffinate recycle is not able to properly purge off the adsorbed  $CO_2$ , as it is strongly adsorbed. On decreasing the intermediate-desorption pressure, product purity gets improved and at  $P_I$  value of 0.3 atm purity of both the end products reached 99.9%.

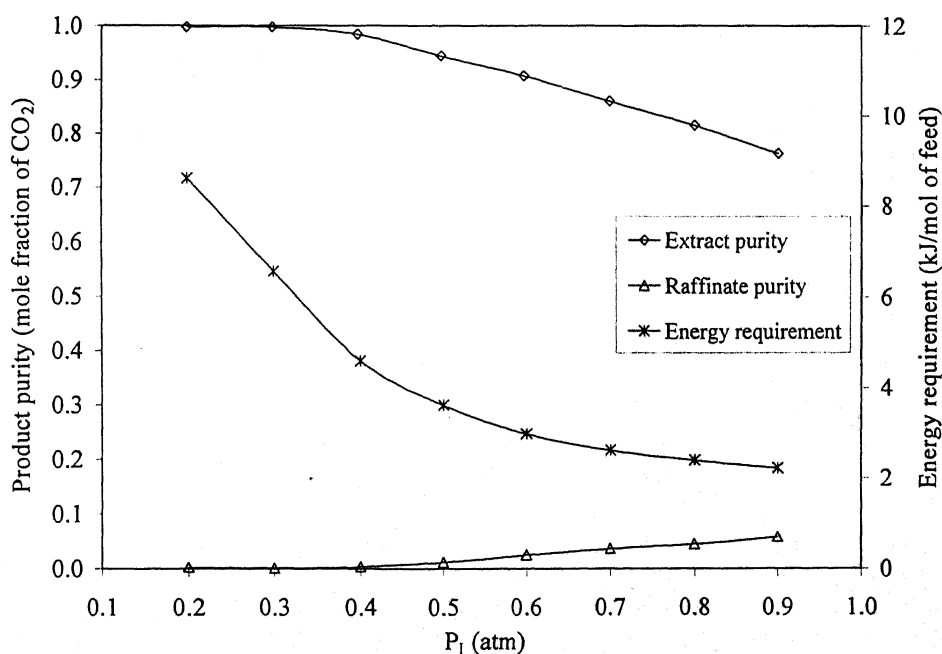


Fig.5.20 Effect of intermediate-desorption pressure;  $F=60\text{mmol/half cycle}$ ,  $P_H=1\text{atm}$ ,  $R_R=0.4$

As  $P_I$  decreases, the corresponding pressure ( $P_L$ ) in the bed undergoing purge also decreases. As the outgoing stream from purge (extract recycle) has to be compressed from  $P_L$  to  $P_H$  (1 atm) before recycling it into the bed undergoing feed, the increase in energy requirement is obvious with decrease in  $P_I$ .

### 5.1.7 Comparison of MV-II duplex and Original duplex PSA

Figures 5.21, 5.22 and 5.23 show the comparative performance of MV-II duplex and Original duplex PSA with change in raffinate recycle ratio, feed and desorption pressure respectively. It can be seen that in all cases, the product purity in MV-II duplex improved drastically over the purities obtained with the Original duplex.

#### *Effect of raffinate recycle ratio*

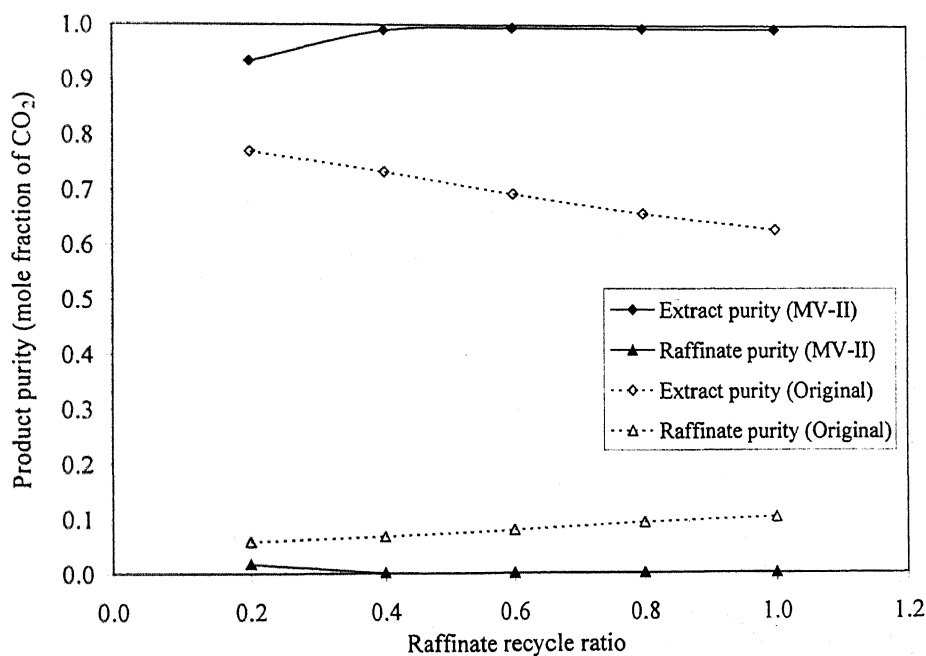


Fig.5.21 Effect of raffinate recycle ratio;  $F=100\text{mmol/half cycle}$ ,  $P_H=1\text{atm}$ ,  $P_I=0.5\text{atm}$  (MV-II),  $P_L=0.3\text{atm}$  (Original)

## Effect of feed

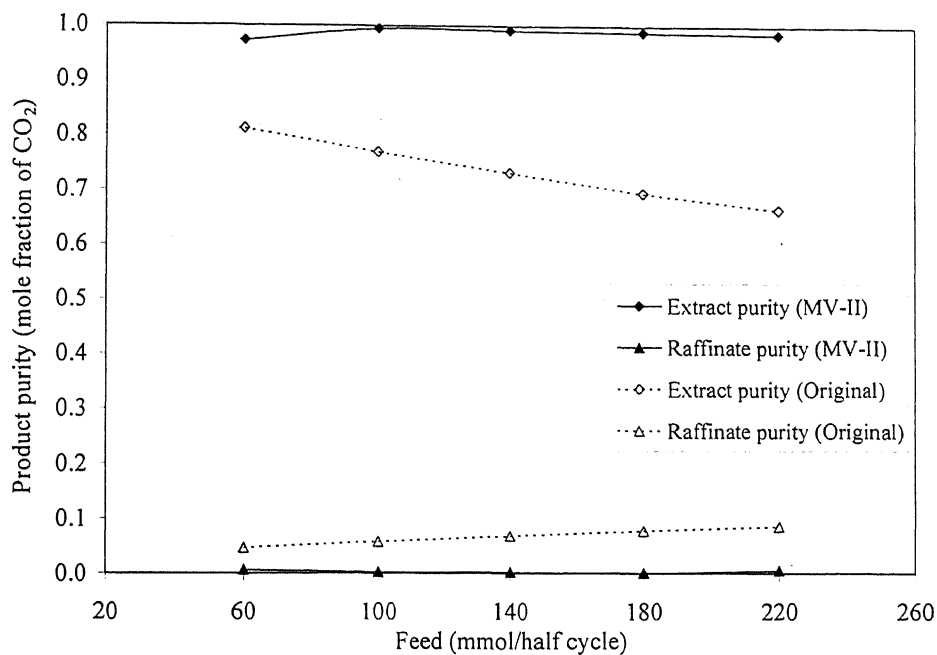


Fig.5.22 Effect of feed;  $P_H=1\text{ atm}$ ,  $P_I=0.5\text{ atm}$  (MV-II),  $P_L=0.3\text{ atm}$  (Original)  
 $R_R=0.6$  (MV-II),  $R_R=0.2$  (Original)

## Effect of desorption pressure

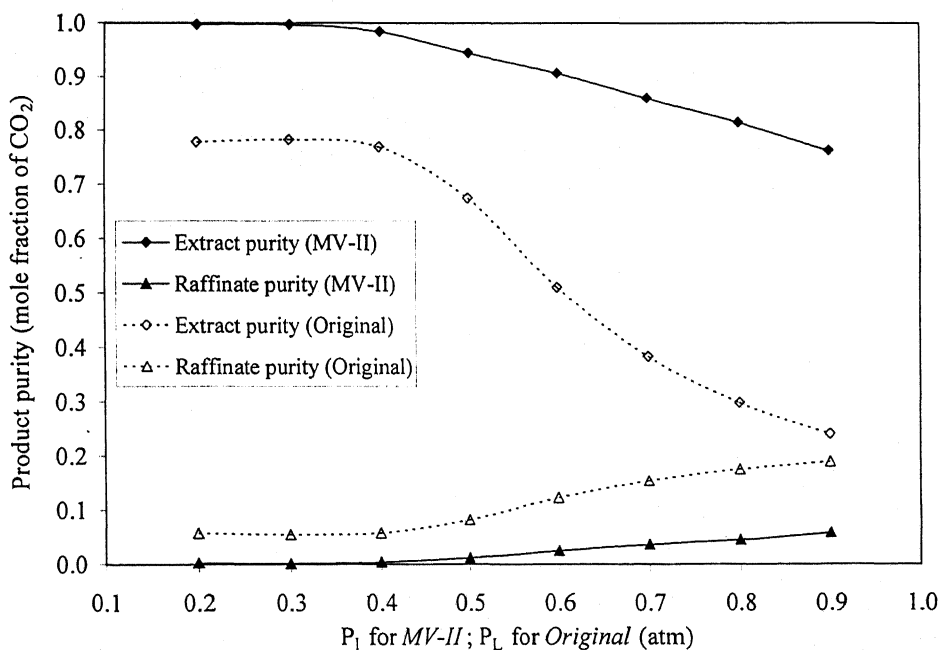


Fig.5.23 Effect of intermediate-desorption (MV-II) or desorption pressure (Original);  
 $F=60\text{ mmol/half cycle}$ ,  $P_H=1\text{ atm}$ ,  $R_R=0.4$

## 5.2 Fractionation of methane-hydrogen (CH<sub>4</sub>-H<sub>2</sub>) mixture

The separation of CH<sub>4</sub>-H<sub>2</sub> is important in petroleum and chemical process industries. We have assessed the performance of the duplex PSA for clean separation with CH<sub>4</sub>-H<sub>2</sub> mixture. The parameters used in simulation are listed in Table 5.2.

Table 5.2 Parameters used in simulation of fractionation of methane-hydrogen mixture

---

1. Molar feed composition	:	30% CH <sub>4</sub> , 70% H <sub>2</sub>
2. Adsorbent	:	Activated carbon
3. Particle diameter, <i>cm</i>	:	0.0707
4. Bed voidage	:	0.4
5. Bulk density, <i>kg/m<sup>3</sup></i>	:	480
6. Bed length, <i>cm</i>	:	100
7. Bed diameter, <i>cm</i>	:	2.5
8. Langmuir constant for CH <sub>4</sub> ( <i>b</i> ), <i>m<sup>3</sup>/mol</i>	:	3.91E-03
9. Saturation constant for CH <sub>4</sub> ( <i>q<sub>s</sub></i> ), <i>mol/m<sup>3</sup></i>	:	5067.0
10. LDF constant for CH <sub>4</sub> , <i>s<sup>-1</sup></i>	:	3.01
11. Operating temperature, <i>K</i>	:	298.15
12. Cycle time, <i>s</i> (Original and MV-I duplex)	:	50
Feed ( <i>t<sub>F</sub></i> ), <i>s</i>	:	20
Blowdown ( <i>t<sub>B</sub></i> ), <i>s</i>	:	5
Purge ( <i>t<sub>P</sub></i> ), <i>s</i>	:	20
Pressurization ( <i>t<sub>PR</sub></i> ), <i>s</i>	:	5
13. Cycle time, <i>s</i> (MV-II duplex)	:	54
Feed ( <i>t<sub>F</sub></i> ), <i>s</i>	:	20
Intermediate-blowdown ( <i>t<sub>BI</sub></i> ), <i>s</i>	:	5
Final-blowdown ( <i>t<sub>BF</sub></i> ), <i>s</i>	:	2
Purge ( <i>t<sub>P</sub></i> ), <i>s</i>	:	20
Pressurization ( <i>t<sub>PR</sub></i> ), <i>s</i>	:	5
Frozen ( <i>t<sub>FR</sub></i> ), <i>s</i>	:	2

---

The equilibrium data for methane-hydrogen mixture over Activated carbon reported by Malek and Farooq (1996) has been used. The amount of hydrogen adsorbed is negligible over a wide range of pressure and it can be considered as non-adsorbing component. Figure 5.24 shows the adsorption isotherm of methane on Activated carbon for different pressures at 298.15 K.

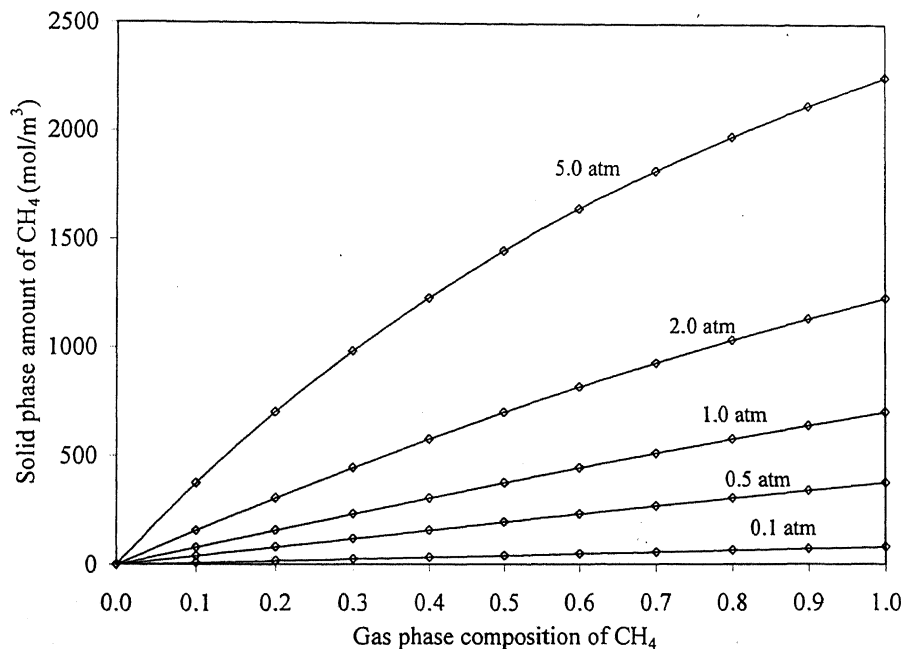


Fig.5.24 Adsorption isotherm of methane on Activated carbon at 298.15 K

As composition of feed in the CH<sub>4</sub>-H<sub>2</sub> system ( $X_F = 0.3$ ) is different from that of the CO<sub>2</sub>-N<sub>2</sub> system ( $X_F = 0.2$ ), we first studied the effect of feed position on the product purity. In CO<sub>2</sub>-N<sub>2</sub> system, optimum feed position was middle of the bed (Hirose et. al. 1995). We observed that in CH<sub>4</sub>-H<sub>2</sub> system, optimum feed position has shifted towards the top (extract recycle end) of the bed.

### 5.2.1 Effect of feed position

Figure 5.25 shows the effect of feed position on the product purity. In the study, the total length of the bed has been divided into 53 equispaced grids. It can be seen that on introducing feed in the middle, the system performance is poor. The highest purity is obtained on introducing feed at 10<sup>th</sup> grid (10 / 53 grid) from extract recycle end of the bed.

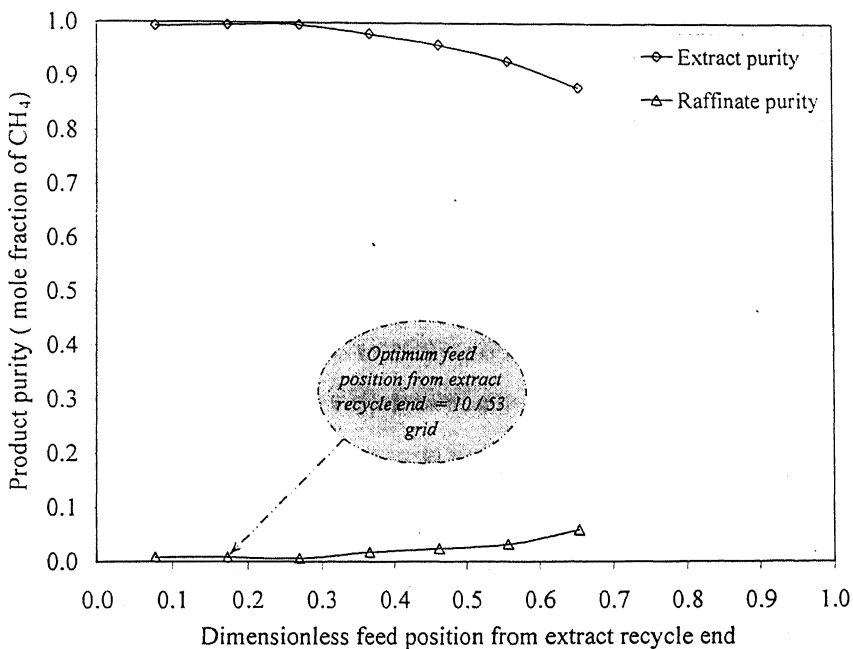


Fig.5.25 Variation in product purity with different position of feed;  $F=60$  mmol/half cycle,  $P_H=1$  atm,  $P_L=0.5$  atm,  $R_R=0.5$

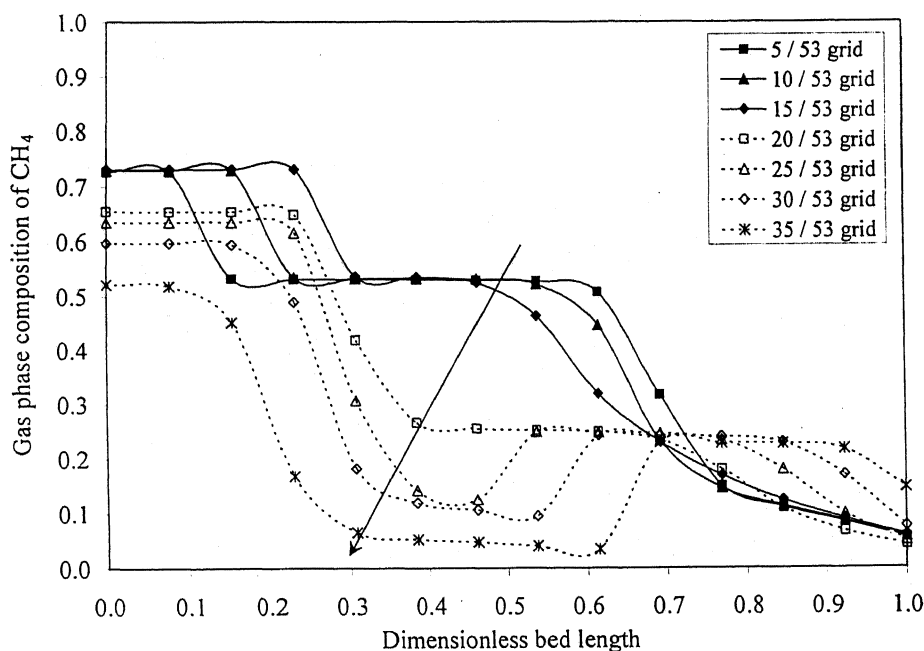


Fig.5.26 Final gas phase concentration profile of  $CH_4$  in bed undergoing feed;  $F=60$  mmol/half cycle,  $P_H=1$  atm,  $P_L=0.5$  atm,  $R_R=0.5$

The reason can be understood by analyzing the final gas phase concentration profile in the bed undergoing the feed step. Figure 5.26 shows the profile corresponding to different



feed location. On introducing the feed between 5<sup>th</sup> to 15<sup>th</sup> grids from extract recycle end, there is smooth transition in the profile throughout the bed length. Whereas, on introducing feed after 20<sup>th</sup> grid from extract recycle end, feed breaks through the bed resulting in poor product purity.

Here onwards we have taken 10<sup>th</sup> grid (optimum) from extract recycle end as the feed position (with total number of grids equal to 53).

The comparative performance of the Original duplex, MV-I duplex and MV-II duplex PSA has been studied with variation in raffinate recycle ratio, feed and desorption pressure respectively. It has been observed that the trend in product purity with variation in simulation parameters is same as that of the CO<sub>2</sub>-N<sub>2</sub> system studied earlier. This is obvious as in both the systems, only one component gets adsorbed and other is non-adsorbing.

### 5.2.2 Original duplex and MV-I duplex PSA

Figure 5.27 shows the mass balance sheet of the Original duplex PSA. For a feed rate of 60 mmol/half cycle, purity of extract (rich in CH<sub>4</sub>) is 78.5% and that of raffinate (rich in H<sub>2</sub>) is 90.3%.

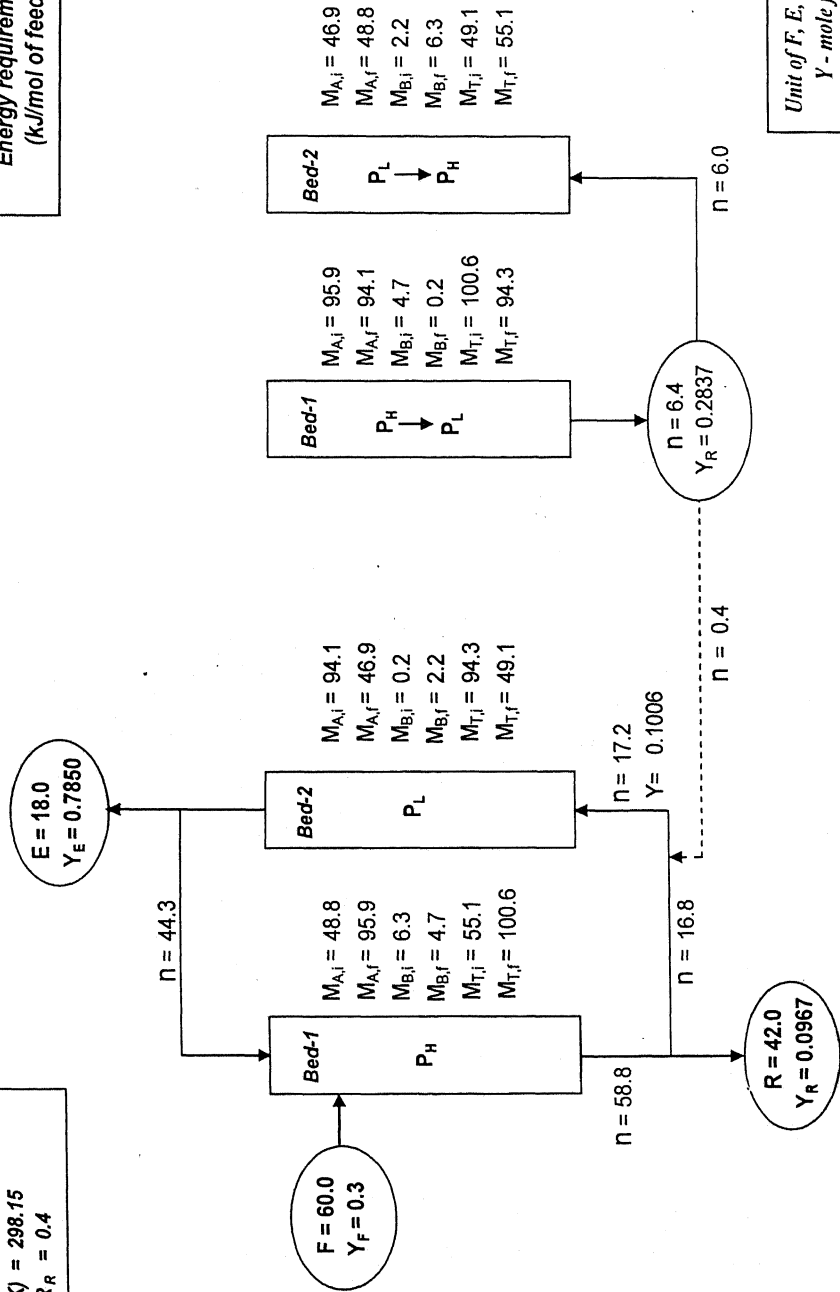
As H<sub>2</sub> is not getting adsorbed, it affects the extract purity in same way as that of N<sub>2</sub> (non-adsorbing) in CO<sub>2</sub>-N<sub>2</sub> system.

Figure 5.28 shows the mass balance sheet of the MV-I duplex with operating parameters same as that of the Original duplex (Figure 5.27). In MV-I duplex, the first part (I) of the outgoing stream from the bed undergoing purge is collected as extract product (rich in CH<sub>4</sub>) and the remaining amount (II) is recycled to the top of the bed undergoing feed as extract recycle. It can be seen that in MV-I duplex, the extract purity improved from 78.5% to 87.9% and that of the raffinate from 90.3% to 94.4% over Original duplex.

	CH <sub>4</sub>	H <sub>2</sub>
Purity (%)	78.50	90.33
Recovery (%)	78.5	90.3
Productivity (mol/kg-h)	4.0	10.7
Energy requirement (kJ/mol of feed)	3.0	

System : CH<sub>4</sub> - H<sub>2</sub>  
Adsorbent : Activated carbon

Bed length (cm) = 100  
Bed diameter (cm) = 2.5  
Feed (mmol/half cycle) = 60  
Half cycle time (s) = 20 + 5  
 $P_H$  (atm) = 1.0  
 $P_L$  (atm) = 0.4  
 $T$  (K) = 298.15  
 $R_R = 0.4$



Unit of F, E, R, M and n - mmol  
Y - mole fraction of CH<sub>4</sub>

Fig.5.27 Mass balance sheet of Original duplex PSA

	CH <sub>4</sub>	H <sub>2</sub>
Purity (%)	87.85	94.41
Recovery (%)	87.9	94.4
Productivity (mol/kg-h)	4.5	11.2
Energy requirement (kJ/mol of feed)	2.7	

System : CH<sub>4</sub> - H<sub>2</sub>  
Adsorbent : Activated carbon

Bed length (cm) = 100  
Bed diameter (cm) = 2.5  
Feed (mmol/half cycle) = 60  
Half cycle time (s) = 20 + 5  
P<sub>H</sub> (atm) = 1.0  
P<sub>L</sub> (atm) = 0.4  
T (K) = 298.15  
R<sub>R</sub> = 0.4

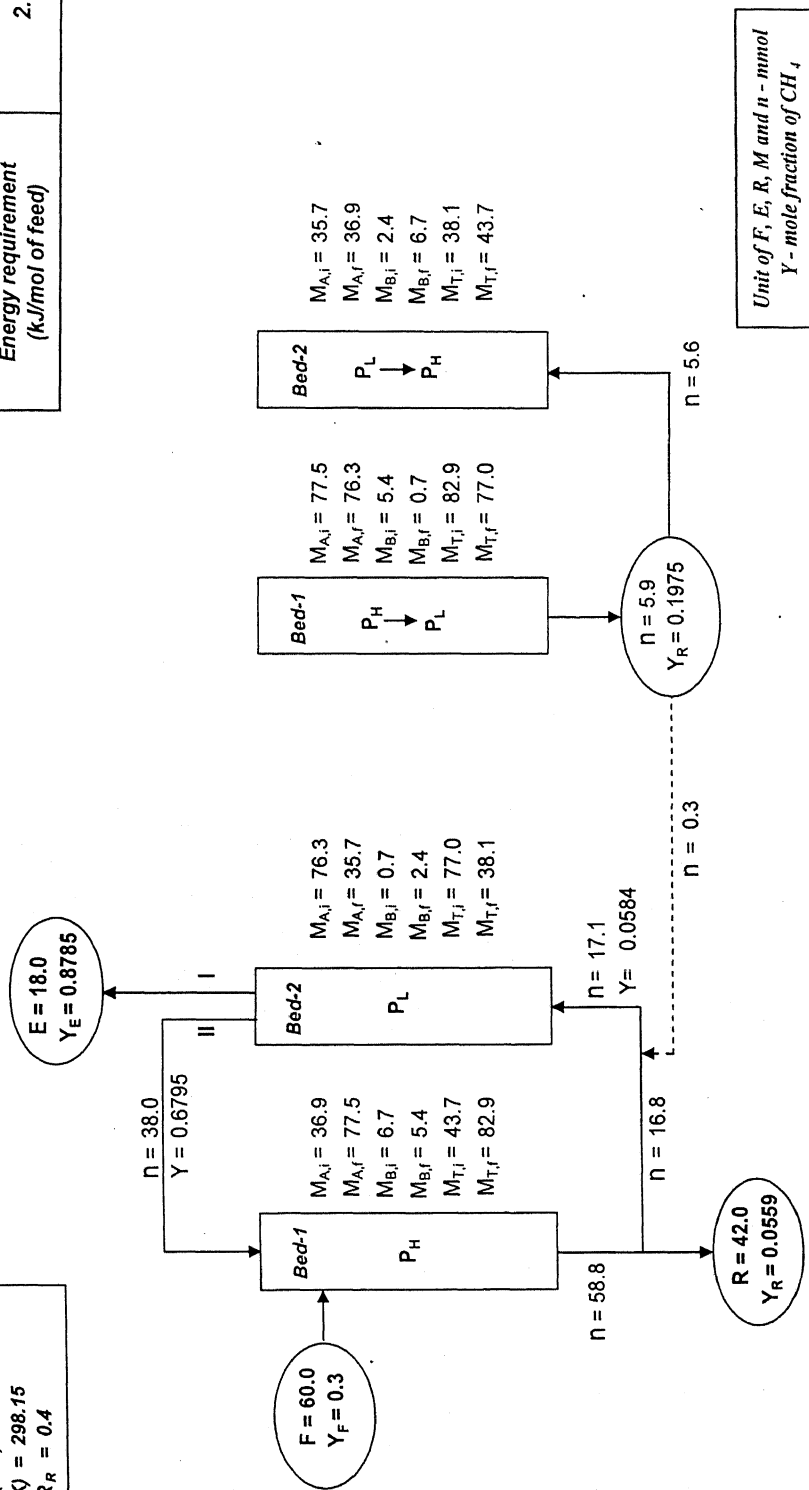


Fig.5.28 Mass balance sheet of MV-I duplex PSA

### 5.2.3 Comparison of MV-I duplex and Original duplex PSA

Figures 5.29, 5.30 and 5.31 show the comparative performance of the MV-I duplex and the Original duplex PSA with change in raffinate recycle ratio, feed and desorption pressure respectively. It can be seen that in all cases, performance of MV-I duplex improved over Original duplex. The trend is similar to that of the  $\text{CO}_2\text{-N}_2$  system and can be explained in the same way.

Figures 5.29 and 5.31 show that at low value of raffinate recycle ratio (0.2) or at a large value of desorption pressure ( $>0.5$ ) there is no improvement in product purity because  $\text{CH}_4$  is not properly purged off from the bed undergoing purge step.

#### *Effect of raffinate recycle ratio, $R_R$*

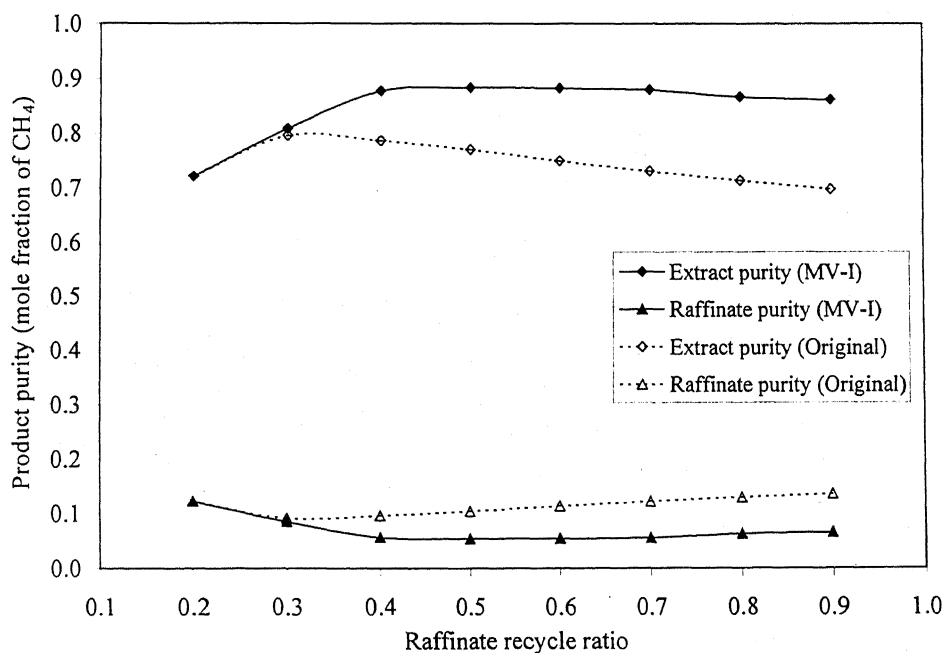


Fig.5.29 Effect of raffinate recycle ratio;  $F=60\text{mmol/half cycle}$ ,  $P_H=1\text{ atm}$ ,  $P_L=0.4\text{ atm}$

### Effect of feed, $F$

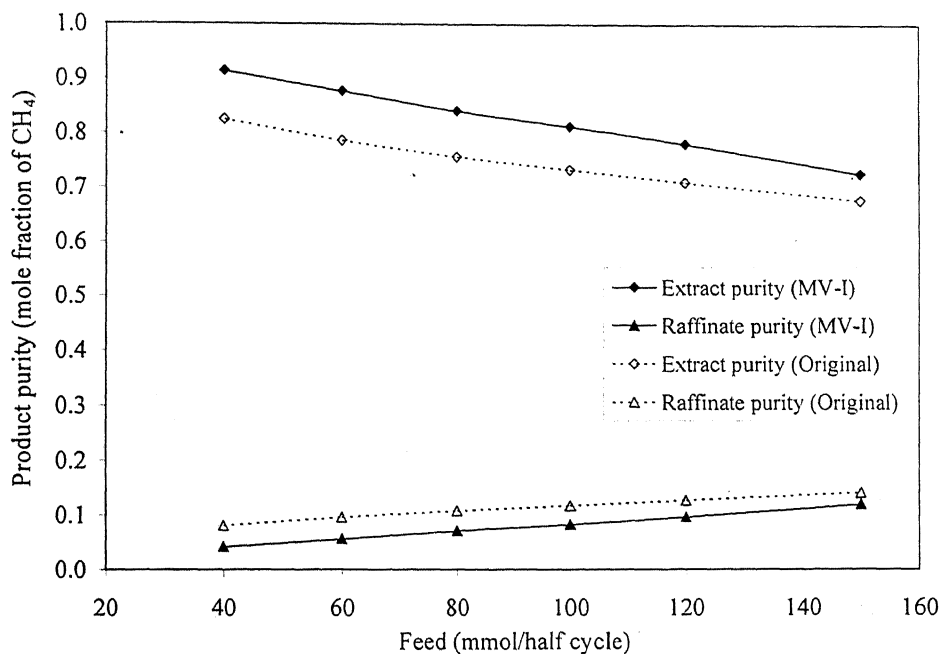


Fig.5.30 Effect of feed;  $P_H=1\text{ atm}$ ,  $P_L=0.4\text{ atm}$ ,  $R_R=0.4$

### Effect of desorption pressure, $P_L$

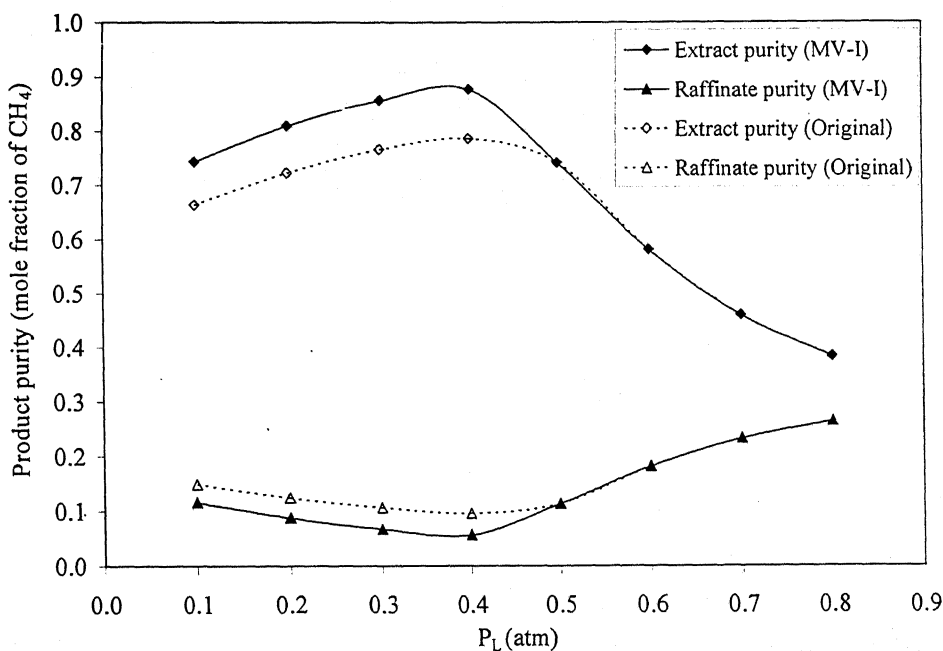


Fig.5.31 Effect of desorption pressure;  $F=60\text{ mmol/half cycle}$ ,  $P_H=1\text{ atm}$ ,  $R_R=0.4\text{ atm}$

#### 5.2.4 MV-II duplex PSA

From the parametric study presented in section 5.2.3, it can be concluded that the clean separation is not feasible in Original and MV-I duplex PSA because of the non-adsorbing nature of  $H_2$ .

We studied the performance of MV-II duplex to get clean separation with  $CH_4-H_2$  system. Figure 5.32 shows the mass balance sheet of MV-II duplex for 60 mmol/half cycle of feed. It can be seen that in MV-II duplex, the extract purity improved dramatically from 78.5% to 99.9% with 99.9% recovery and that of the raffinate from 90.3% to 99.9% with 99.9% recovery over Original duplex.

The gas and solid phase concentration profile of the bed undergoing intermediate-blowdown, final-blowdown, purge and pressurization step has not been shown as they exhibit almost the same trend as that of the  $CO_2-N_2$  system. There is change only in the feed profile as feed location is different. Figures 5.33 (a) and (b) show the gas and the solid phase concentration profiles in the bed undergoing feed step.

	CH <sub>4</sub>	H <sub>2</sub>
Purity (%)	99.98	99.94
Recovery (%)	100.0	99.9
Productivity (mol/kg-h)	4.7	11.0
Energy requirement (kJ/mol of feed)	4.6	

System : CH<sub>4</sub> - H<sub>2</sub>  
 Adsorbent : Activated carbon

Bed length (cm) = 100  
 Bed diameter (cm) = 2.5  
 Feed (mmol/half cycle) = 60  
 Half cycle time (s) = 20 + 5 + 2  
 $P_H$  (atm) = 1.0  
 $P_L$  (atm) = 0.4  
 $T$  (K) = 298.15  
 $R_R = 0.4$

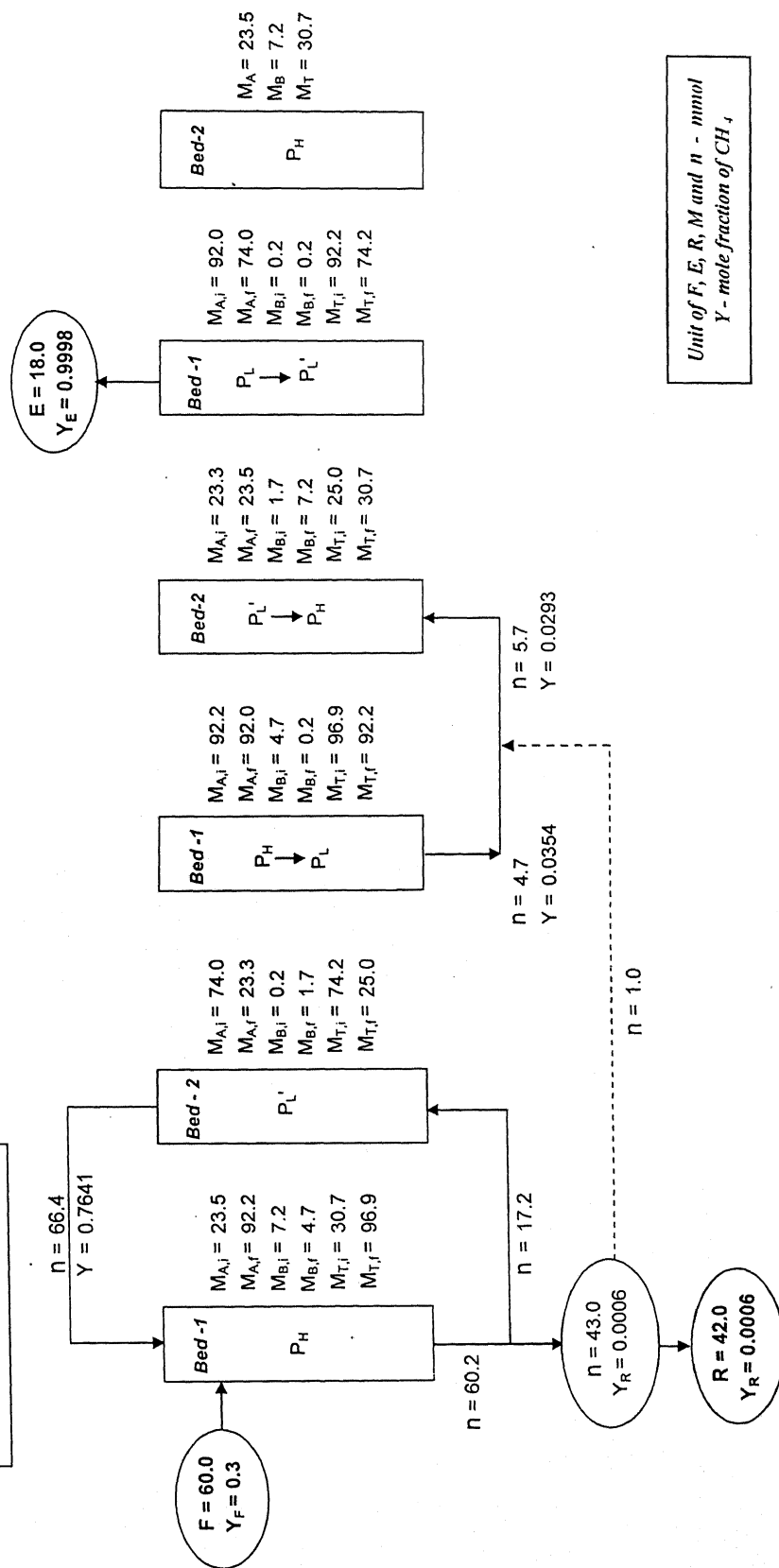


Fig.5.32 Mass balance sheet of MV-II duplex PSA

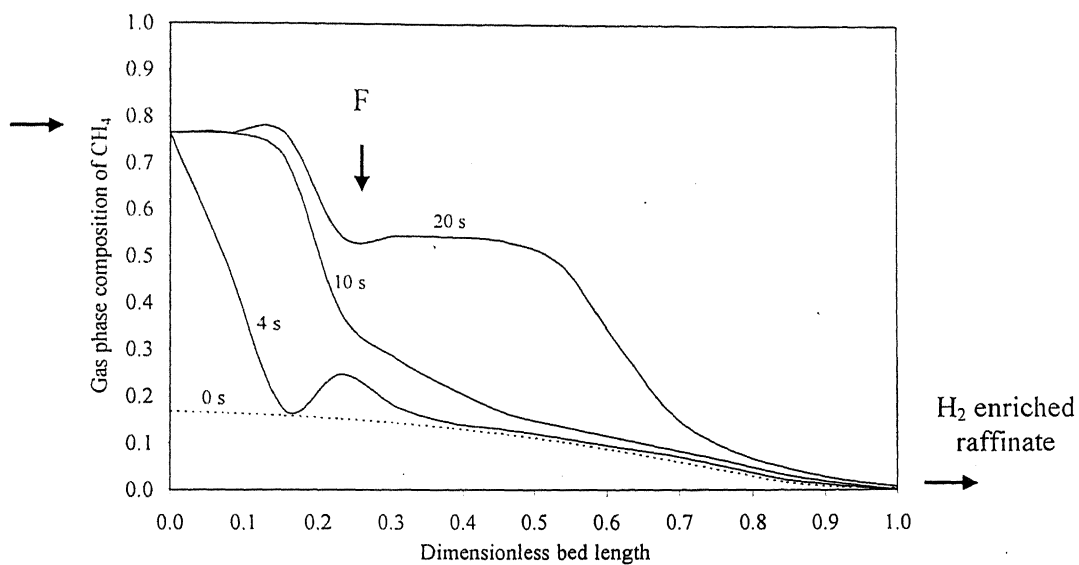


Fig.5.33 (a) Gas phase concentration profile in the bed undergoing feed step (MV-II duplex)

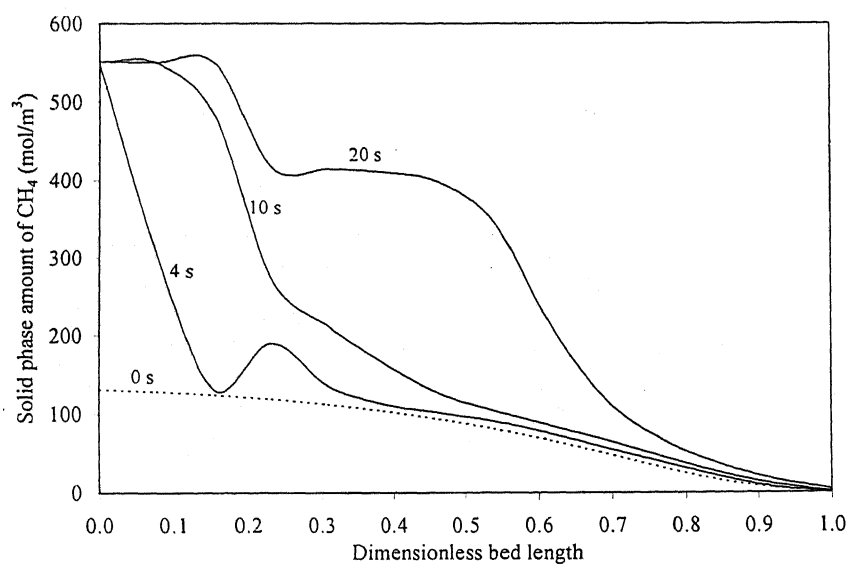


Fig.5.33 (b) Solid phase concentration profile in the bed undergoing feed step (MV-II duplex)



### 5.2.5 Parametric study of MV-II duplex PSA

The effect of raffinate recycle ratio, feed and desorption pressure on the performance of MV-II duplex PSA has been studied. The trend in product purities and energy requirement is the same as that of the CO<sub>2</sub>-N<sub>2</sub> system.

#### *Effect of raffinate recycle ratio, $R_R$*

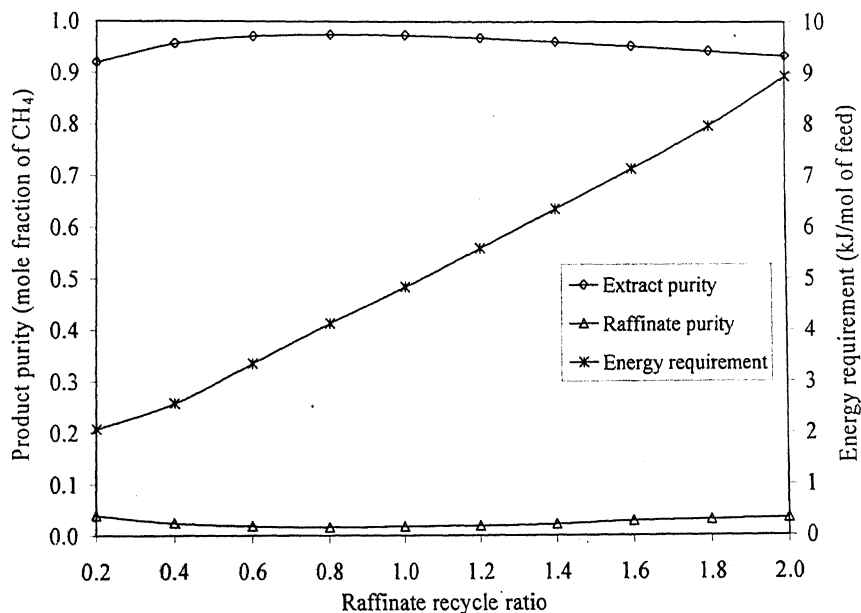


Fig.5.34 Effect of raffinate recycle ratio;  $F=60\text{mmol/half cycle}$ ,  $P_H=1\text{ atm}$ ,  $P_I=0.6\text{ atm}$

#### *Effect of feed, $F$*

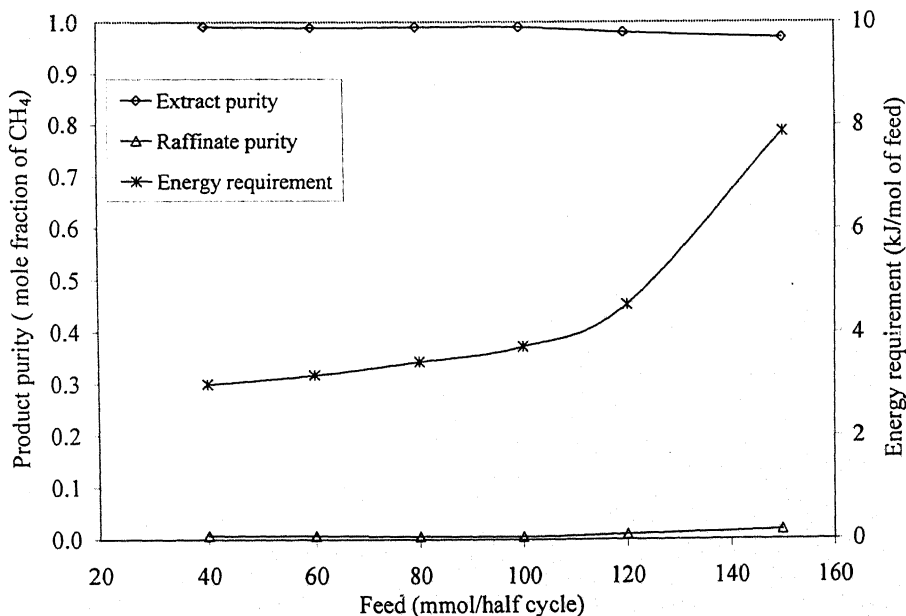


Fig.5.35 Effect of feed;  $P_H=1\text{ atm}$ ,  $P_I=0.5\text{ atm}$ ,  $R_R=0.5$

### Effect of intermediate-desorption pressure, $P_I$

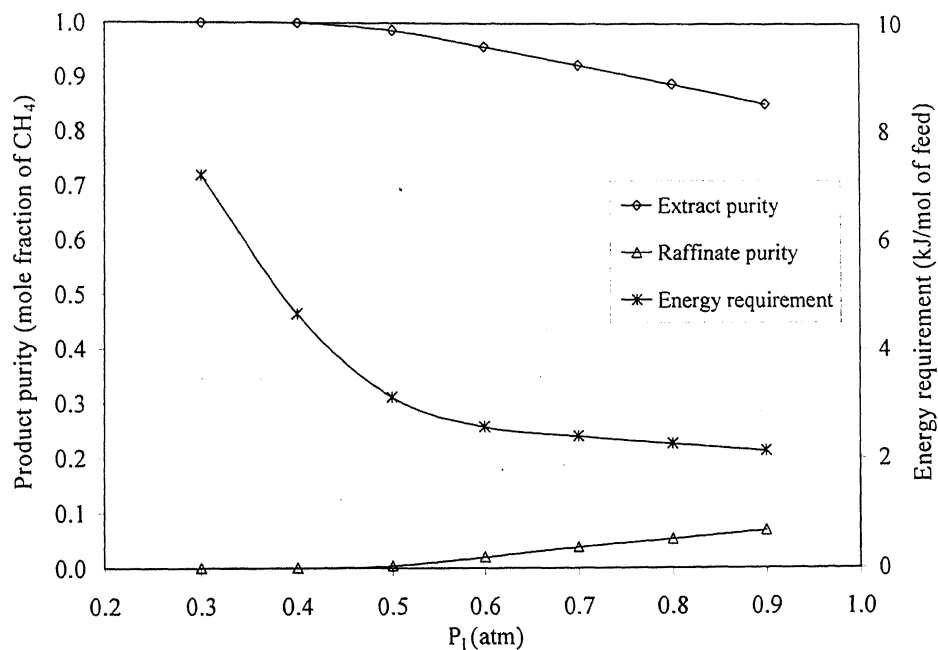


Fig.5.36 Effect of intermediate-desorption pressure;  $F=60$  mmol/half cycle,  $P_H=1$  atm,  $R_R=0.4$

### 5.2.6 Comparison of MV-II duplex and Original duplex PSA

Figures 5.37, 5.38 and 5.39 show the comparative performance of MV-II duplex and Original duplex PSA with change in raffinate recycle ratio, feed and desorption pressure respectively. It can be seen that in all cases, the product purity in the MV-II duplex improved drastically over the purities obtained with the Original duplex.

### Effect of raffinate recycle ratio

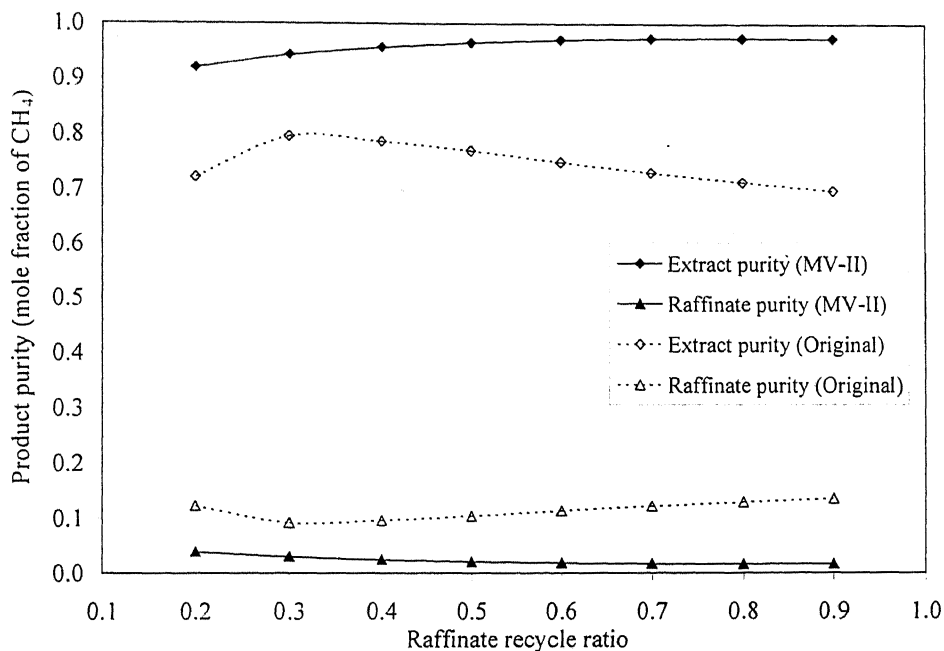


Fig.5.37 Effect of raffinate recycle ratio;  $F=60$  mmol/half cycle,  $P_H=1$  atm,  $P_I=0.6$  atm (MV-II),  $P_L=0.4$  atm (Original)

### Effect of feed

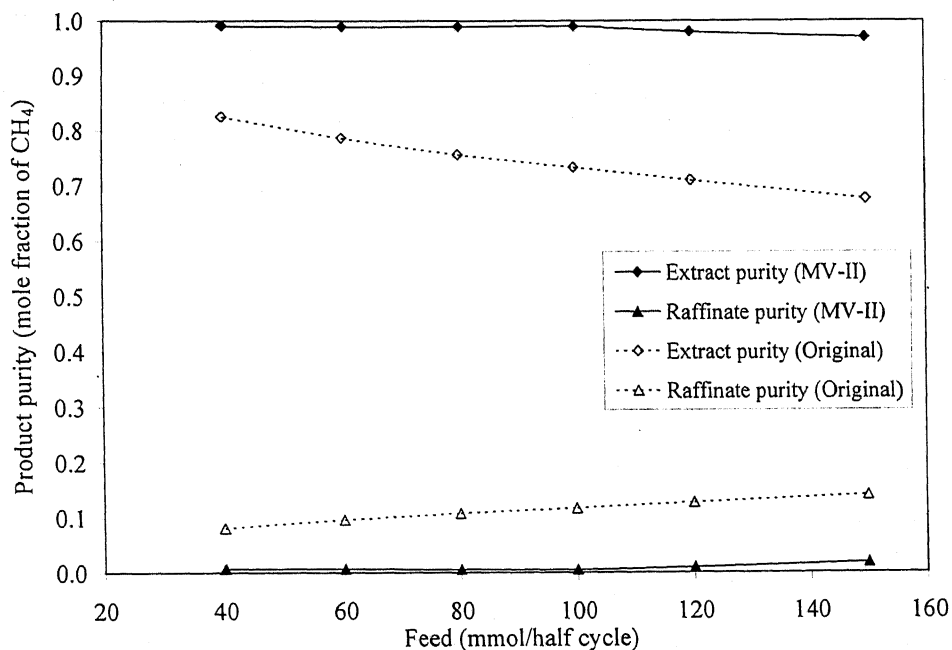


Fig.5.38 Effect of feed;  $P_H=1$  atm,  $P_I=0.5$  atm (MV-II),  $P_L=0.4$  atm (Original)  
 $R_R=0.5$  (MV-II),  $R_R=0.4$  (Original)

## Effect of desorption pressure

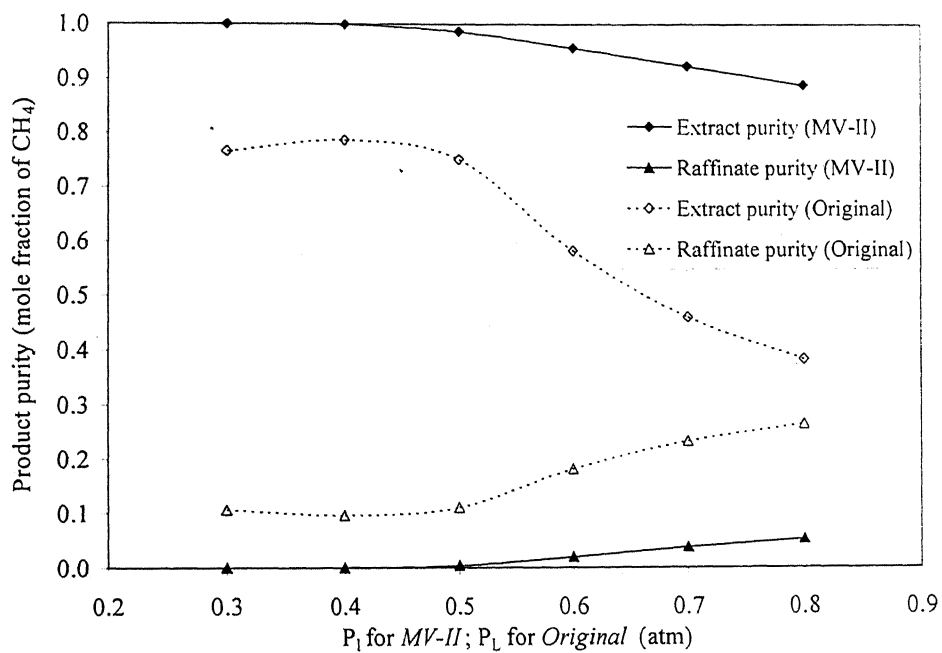


Fig.5.39 Effect of intermediate-desorption (MV-II) or desorption pressure (Original);

$F=60\text{mmol/half cycle}$ ,  $P_H=1\text{ atm}$ ,  $R_R=0.4$

### 5.3 Fractionation of nitrogen-oxygen (N<sub>2</sub>-O<sub>2</sub>) mixture

The equimolar feed composition has been taken to study the fractionation of nitrogen-oxygen system. In this system, both the components get adsorbed unlike the case of CO<sub>2</sub>-N<sub>2</sub> and CH<sub>4</sub>-H<sub>2</sub> systems. We have explored the possibility of fractionation in the duplex PSA. The parameters used in simulation are listed in Table 5.3.

Table 5.3 Parameters used in simulation of fractionation of nitrogen-oxygen mixture

1. Molar feed composition	:	50% N <sub>2</sub> , 50% O <sub>2</sub>
2. Adsorbent	:	Zeolite 5A
3. Particle diameter, <i>cm</i>	:	0.0707
4. Bed voidage	:	0.4
5. Bulk density, <i>kg/m<sup>3</sup></i>	:	670
6. Bed length, <i>cm</i>	:	100
7. Bed diameter, <i>cm</i>	:	2.5
8. Langmuir constant for N <sub>2</sub> (b), <i>m<sup>3</sup>/mol</i>	:	2.813E-03
9. Saturation constant for N <sub>2</sub> (q <sub>s</sub> ), <i>mol/m<sup>3</sup></i>	:	5260.0
10. LDF constant for N <sub>2</sub> , <i>s<sup>-1</sup></i>	:	19.7
11. Langmuir constant for O <sub>2</sub> (b), <i>m<sup>3</sup>/mol</i>	:	8.935E-04
12. Saturation constant for O <sub>2</sub> (q <sub>s</sub> ), <i>mol/m<sup>3</sup></i>	:	5260.0
13. LDF constant for O <sub>2</sub> , <i>s<sup>-1</sup></i>	:	62.0
14. Operating temperature, <i>K</i>	:	298.15
15. Cycle time, <i>s</i> (Original duplex)	:	50
Feed (t <sub>F</sub> ), <i>s</i>	:	20
Blowdown (t <sub>B</sub> ), <i>s</i>	:	5
Purge (t <sub>P</sub> ), <i>s</i>	:	20
Pressurization (t <sub>PR</sub> ), <i>s</i>	:	5
16. Cycle time, <i>s</i> (MV-II duplex)	:	60
Feed (t <sub>F</sub> ), <i>s</i>	:	20
Intermediate-blowdown (t <sub>BI</sub> ), <i>s</i>	:	5
Final-blowdown (t <sub>BF</sub> ), <i>s</i>	:	5
Purge (t <sub>P</sub> ), <i>s</i>	:	20

Pressurization ( $t_{PR}$ ), s	:	5
Frozen ( $t_{FR}$ ), s	:	5

The equilibrium data for nitrogen-oxygen mixture over Zeolite 5A reported by Farooq et. al. (1996) has been used. Figure 5.40 (a) shows the adsorption equilibrium isotherm (total solid phase amount vs. gas phase composition of  $N_2$ ) for different pressures at 298.15 K. Figure 5.40 (b) shows that the separation factor is 3.15 in favor of nitrogen.

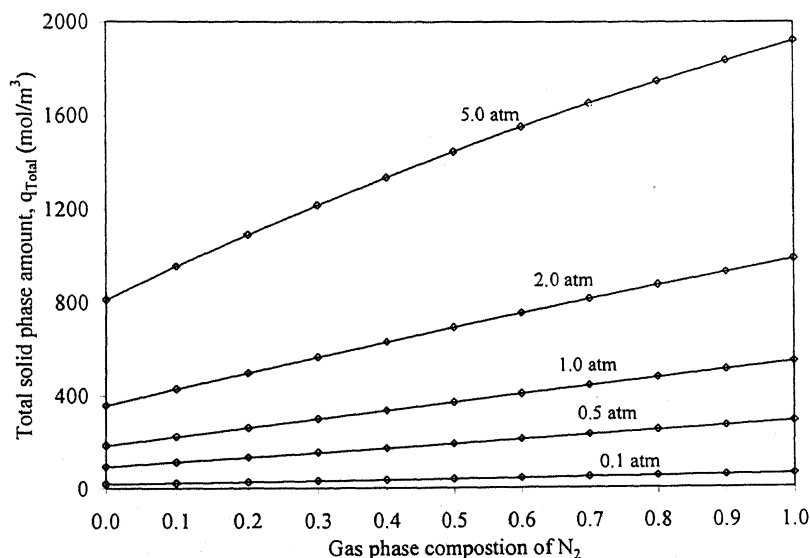


Fig.5.40 (a) Adsorption isotherm of nitrogen-oxygen on Zeolite 5A at 298.15 K

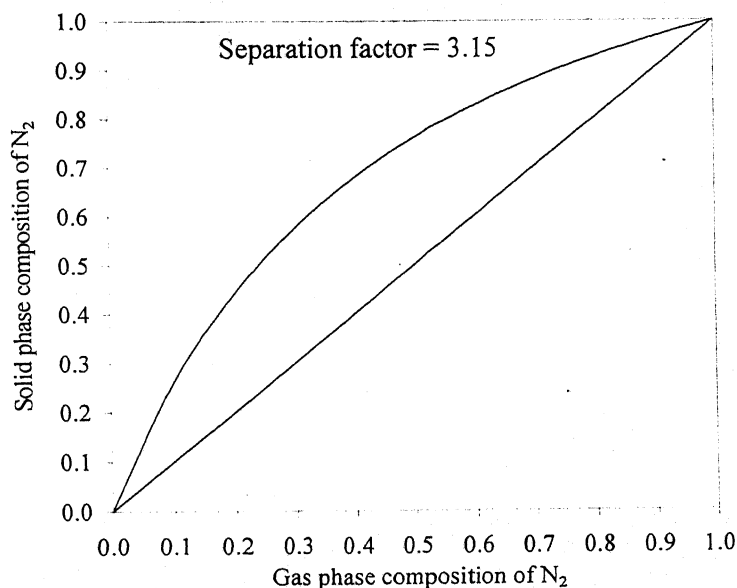


Fig.5.40 (b) Solid phase composition vs. gas phase composition of  $N_2$  at 298.15 K

### 5.3.1 Effect of feed position

Figure 5.41 shows the effect of feed position on the product purity. In the study, the total length of the bed has been divided into 209 equispaced grids. The optimum purity is obtained on introducing feed at 60<sup>th</sup> grid (60 / 209 grid) from extract recycle end of the bed. Figure 5.42 shows the final gas phase concentration profile in the bed undergoing feed step from different positions along the length of the bed.

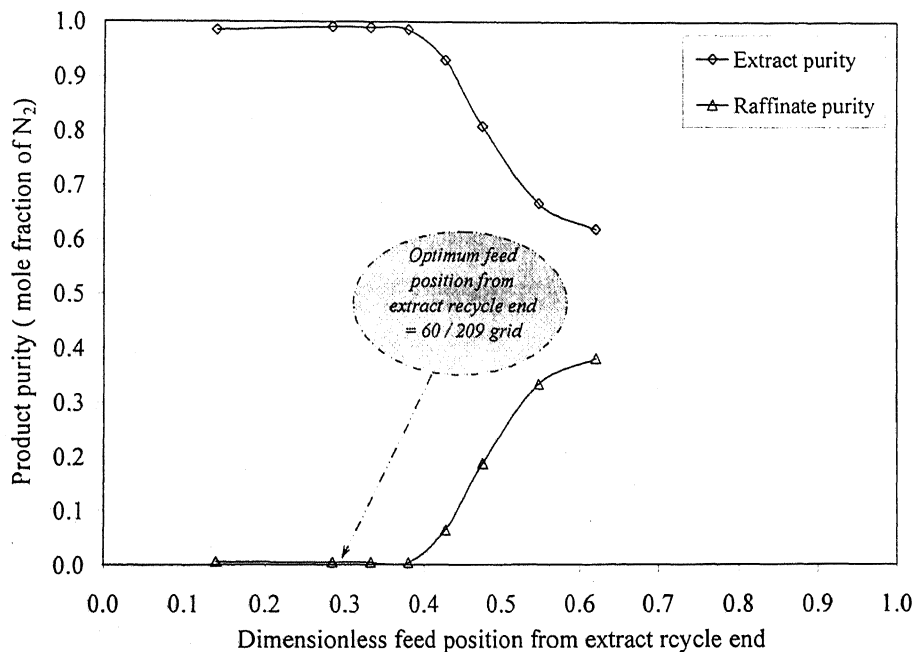


Fig.5.41 Variation in product purity with different position of feed;  $F=60$  mmol/half cycle,  $P_H=4$  atm,  $P_L=1.5$  atm,  $R_R=1.0$

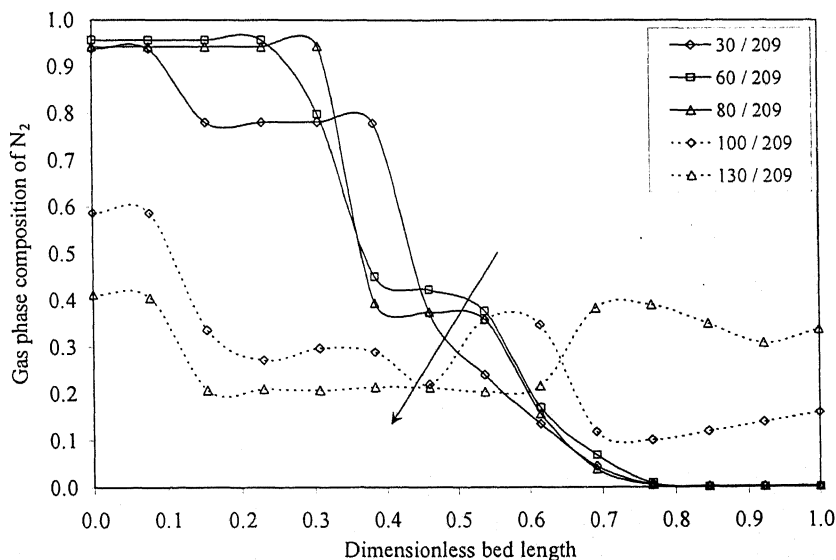


Fig.5.42 Final gas phase concentration profile of  $N_2$  in bed undergoing feed;  $F=60$  mmol/half cycle,  $P_H=4$  atm,  $P_L=1.5$  atm,  $R_R=1.0$

Here onwards we have taken 60<sup>th</sup> grid (optimum) from extract recycle end as the feed position (with total number of grids equal to 209).

### 5.3.2 Original duplex PSA

Figure 5.43 shows the mass balance sheet of the Original duplex for 60 mmol/half cycle of feed. The purity of extract (rich in N<sub>2</sub>) and that of raffinate (rich in O<sub>2</sub>) is only 72%. Figures 5.44 (a, b, c, d, e, f, g, h) show the gas and the solid phase concentration profiles in the bed undergoing feed, blowdown, purge and pressurization step respectively.

It can be seen that, the gas and the solid phase concentration profiles in the bed undergoing feed is not stretched like that of CO<sub>2</sub>-N<sub>2</sub> and CH<sub>4</sub>-H<sub>2</sub> systems. Subsequently, this bed will go for other steps like blowdown, purge and pressurization affecting the overall performance of the Original duplex.

It has been observed that in MV-II duplex PSA, the bed profiles gets stretched throughout the length during the feed step leading to dramatic improvement in product purity.



	N <sub>2</sub>	O <sub>2</sub>
Purity (%)	72.15	72.24
Recovery (%)	72.2	72.0
Productivity (mol/kg-h)	4.7	4.7
Energy requirement (kJ/mol of feed)	9.1	

System : N<sub>2</sub>-O<sub>2</sub>  
Adsorbent : Zeolite 5A

Bed length (cm) = 100  
Bed diameter (cm) = 2.5  
Feed (mmol/half cycle) = 60  
Half cycle time (s) = 20 + 5  
P<sub>H</sub> (atm) = 4.0  
P<sub>L</sub> (atm) = 1.5  
T (K) = 298.15  
R<sub>R</sub> = 1.0

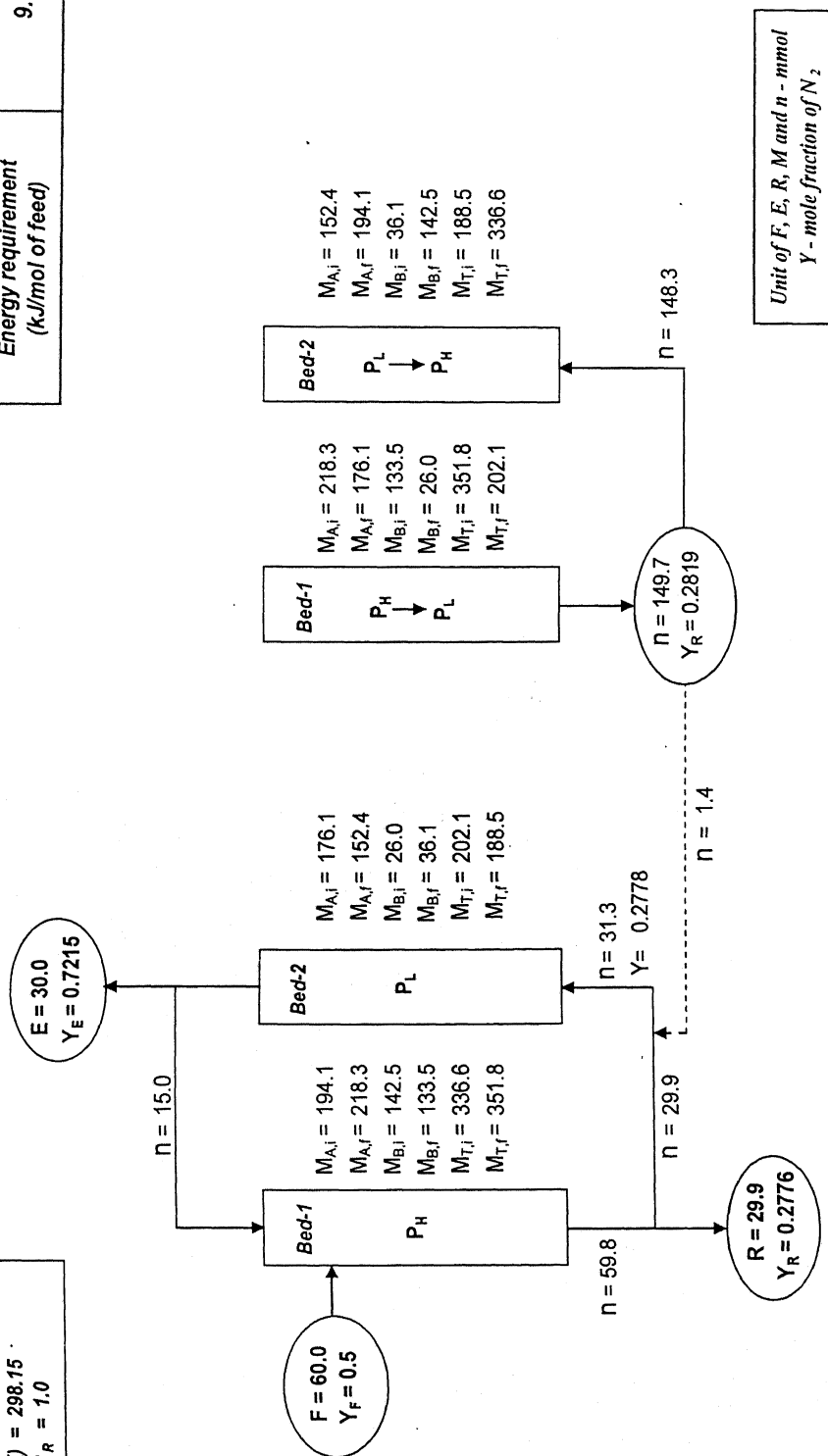


Fig.5.43 Mass balance sheet of Original duplex PSA

Feed

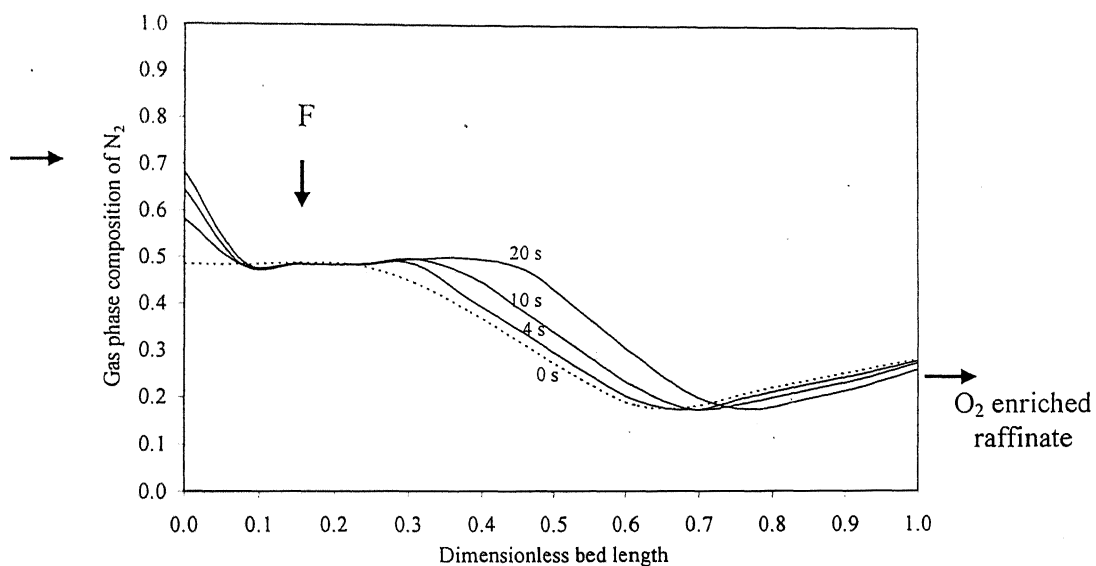


Fig.5.44 (a) Gas phase concentration profile in the bed undergoing feed step (Original duplex)

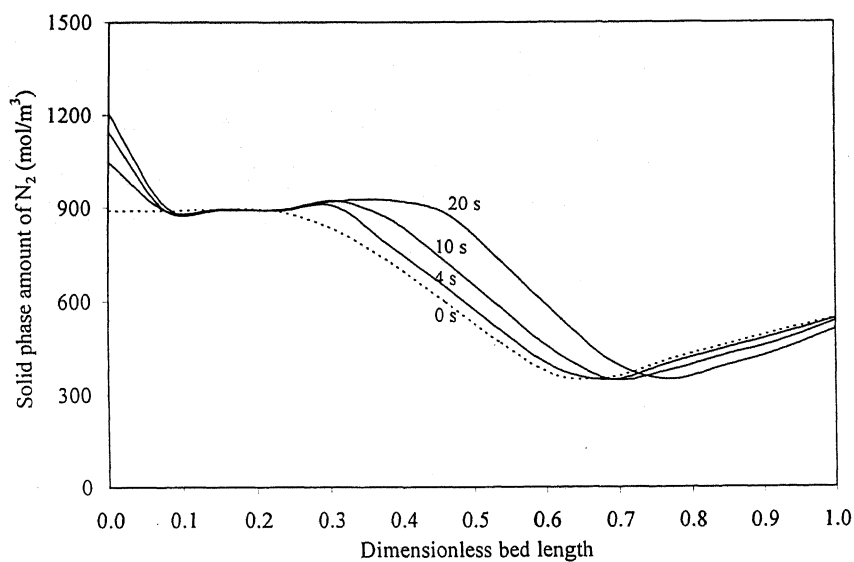


Fig. 5.44 (b) Solid phase concentration profile in the bed undergoing feed step (Original duplex)

## Blowdown

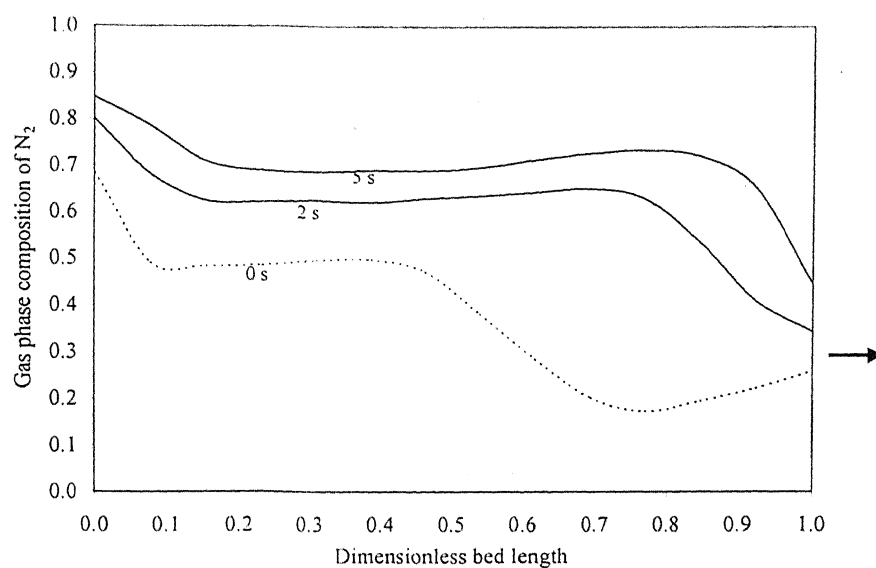


Fig.5.44 (c) Gas phase concentration profile in the bed undergoing blowdown step (Original duplex)

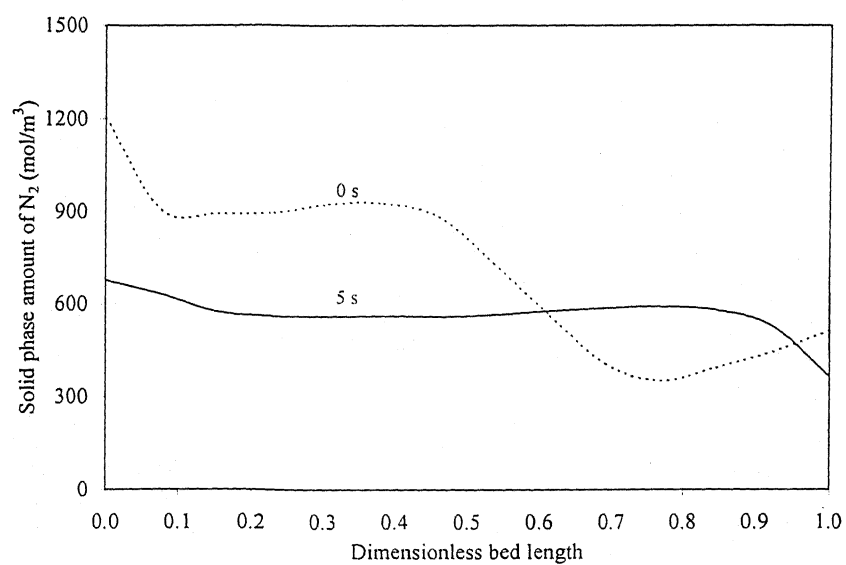


Fig. 5.44 (d) Gas phase concentration profile in the bed undergoing blowdown step (Original duplex)

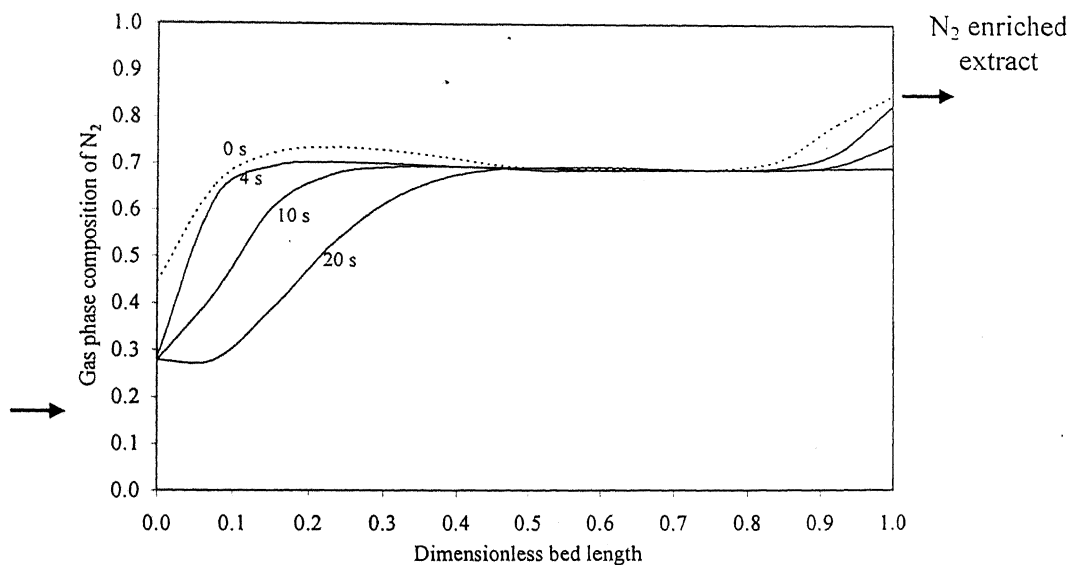


Fig.5.44 (e) Gas phase concentration profile in the bed undergoing purge step (Original duplex)

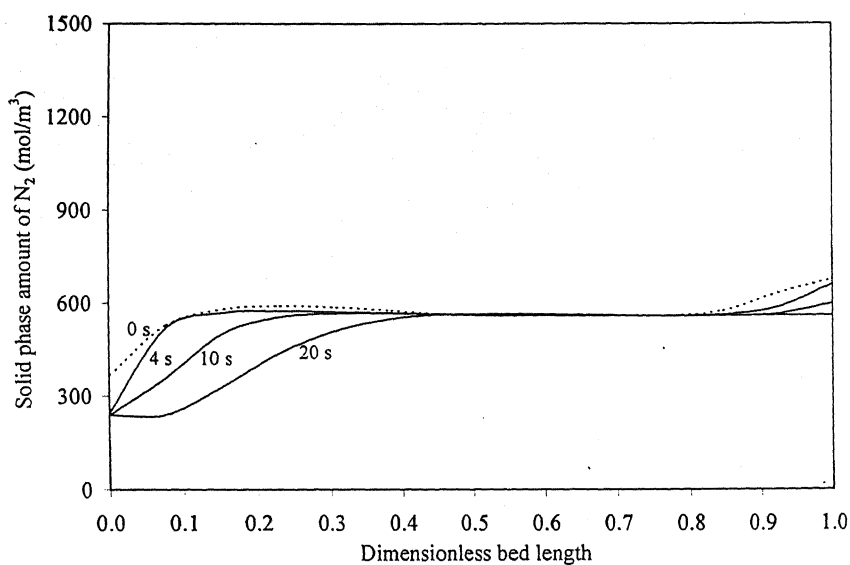


Fig.5.44 (f) Solid phase concentration profile in the bed undergoing purge step (Original duplex)

## Pressurization

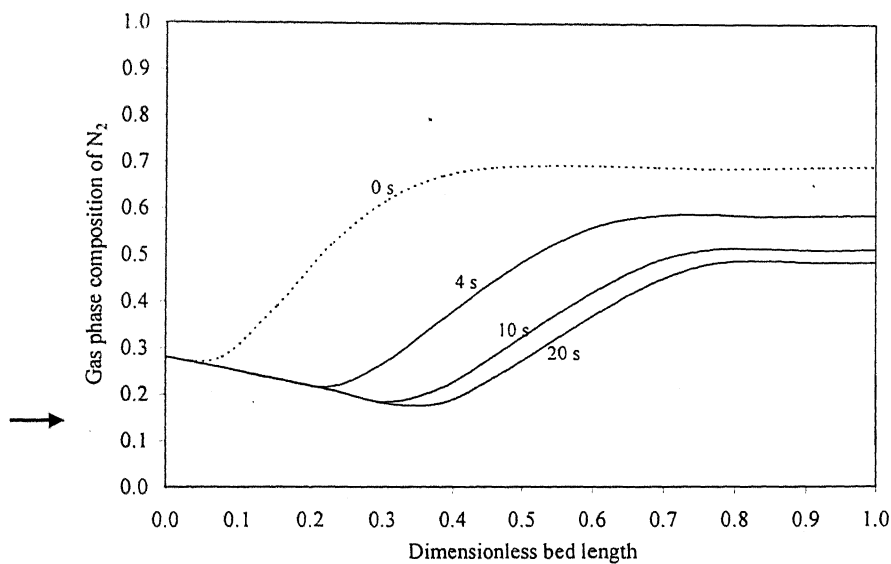


Fig.5.44 (g) Gas phase concentration profile in the bed undergoing pressurization step (Original duplex)

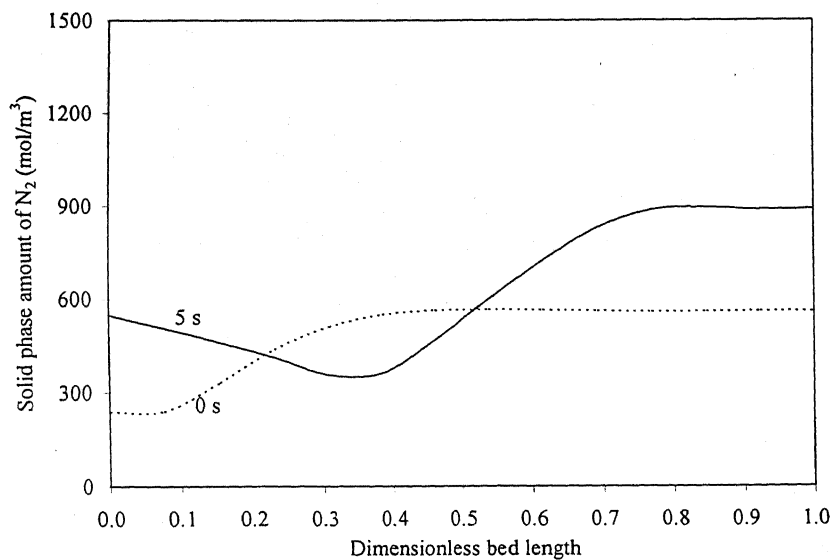


Fig.5.44 (h) Solid phase concentration profile in the bed undergoing pressurization step (Original duplex)

### 5.3.3 MV-II duplex PSA

Figure 5.45 shows the mass balance sheet for MV-II duplex PSA. The purity of extract (rich in  $N_2$ ) improved from 72% to 99.3% with 99.7% recovery and that of raffinate (rich in  $O_2$ ) from 72% to 99.6% with 99.0% recovery over the Original duplex.

The total gas coming out from the bed undergoing intermediate-blowdown step is very large (123 mmol) compared to that of  $CO_2-N_2$  and  $CH_4-H_2$  systems ( $<10$  mmol). This is because of the light component,  $O_2$  is also desorbed significantly when pressure is reduced in the bed from  $P_H$  to  $P_L$  unlike  $N_2$  (non-adsorbing) in the  $CO_2-N_2$  and  $H_2$  (non-adsorbing) in the  $CH_4-H_2$  systems.

As a large amount has to be drawn from the bed undergoing blowdown to reduce the pressure, energy requirement is also large (12.2 kJ/mol of feed) compared to that of  $CO_2-N_2$  system (5.4 kJ/mol of feed) and  $CH_4-H_2$  (4.6 kJ/mol of feed).

Figures 5.46 (a, b, c, d, e, f, g, h, i, j) show the change in the gas phase and the solid phase concentration with time in the bed undergoing feed, intermediate-blowdown, final-blowdown, purge and pressurization steps for the mass balance sheet given in Figure 5.45.

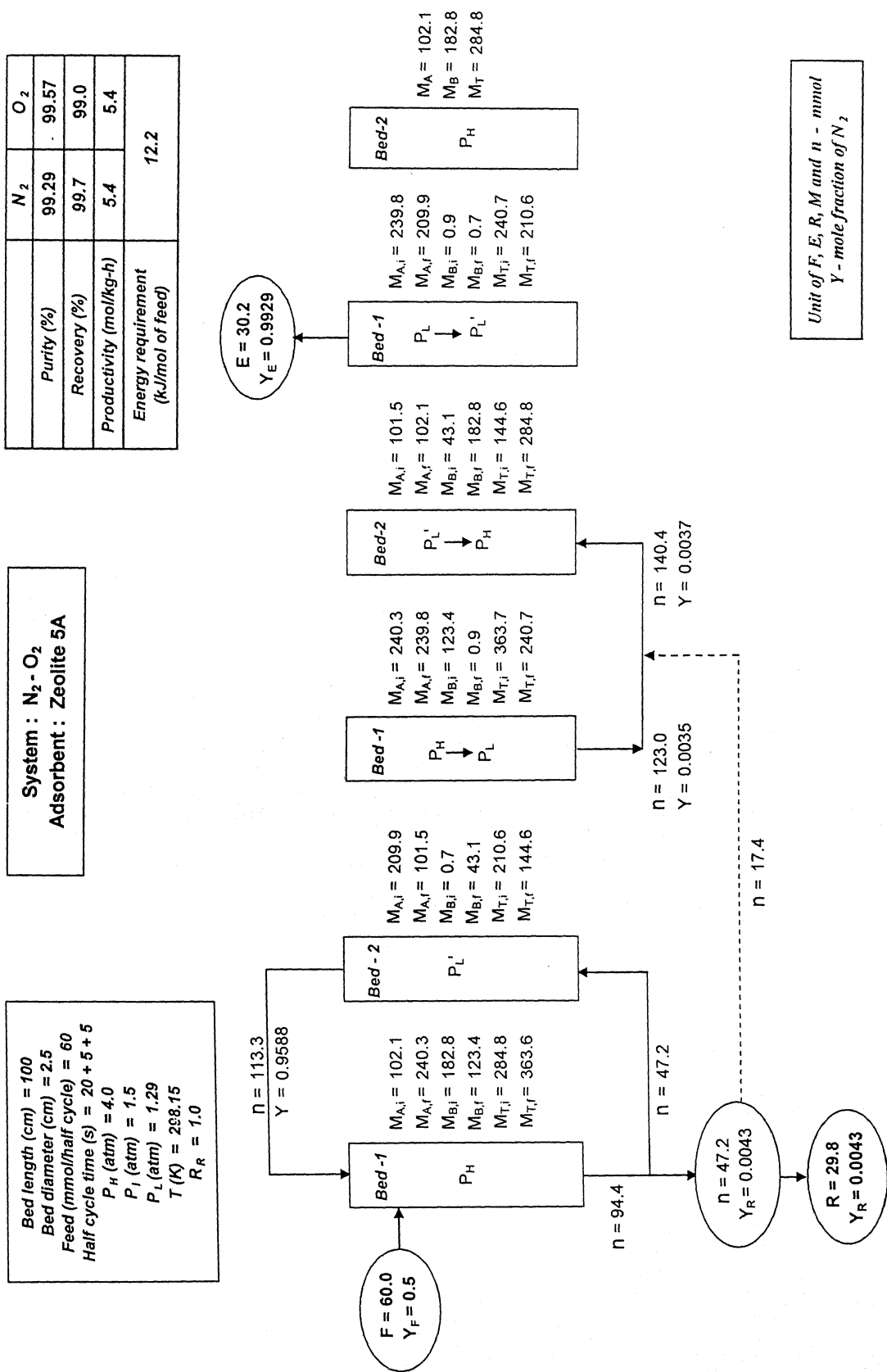


Fig.5.45 Mass balance sheet of MV-II duplex PSA

**Feed:** Figures 5.46 (a) and 5.46 (b) show the gas and the solid phase concentration profile of the feed step. Feed is introduced at 0.28 dimensionless bed length from the extract recycle end (top end). The  $N_2$  from extract recycle and feed gets adsorbed and the raffinate product, rich in  $O_2$  is drawn from the bottom. At the feed position, sudden change in the bed profiles can be observed as feed mixes with a stream of different composition. The bed profiles are stretched throughout the length unlike that of the Original duplex.

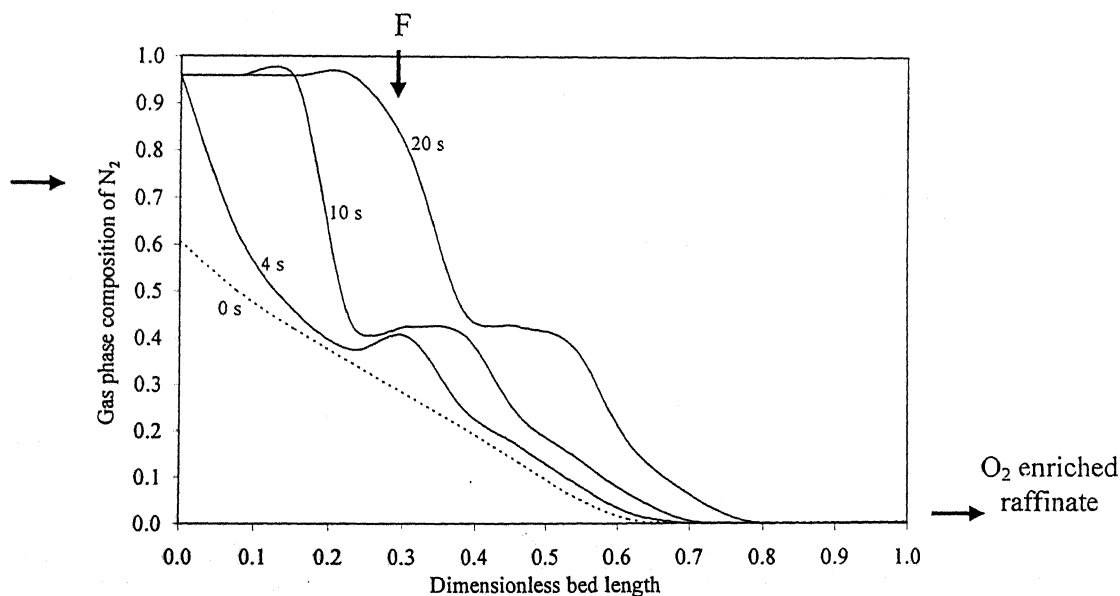


Fig.5.46 (a) Gas phase concentration profile in the bed undergoing feed step (MV-II duplex)

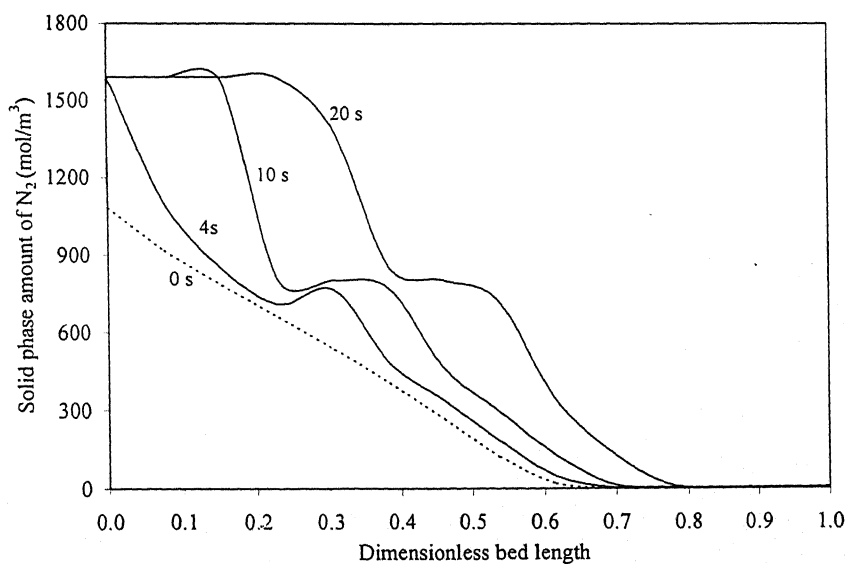


Fig.5.46 (b) Solid phase concentration profile in the bed undergoing feed step (MV-II duplex)



**Intermediate-blowdown:** Figures 5.46 (c) and 5.46 (d) show the gas and the solid phase concentration profiles of the intermediate-blowdown step. The solid phase concentration profile shows that as the pressure reduces from  $P_H$  (4 atm) to  $P_I$  (1.5 atm), the  $N_2$  gets desorbed and then adsorbed like  $CO_2$  in the  $CO_2$ - $N_2$  system and  $CH_4$  in the  $CH_4$ - $H_2$  system. The overall effect is that a little amount of  $N_2$  (0.44 mmol) comes out from the bed. It can be concluded from the three systems studied that the locking effect is independent of whether only one component is adsorbed or both are adsorbed. The component locked inside the bed is always heavy component.

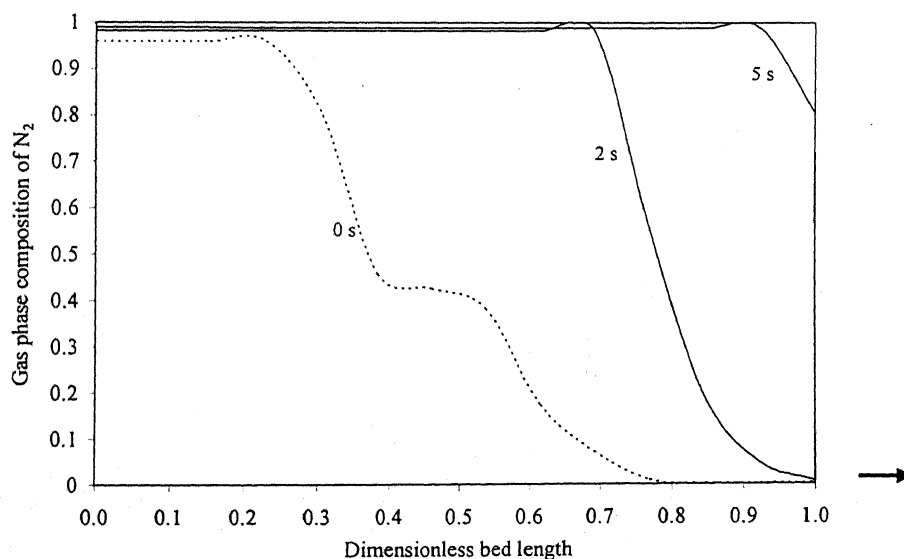


Fig.5.46 (c) Gas phase concentration profile in the bed undergoing intermediate-blowdown step (MV-II duplex)

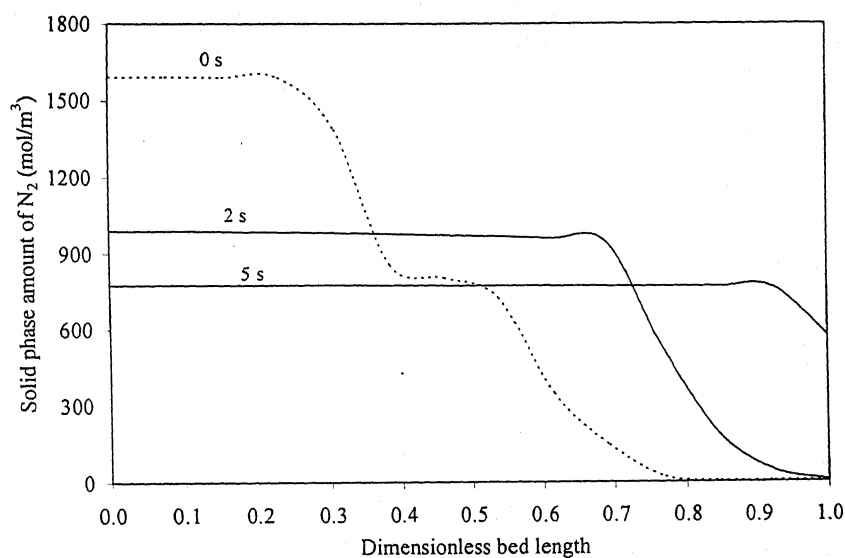


Fig.5.46 (d) Solid phase concentration profile in the bed undergoing intermediate-blowdown step (MV-II duplex)

**Final-blowdown:** Figures 5.46 (e) and 5.46 (f) show the gas and the solid phase concentration profiles of the final-blowdown step. On evacuating the bed from top, the outgoing gas (extract product) is enriched with 99.29%  $N_2$ . To draw 30 mmol extract product, the bed has to be evacuated from  $P_I$  (1.5 atm) to  $P_L$  (1.29 atm).

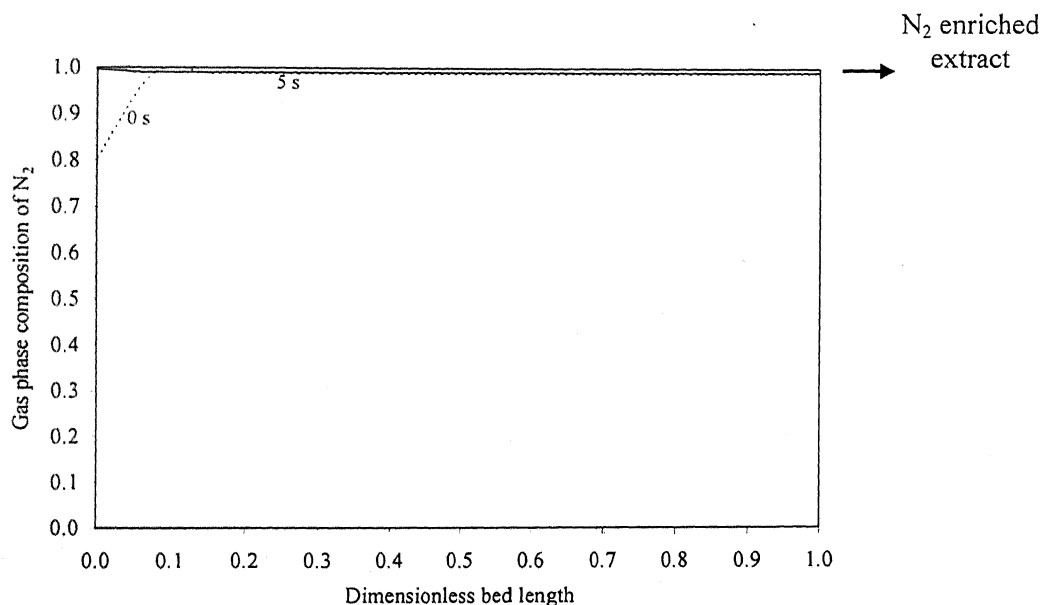


Fig.5.46 (e) Gas phase concentration profile in the bed undergoing final-blowdown step (MV-II duplex)

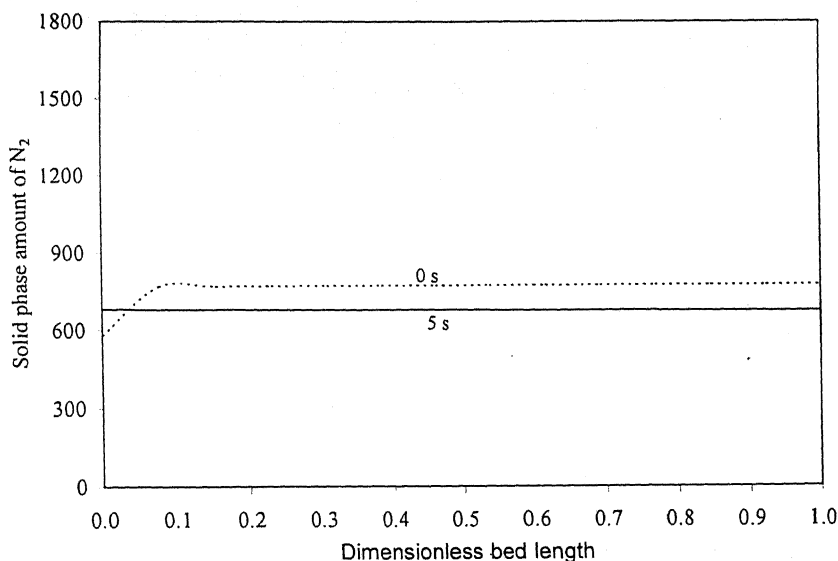


Fig.5.46 (f) Solid phase concentration profile in the bed undergoing final-blowdown step (MV-II duplex)

**Purge:** Figures 5.46 (g) and 5.46 (h) show the gas and the solid phase concentration profiles of the purge step. The bed undergoing purge is at final-desorption pressure (1.29 atm). As the raffinate recycle stream rich in  $O_2$  enters the bed, the gas phase composition of  $N_2$  decreases. This results in the decrease in the partial pressure of  $N_2$  as the total pressure is constant. So, the  $N_2$  gets desorbed and purged off from the bed.

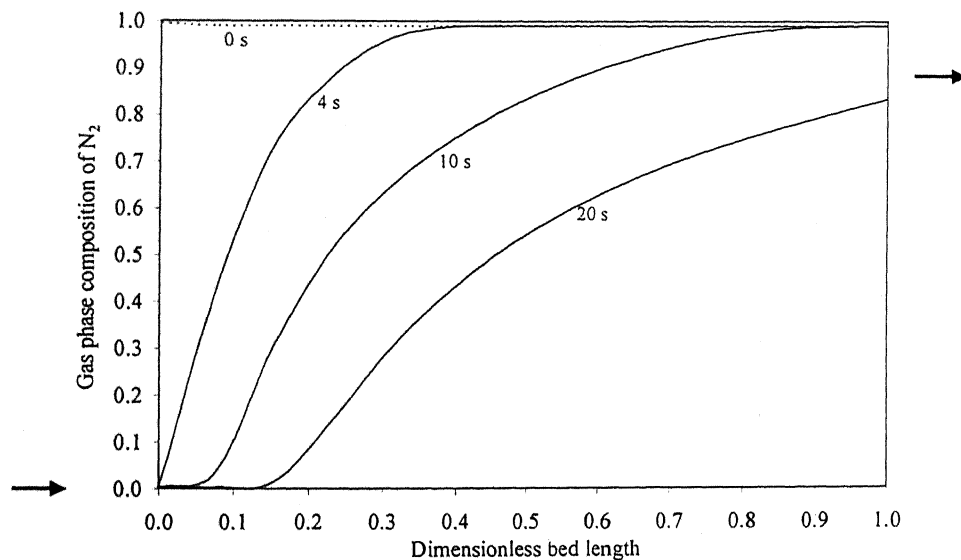


Fig.5.46 (g) Gas phase concentration profile in the bed undergoing purge step (MV-II duplex)

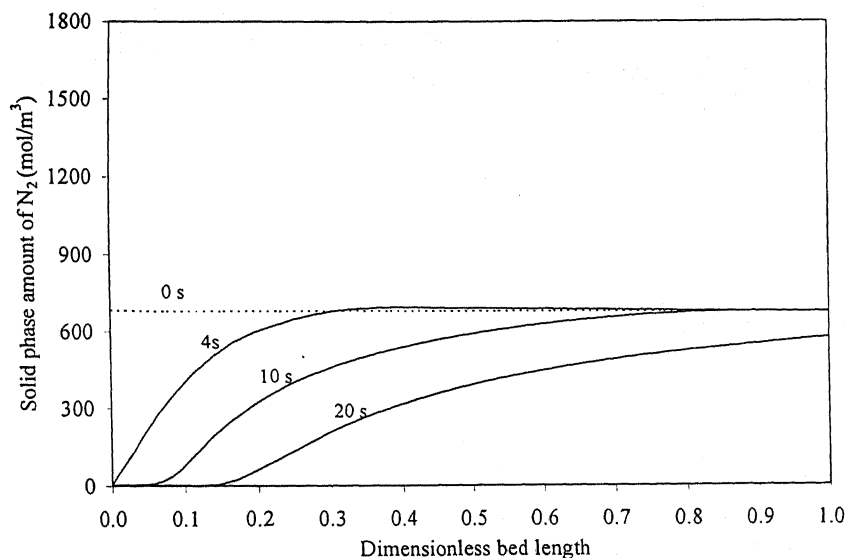


Fig.5.46 (h) Solid phase concentration profile in the bed undergoing purge step (MV-II duplex)

**Pressurization:** Figures 5.46 (i) and 5.46 (j) show the gas and the solid phase concentration profiles of the pressurization step. The bed is pressurized from  $P_I$  (1.29 atm) to  $P_H$  (4 atm). The composition of  $N_2$  in the gas phase decreases as the inlet stream is rich in 99.6%  $O_2$ . The amount required to pressurize the bed is very large (140 mmol) compared to that of the  $CO_2$ - $N_2$  and  $CH_4$ - $H_2$  systems ( $< 10$  mmol) because  $O_2$  entering the bed is also getting adsorbed significantly unlike  $N_2$  and  $H_2$ .

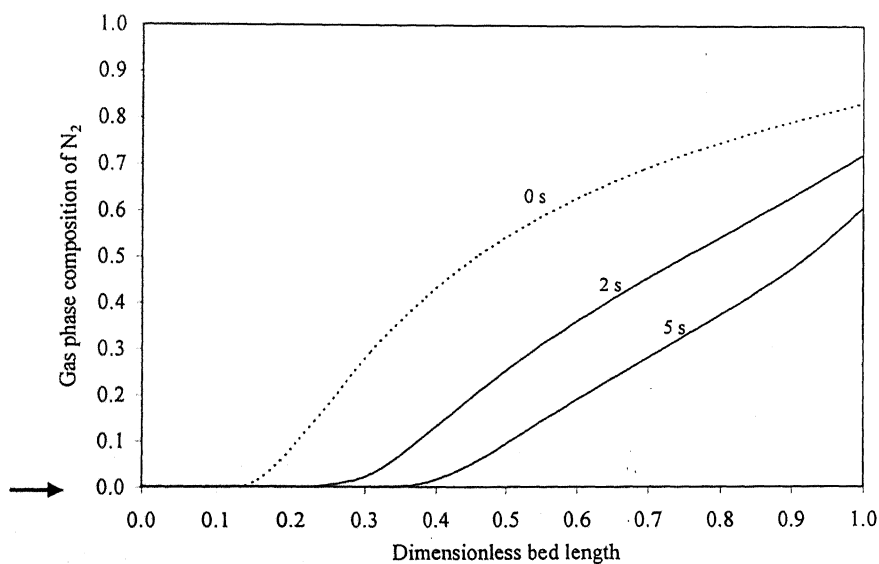


Fig.5.46 (i) Gas phase concentration profile in the bed undergoing pressurization step (MV-II duplex)

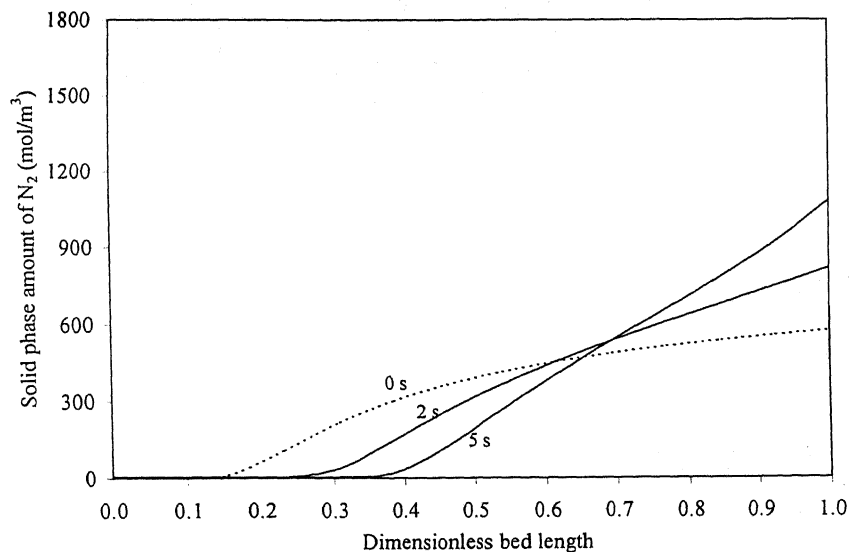


Fig.5.46 (j) Solid phase concentration profile in the bed undergoing pressurization step (MV-II duplex)

### 5.3.4 Comparison of MV-II duplex and Original duplex PSA

Figure 5.47 shows the comparative performance of the MV-II duplex and Original duplex PSA with variation in feed rate. It can be seen that the product purity in MV-II duplex improved drastically over the Original duplex in the feed range studied (60 mmol/half cycle to 100 mmol/half cycle).

*Effect of feed,  $F$*

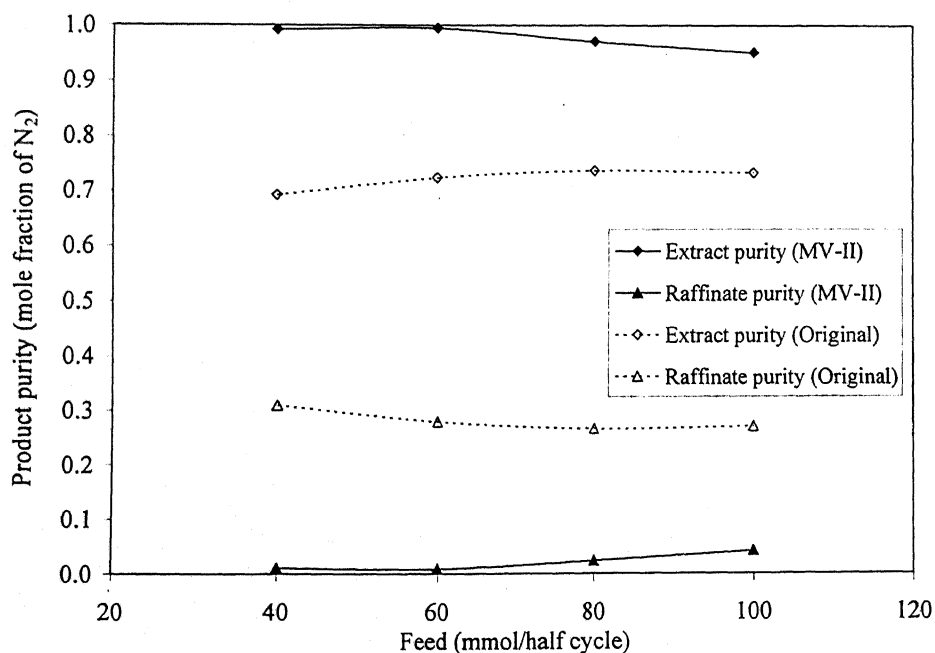


Fig.5.47 Effect of feed;  $P_H=4\text{atm}$ ,  $P_I=1.5\text{ atm}$  (MV-II),  $P_L=1.5\text{ atm}$  (Original)  $R_R=0.5$

## 5.4 Duplex TSA

Carbon dioxide-nitrogen system has been taken to study the possibility of separation in the duplex TSA. The parameters used in simulation are listed in Table 5.4.

Table 5.4 Parameters used in simulation of fractionation of carbon dioxide-nitrogen mixture (TSA)

1. Molar feed composition	:	20% CO <sub>2</sub> , 80% N <sub>2</sub>
2. Feed position	:	middle of the bed
3. Adsorbent	:	Zeolite 13X
4. Particle diameter, <i>cm</i>	:	0.0707
5. Bed voidage	:	0.4
6. Bulk density, <i>kg/m<sup>3</sup></i>	:	750
7. Bed length, <i>cm</i>	:	100
8. Bed diameter, <i>cm</i>	:	2.5
9. Langmuir constant for CO <sub>2</sub> ( <i>b<sub>0</sub></i> ), <i>m<sup>3</sup>/mol</i>	:	303.9
10. Saturation constant for CO <sub>2</sub> ( <i>q<sub>s0</sub></i> ), <i>mol/m<sup>3</sup></i>	:	22352
11. LDF constant for CO <sub>2</sub> , <i>s<sup>-1</sup></i>	:	0.808
12. Heat of adsorption, <i>J/mol</i>	:	3.5E04
13. Temperature parameters, <i>K<sup>-1</sup></i>		
	<i>k<sub>1</sub></i>	: -0.02816
	<i>k<sub>2</sub></i>	: -0.02352
14. Cycle time, <i>s</i>	:	40
	Cooling ( <i>t<sub>C</sub></i> ), <i>s</i>	: 20
	Heating ( <i>t<sub>H</sub></i> ), <i>s</i>	: 20

The temperature dependent Langmuir isotherm data for carbon dioxide-nitrogen mixture over Zeolite 13X reported by Cho et al. (1995) has been used. Nitrogen is non-adsorbing component. Figure 5.48 shows the adsorption isotherm of carbon dioxide on Zeolite 13X at different temperatures and pressures.

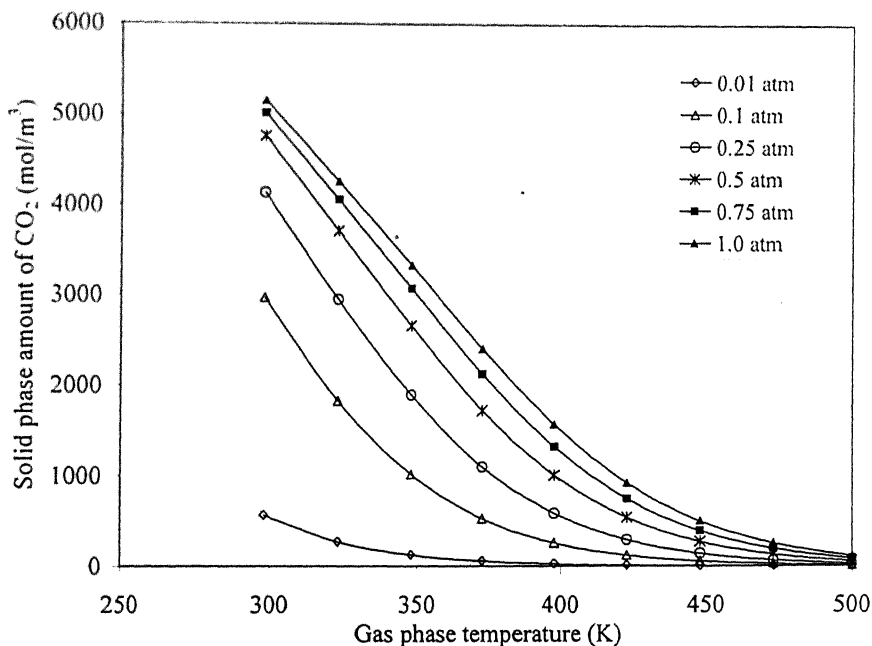


Fig.5.48 Adsorption isotherm of carbon dioxide on Zeolite 13X

In duplex TSA, one bed undergoes cooling (adsorption) and the other bed undergoes heating (desorption). In the present study we have simulated the cooling step and heating step separately. The gas and the solid are at the same temperature. The initial gas phase concentration profile and temperature profile in the bed has been taken to be linear. During the steps, the temperature shift between the two ends of the beds has also been taken as linear. This is the ideal case, and has been taken to study the possible mechanism of separation.

### Cooling step

Figure 5.49 shows the mass balance in cooling step. There are two inlet streams. Feed (10 mmol) is introduced in the middle of the bed. The inlet stream from top of the bed has been taken as pure  $\text{CO}_2$  (20 mmol). Figures 5.50 (a, b, c) show the temperature, gas phase concentration and solid phase concentration profile in the bed. The  $\text{CO}_2$  entering from top end gets adsorbed in the first half. It can be seen from the concentration profiles that at feed position  $\text{CO}_2$  gets desorbed. This may be because of the decrease in gas phase partial pressure of  $\text{CO}_2$  as initial composition of  $\text{CO}_2$  in middle of the bed is 0.5 and feed composition is only 0.2.

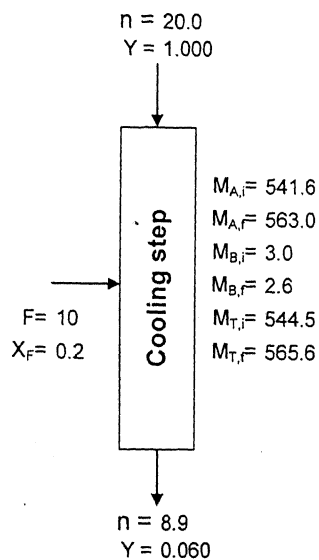


Fig. 5.49 Cooling (feed) step in duplex TSA

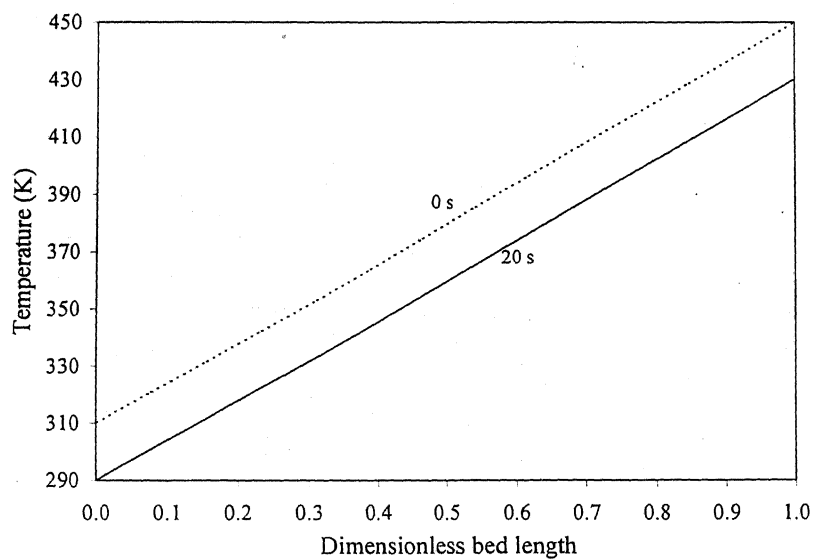


Fig. 5.50 (a) Temperature profile in the bed undergoing cooling step



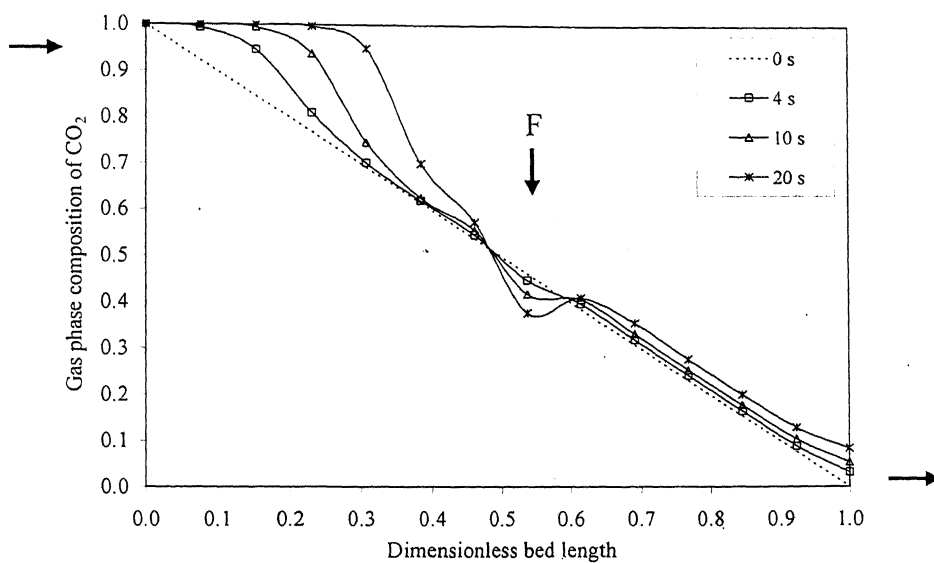


Fig. 5.50 (b) Gas phase concentration profile in the bed undergoing cooling step

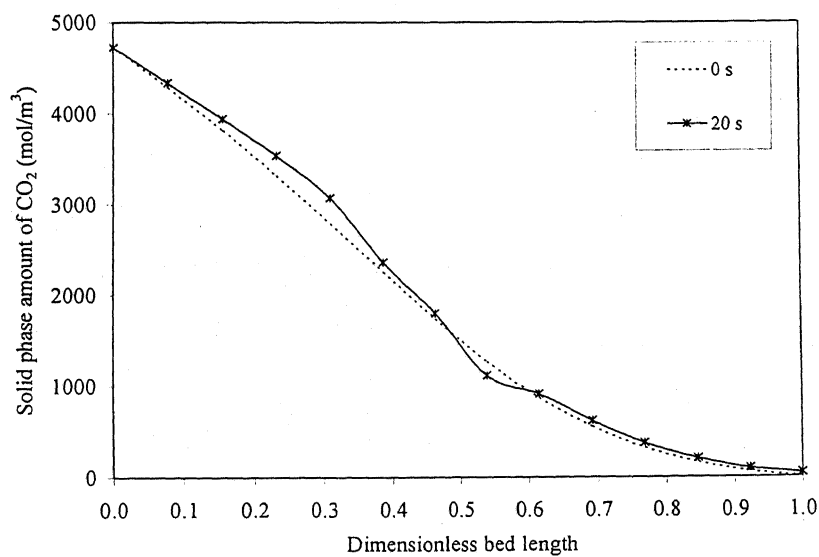


Fig. 5.50 (c) Solid phase concentration profile in the bed undergoing cooling step

## Heating step

Figure 5.51 shows the mass balance in heating step. The inlet stream from bottom of the bed has been taken as pure  $N_2$  (20 mmol). Figures 5.52 (a, b, c) shows the temperature, gas phase concentration and solid phase concentration profile in the bed. The  $CO_2$  gets desorbed as temperature inside the bed increases and then purged off from the top end. The composition of  $CO_2$  in the outgoing stream is 71.8%.

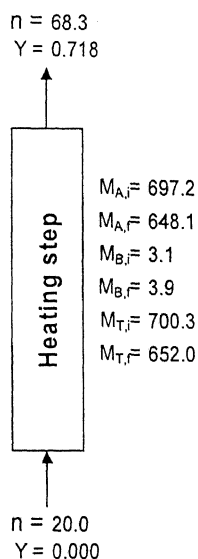


Fig. 5.51 Heating step in duplex TSA

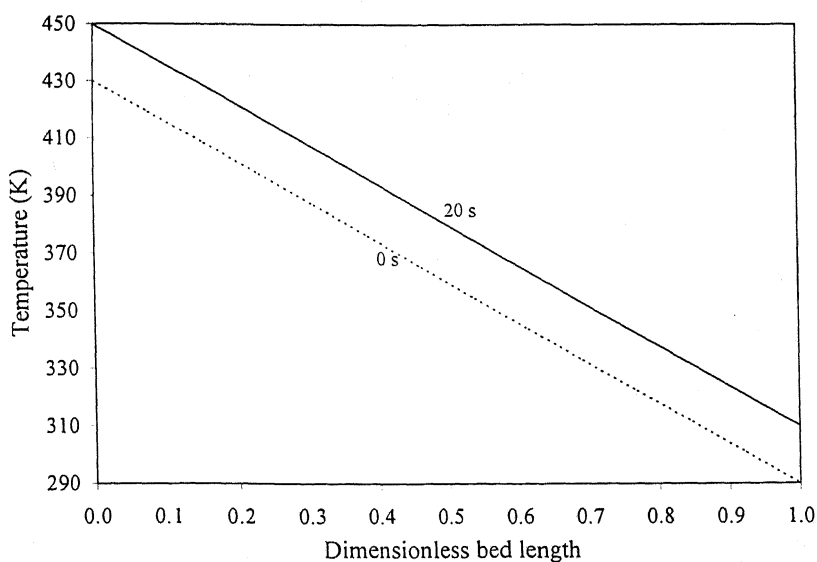


Fig. 5.52 (a) Temperature profile in the bed undergoing heating step

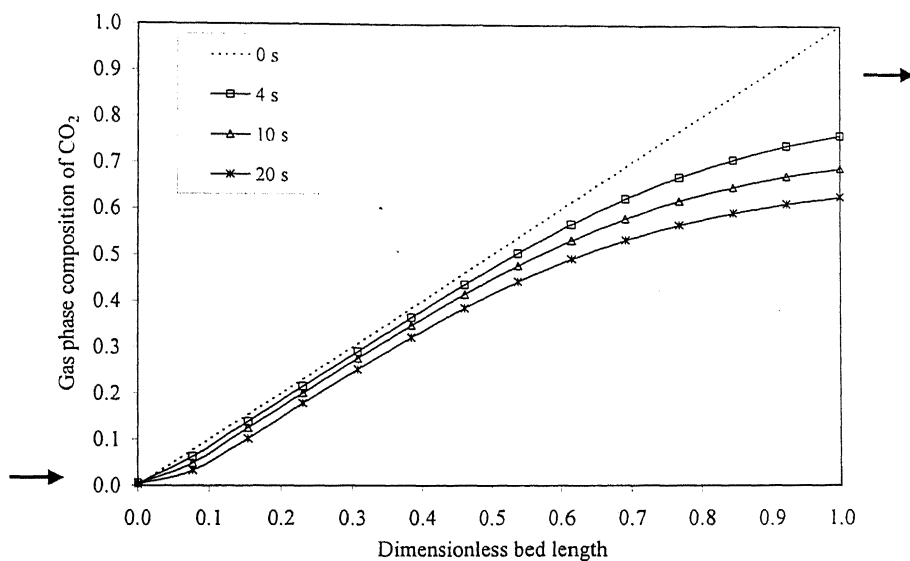


Fig. 5.52 (b) Gas phase concentration profile in the bed undergoing heating step

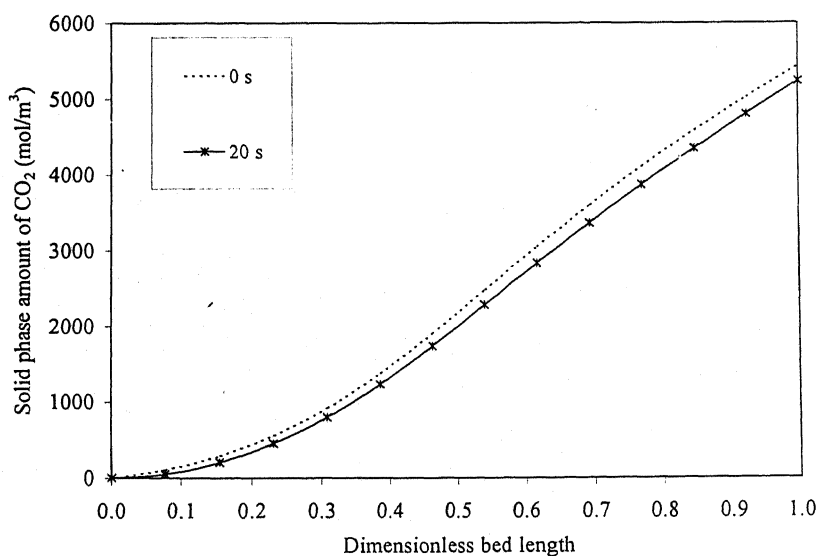


Fig. 5.52 (c) Solid phase concentration profile in the bed undergoing heating step

The above results show that there is a possibility to get separation with the proposed duplex TSA cycle. However, further studies required to develop a feasible process.

### Conclusions

The Original duplex was not able to give sharp separation. To overcome this, modifications in the duplex PSA has been proposed to improve the performance. The parametric studies such as the effect of feed inlet position, raffinate recycle ratio, gas flow rate and desorption pressure were performed to assess the comparative performance of the Original duplex, MV-I duplex and MV-II duplex PSA with  $\text{CO}_2\text{-N}_2$  system ( $\text{N}_2$  was non-adsorbing),  $\text{CH}_4\text{-H}_2$  system ( $\text{H}_2$  was non-adsorbing) and  $\text{N}_2\text{-O}_2$  system (both the components were adsorbing).

In the original duplex PSA, the maximum purity obtained of the heavy component ( $\text{CO}_2$  and  $\text{CH}_4$ ) was 90% and that of the light component ( $\text{N}_2$  and  $\text{H}_2$ ) was 95%. In the  $\text{N}_2\text{-O}_2$  system, maximum purity of both the products obtained was only 75%. The MV-I duplex showed a marginal improvement in the product purity over that of the Original duplex whereas in the MV-II duplex, the purity of both the products improved dramatically to 99+% with 99+% recoveries. The productivity in MV-II duplex PSA was 5-10 times greater than that of the conventional PSAs because of the small cycle time and extended mass transfer zone in the bed.

The equalization and pressurization from both end of the bed viz. rich end (mode-I) and lean end (mode-II) was studied with the  $\text{CO}_2\text{-N}_2$  system. It was observed that the product purity for both the modes was about the same but the energy requirement in the mode-I was 1.5 times more than that in the mode-II.

The energy requirement with the  $\text{N}_2\text{-O}_2$  system (12.2 kJ/mol of feed) was found to be quite large compared to that of the  $\text{CO}_2\text{-N}_2$  system (5.4 kJ/mol of feed) and the  $\text{CH}_4\text{-H}_2$  system (4.6 kJ/mol of feed). This was because of the light component;  $\text{O}_2$  was also desorbed significantly when pressure in the bed was reduced from  $P_H$  to  $P_L$  unlike  $\text{N}_2$  in the  $\text{CO}_2\text{-N}_2$  and  $\text{H}_2$  in the  $\text{CH}_4\text{-H}_2$  system.

Exploratory studies have been made to examine the feasibility of temperature swing adsorption. However, further studies required to establish the feasibility.

## 6.1 Scope of future studies

The possible areas of future studies are as follows:

- Fractionation of multicomponent mixture
- Development of a duplex TSA cycle
- Experimental validation of the simulation study

# References

- Alpay, E. and Scott, D. M., "The Linear Driving Force Model for Fast-cycle Adsorption and Desorption in a Spherical Particle", *Chem. Eng. Sci.*, 47 (2), 499 (1992)
- Chahbani, M. H. and Tondeur, D., "Mass Transfer Kinetics in Pressure Swing Adsorption", *Sep. and Puri. Tech.*, 20, 185 (2000)
- Choong, T. S. Y., Paterson, W. R. and Scott, D. M., "Axial Dispersion in Rich, Binary Gas Mixtures: Model form and Boundary Conditions", *Chem. Eng. Sci.*, 53 (24), 4147 (1998)
- Chue, K. T., Kim, J. N., Yoo, Y. J., Cho, S. H. and Yang, R. T., "Comparison of Activated Carbon and Zeolite 13X for CO<sub>2</sub> Recovery from Flue Gas by Pressure Swing Adsorption", *Ind. Eng. Chem. Res.*, 34 (2), 591 (1995)
- Diagne, D., Goto, M. and Hirose, T., "Parametric Studies on CO<sub>2</sub> Separation and Recovery by a Dual Reflux PSA Process Consisting of both Rectifying and Stripping Sections", *Ind. Eng. Chem. Res.*, 34 (9), 3083 (1995)
- Diagne, D., Goto, M. and Hirose, T., "New PSA Process with Intermediate Feed Inlet Position Operated with Dual Refluxes: Application to Carbon Dioxide Removal and Enrichment", *J. Chem. Eng. Japan*, 27, 85 (1994)
- Diagne, D., Goto, M. and Hirose, T., "Numerical Analysis of a Dual Refluxed PSA Process during Simultaneous Removal and Concentration of Carbon Dioxide Dilute Gas from Air", *J. Chem. Tech. Biotechnol.*, 65, 29 (1996)
- Dong, F., Lou, H., Goto, M. and Hirose, T., "A New Process as an Extension of the Petlyuk Distillation Concept", *Sep. and Puri. Tech.*, 15, 31 (1999)
- Ebner, A.D. and Ritter, J.A., "Equilibrium Theory Analysis of Dual Reflux PSA for Separation of a Binary Mixture", *AIChE J.*, 50 (10), 2418 (2004)
- Farooq, S., Ruthven, D. M. and Boniface, H. A., "Numerical Simulation of a Pressure Swing Adsorption Oxygen Unit", *Chem. Eng. Sci.*, 44 (12), 2809 (1989)
- Fernandes, G.F. and Kenney, C. N., "Modeling of the Pressure Swing Air Separation Process", *Chem. Eng. Sci.*, 38 (6), 827 (1983)

- Hassan, M. M., Raghavan, N. S. and Ruthven, D. M., "Air Separation by Pressure Swing Adsorption on a Carbon Molecular Sieve", *Chem. Eng. Sci.*, 41 (5), 1333 (1986)
- Huang, W. and Chou, C., "A Moving Finite Element Simulation of a Pressure Swing Adsorption Process", *Comp & Chem. Eng.*, 21 (3), 301 (1997)
- Kaczmarek, K., Mazzotti, M., Storti, G. and Morbidelli, M., "Modeling Fixed Bed Adsorption Columns through Orthogonal Collocations on Moving Finite Elements", *Comp & Chem. Eng.*, 21 (6), 641 (1995)
- Keith, P. M., "Industrial Gas: Surveying Onsite Supply Options," *Chem. Eng.*, 72 (1997)
- Keller II, G.E. and Kuo, C.H.A., US Patent 4,354,859 (1982)
- Kikkinides, E. S., Yang, R. T. and Cho, S. H., "Concentration and Recovery of CO<sub>2</sub> from Flue Gas by Pressure Swing Adsorption", *Ind. Eng. Chem. Res.*, 32 (11), 2714 (1993)
- Knaebel, K.S., and Hill, F.B., "Pressure Swing Adsorption: Development of an Equilibrium Theory for Gas Separation." *Chem. Eng. Sci.*, 40 (12), 2351 (1993)
- Knaebel, K.S., US Patent 5,032,150 (1989)
- Ko, D., Kim, M., Moon, H. and Choi, D., "Analysis of Purge Gas Temperature in Cyclic TSA Process", *Chem. Eng. Sci.*, 57 (1), 179 (2002)
- Krishnamoorthy C. P., "Bulk Separation of Gas Mixture using a Novel PSA: Modeling and Simulation", *M.Tech. Thesis*, I.I.T., Kanpur (2002)
- Leavitt, F. W., US Patent No: 5,085,674 (1992)
- Lu, Z.P., Loureiro, J.M. and Rodrigues, A.E., "Simulation of a Three-Step One Column Pressure Swing Adsorption Process," *AIChE J.*, 39 (9), 1483 (1993)
- Malek, A., and Farooq, S. "Comparison of Isotherm Models for Hydrocarbon Adsorption on Activated Carbon", *AIChE J.*, 42 (11), 3191 (1996)
- Malek, A., and Farooq, S., "Hydrogen Purification from Refinery Fuel Gas by Pressure Swing Adsorption," *AIChE J.*, 44 (9), 1985 (1998)
- Mc Intyre, J. A., Holland, C. E. and Ritter, J. A., "High Enrichment and Recovery of Dilute Hydrocarbons by Dual-reflux Pressure-Swing Adsorption", *Ind. Eng. Chem. Res.*, 41 (14), 3499 (2002)
- Mittal, C.P., "Exploratory studies of process intensification in heat regenerator and adsorbers", *M.Tech Thesis*, IIT Kanpur (2004)

- Murthy, D.S., Sivakumar, S.V., Kant, K. and Rao, D.P., "Process Intensification in a Simulated Moving Bed Heat Regenerator", *ASME Heat Trans. /Fluids Eng. Summer Conference*, U.S.A, July 2004
- Nair, A.P., "Simulation Studies on a New Pressure Swing Adsorber similar to Distillation for Fractionation of Gas Mixtures," *M.Tech Thesis*, I.I.T Kanpur (2001)
- Raghavan, N. S., Hassan, M. M. and Ruthven, D. M., "Numerical Simulation of a PSA System-Part-I: Isothermal Trace Component System with Linear Equilibrium and Finite Mass Transfer Resistance," *AIChE J.*, 31 (3), 385 (1985)
- Raghavan, N. S. and Ruthven, D. M., "Pressure Swing Adsorption Part-III: Numerical Simulation of a Kinetically Controlled Bulk Gas Separation," *AIChE J.*, 31 (12), (1985)
- Raghavan, N. S., Hassan M. M. and Ruthven, D. M., "Numerical Simulation of a PSA System Using a Pore Diffusion Model," *Chem. Eng. Sci.*, 41 (11), 2787 (1986)
- Rao, D. P., Sivakumar, S. V., Mandal, S., Kota, S., Ramprasad, B. S. G., "Novel Simulated Moving-Bed Adsorber for the Fractionation of Gas Mixture," *J. Chromatography A*, 1069, 141 (2005)
- Rao, D. P., "The Futility of Raffinate Reflux Revised", *Can. J. of Chem. Eng.*, 77, 74 (1999)
- Rege, S.U. and Yang, R.T., "Limits for Air Separation by Adsorption with LiX Zeolite", *Ind. Eng. Chem. Res.*, 36 (12), 5358 (1997)
- Ruthven, D. M., Farooq, S. and Knaebel, K. S., "Pressure Swing Adsorption", VCH Publishers, New York (1993)
- Sircar, S. and Zondlo, J. W., US Patent 4,013,429 (1977)
- Sun, L.M., and Meunier, F., "An Improved Finite Difference Method for Fixed-Bed Multicomponent Sorption," *AIChE J.*, 37 (2), 244 (1991)
- Sun, L.M., Le Quere, P. and Levan, M.D., "Numerical Simulation of Diffusion-limited PSA Process Models by Finite Difference Methods," *Chem. Eng. Sci.*, 51 (24), 5341 (1996)
- Wakao, N. and Kaguei, S., "Heat and Mass Transfer in Packed Beds", Gordon and Breach Science Publishers (1982)
- Wen, C. Y., Fan, L. T. and Dekker, M., "Models for Flow Systems and Chemical Reactor", *Math. and Comp. in Simu*, 20 (3), 211 (1978)
- Wilson, P., US Patent 4,359,328 (1982)

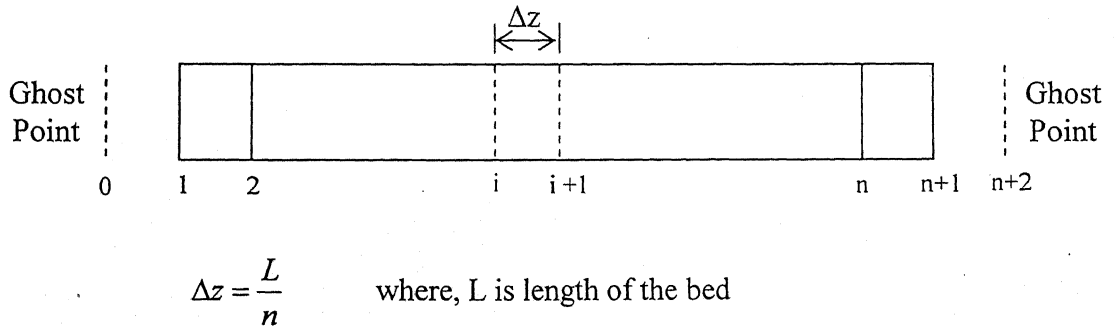


- Yang, R. T., "Gas Separation by Adsorption Processes", Butterworths Publishers, Boston (1987)
- Yang, R.T. and Cen, P., "Bulk Gas Separation by Pressure Swing Adsorption," *Ind. Eng. Chem. Fundam.*, 25, 758 (1986)
- Yang, R.T. and Doong, S. J., "Gas Separation by Pressure Swing Adsorption: A Pore Diffusion Model for Bulk Separation," *AIChE J.*, 31 (11), 1829 (1985)
- Yang, R. T. and Doong, S. J., "Bulk Separation of Multicomponent Gas Mixtures by Pressure Swing Adsorption: Pore / Surface Diffusion and Equilibrium Models," *AIChE J.*, 32 (3), 397 (1986)
- Yoshida, M., Ritter, J. A., Kodama, A., Goto, M. and Hirose, T., "Enriching Reflux and Parallel Equalization PSA Process for Concentrating Trace Components in Air," *Ind. Eng. Chem. Res.*, 42 (8), 1795 (2003)

## Appendix - A

The governing partial differential equations (PDE's) with the boundary conditions derived in Chapter-4 are discretized in space domain using central difference scheme of the finite difference method (FDM).

A schematic diagram of the bed with grids is shown below. The total length of the bed has been divided into  $n+1$  grids. Grid '0' and 'n+2' represents ghost points. In the discretized equations at grid '1' and 'n+1', we need values of variables at ghost point '0' and 'n+2' respectively which are not known. These ghost point values are replaced by the known values at the nearby grids using the appropriate boundary conditions.



The discretized governing equations and the boundary conditions for the duplex PSA and the duplex TSA are given below. In equations, subscript  $i$  represents grid and  $j$  represents component.

### A.1 Discretized governing equations

#### A.1.1 Duplex PSA

Pressure profile; Equation (4.16)

$$\frac{dP_i}{dt} = K \left[ P_i \left( \frac{P_{i+1} - 2P_i + P_{i-1}}{(\Delta z)^2} \right) + \left( \frac{P_{i+1} - P_{i-1}}{2\Delta z} \right)^2 \right] - \frac{(1-\varepsilon)}{\varepsilon} RT_g \sum_{j=1}^N \frac{dq_{i,j}}{dt}$$

Concentration profile in the gas phase; Equation (4.17)

$$\frac{dy_i}{dt} = \frac{D_{i,o}}{P_i} \left( \frac{y_{i+1} - 2y_i + y_{i-1}}{(\Delta z)^2} \right) + K \left( \frac{y_{i+1} - y_{i-1}}{2\Delta z} \right) \left( \frac{P_{i+1} - P_{i-1}}{2\Delta z} \right) + \frac{(1-\varepsilon)}{\varepsilon} \frac{RT_g}{P_i} \left( y_i \sum_{j=1}^N \frac{dq_{i,j}}{dt} - \frac{dq_{i,1}}{dt} \right)$$

Concentration profile in the solid phase; Equation (4.18)

$$\frac{dq_{i,j}}{dt} = k_j (q_{i,j}^* - q_{i,j})$$

### A.1.2 Duplex TSA

Pressure profile; Equation (4.14)

$$\begin{aligned} \frac{dP_i}{dt} = D_{i,o} & \left[ \frac{2}{T_{g,i}^2} \left( \frac{T_{g,i+1} - T_{g,i-1}}{2\Delta z} \right)^2 - \frac{1}{T_{g,i}} \left( \frac{T_{g,i+1} - 2T_{g,i} + T_{g,i-1}}{(\Delta z)^2} \right) \right] + K \left[ P_i \left( \frac{P_{i+1} - 2P_i + P_{i-1}}{(\Delta z)^2} \right) \right. \\ & \left. + \left( \frac{P_{i+1} - P_{i-1}}{2\Delta z} \right)^2 - \frac{P_i}{T_{g,i}} \left( \frac{P_{i+1} - P_{i-1}}{2\Delta z} \right) \left( \frac{T_{g,i+1} - T_{g,i-1}}{2\Delta z} \right) + \frac{P_i}{T_{g,i}} \left( \frac{\partial T_{g,i}}{\partial t} \right) - RT_{g,i} \frac{(1-\varepsilon)}{\varepsilon} \sum_{j=1}^N \frac{dq_{i,j}}{dt} \right] \end{aligned}$$

Concentration profile in the gas phase; Equation (4.15)

$$\begin{aligned} \frac{dy_i}{dt} = \frac{D_{i,o}}{P_i} & \left[ \left( \frac{y_{i+1} - 2y_i + y_{i-1}}{(\Delta z)^2} \right) - \frac{2}{T_{g,i}} \left( \frac{y_{i+1} - y_{i-1}}{2\Delta z} \right) \left( \frac{T_{g,i+1} - T_{g,i-1}}{2\Delta z} \right) \right] + K \left( \frac{y_{i+1} - y_{i-1}}{2\Delta z} \right) \left( \frac{P_{i+1} - P_{i-1}}{2\Delta z} \right) \\ & + \frac{(1-\varepsilon)}{\varepsilon} \frac{RT_{g,i}}{P_i} \left[ y_i \sum_{j=1}^N \frac{dq_{i,j}}{dt} - \frac{dq_{i,1}}{dt} \right] \end{aligned}$$

Concentration profile in the solid phase; Equation (4.18)

$$\frac{dq_{i,j}}{dt} = k_j (q_{i,j}^* - q_{i,j})$$

Temperature profile in the gas phase; Equation (4.21)

$$\frac{dT_{g,i}}{dt} = \alpha \left( \frac{T_{g,i+1} - 2T_{g,i} + T_{g,i-1}}{(\Delta z)^2} \right) + K \left( \frac{P_{i+1} - P_{i-1}}{2\Delta z} \right) \left( \frac{T_{g,i+1} - T_{g,i-1}}{2\Delta z} \right) - \frac{h_p a_s}{\varepsilon \rho_g C_{pg}} (T_{g,i} - T_{s,i})$$

Temperature profile in the solid phase; Equation (4.23)

$$\frac{dT_{s,i}}{dt} = \frac{1}{\rho_s C_{ps}} \sum_{j=1}^N (-\Delta H)_j \frac{\partial q_{i,j}}{\partial t} - \frac{h_p a_s}{\rho_s C_{ps} (1 - \varepsilon)} (T_{g,i} - T_{s,i})$$

## A.2 Discretized boundary conditions

### A.2.1 Duplex PSA

#### ➤ *Blowdown step*

- at  $z = 0$

$$\left. \frac{\partial y}{\partial z} \right|_{z=0} = 0 \quad \Rightarrow \quad y_0 = y_2$$

$$\left. \frac{\partial P}{\partial z} \right|_{z=0} = 0 \quad \Rightarrow \quad P_0 = P_2$$

- at  $z = L$

$$\left. \frac{\partial y}{\partial z} \right|_{z=L} = 0 \quad \Rightarrow \quad y_{n+2} = y_n$$

$$\left. \frac{\partial P}{\partial z} \right|_{z=L} = -\frac{v_f}{K} \quad \Rightarrow \quad P_{n+2} = P_n - 2\Delta z \left( \frac{v_f}{K} \right)$$

#### ➤ *Purge step*

- at  $z = 0$

$$\left. \frac{\partial y}{\partial z} \right|_{z=0} = -\frac{v_f}{D_L} (y_{in} - y|_{z=0}) \quad \Rightarrow \quad y_0 = y_2 + 2\Delta z \left( \frac{v_f}{D_L} \right) (y_{in} - y_1)$$

$$\left. \frac{\partial P}{\partial z} \right|_{z=0} = -\frac{v_f}{K} \quad \Rightarrow \quad P_0 = P_2 + 2\Delta z \left( \frac{v_f}{K} \right)$$

- at  $z = L$

$$\left. \frac{\partial y}{\partial z} \right|_{z=L} = 0 \quad \Rightarrow \quad y_{n+2} = y_n$$

$$\left. \frac{\partial P}{\partial t} \right|_{z=L} = 0$$

### ➤ Pressurization step

- at  $z = 0$

$$\left. \frac{\partial y}{\partial z} \right|_{z=0} = -\frac{v_f}{D_L} (y_{in} - y|_{z=0}) \quad \Rightarrow \quad y_0 = y_2 + 2\Delta z \left( \frac{v_f}{D_L} \right) (y_{in} - y_1)$$

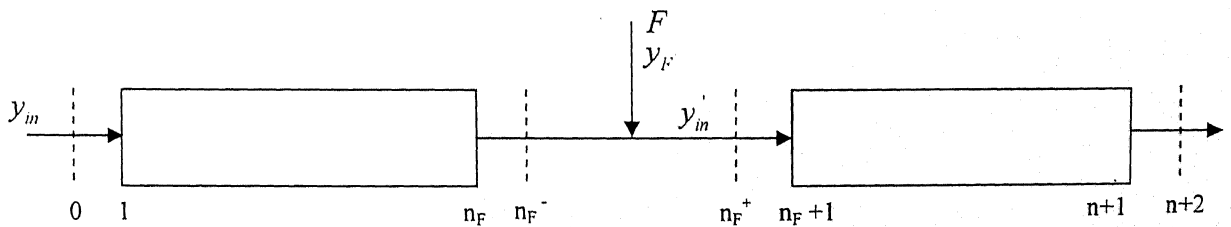
$$\left. \frac{\partial P}{\partial z} \right|_{z=0} = -\frac{v_f}{K} \quad \Rightarrow \quad P_0 = P_2 + 2\Delta z \left( \frac{v_f}{K} \right)$$

- at  $z = L$

$$\left. \frac{\partial y}{\partial z} \right|_{z=L} = 0 \quad \Rightarrow \quad y_{n+2} = y_n$$

$$\left. \frac{\partial P}{\partial z} \right|_{z=L} = 0 \quad \Rightarrow \quad P_{n+2} = P_n$$

### ➤ Feed step



- at  $z = 0$

$$\left. \frac{\partial y}{\partial z} \right|_{z=0} = -\frac{v_f}{D_L} (y_m - y|_{z=0}) \Rightarrow y_0 = y_2 + 2 \Delta z \left( \frac{v_f}{D_L} \right) (y_m - y_1)$$

$$\left. \frac{\partial P}{\partial z} \right|_{z=0} = -\frac{v_f}{K} \Rightarrow P_0 = P_2 + 2 \Delta z \left( \frac{v_f}{K} \right)$$

- at  $z = z_F^-$

$$\left. \frac{\partial y}{\partial z} \right|_{z=z_F^-} = 0 \Rightarrow y_{n_F^-} = y_{n_F-1}$$

$$\left. \frac{\partial P}{\partial t} \right|_{z=z_F^-} = 0$$

- at  $z = z_F^+$

$$\left. \frac{\partial y}{\partial z} \right|_{z=z_F^+} = -\frac{v_f}{D_L} (y_m - y|_{z=z_F^+}) \Rightarrow y_{n_F^+} = y_{n_F+2} + 2 \Delta z \left( \frac{v_f}{D_L} \right) (y_m - y_{n_F+1})$$

$$\left. \frac{\partial P}{\partial z} \right|_{z=z_F^+} = -\frac{v_f}{K} \Rightarrow P_{n_F^+} = P_{n_F+2} + 2 \Delta z \left( \frac{v_f}{K} \right)$$

- at  $z = L$

$$\left. \frac{\partial y}{\partial z} \right|_{z=L} = 0 \Rightarrow y_{n+2} = y_n$$

$$\left. \frac{\partial P}{\partial t} \right|_{z=L} = 0$$

$z_F^-$  and  $z_F^+$  represents the bed position just before and after the feed inlet position respectively. Expression for composition of the mixed stream,  $y_m$  is given below.

From component mole balance at the mixing point we get,

$$y_{in} = \frac{1}{P_{n_F+1} v_{f,n_F+1}} \left( y_{n_F} P_{n_F} v_{f,n_F} + \frac{(F/t_F) y_F R T_g}{\varepsilon A} \right)$$

where  $v_{f,n_F+1}$  is calculated from total mole balance at mixing point

$$v_{f,n_F+1} = \frac{1}{P_{n_F+1}} \left( P_{n_F} v_{f,n_F} + \frac{(F/t_F) R T_g}{\varepsilon A} \right)$$

In expression of  $v_{f,n_F+1}$ ,  $v_{f,n_F}$  is calculated by discretizing the Blake-kozeny equation using backward difference scheme as

$$v_{f,n_F} = -K \left( \frac{3P_{n_F} - 4P_{n_F-1} + P_{n_F-2}}{2\Delta z} \right)$$

### A.2.2 Duplex TSA

#### ➤ Heating step

- at  $z = 0$

$$\left. \frac{\partial y}{\partial z} \right|_{z=0} = -\frac{v_f}{D_L} (y_{in} - y|_{z=0}) \Rightarrow y_0 = y_2 + 2\Delta z \left( \frac{v_f}{D_L} \right) (y_{in} - y_1)$$

$$\left. \frac{\partial P}{\partial z} \right|_{z=0} = -\frac{v_f}{K} \Rightarrow P_0 = P_2 + 2\Delta z \left( \frac{v_f}{K} \right)$$

$$\left. \frac{\partial T_g}{\partial z} \right|_{z=0} = -\frac{v_f}{\alpha} (T_{g,in} - T_g|_{z=0}) \Rightarrow T_{g,0} = T_{g,2} + 2\Delta z \left( \frac{v_f}{\alpha} \right) (T_{g,in} - T_{g,1})$$

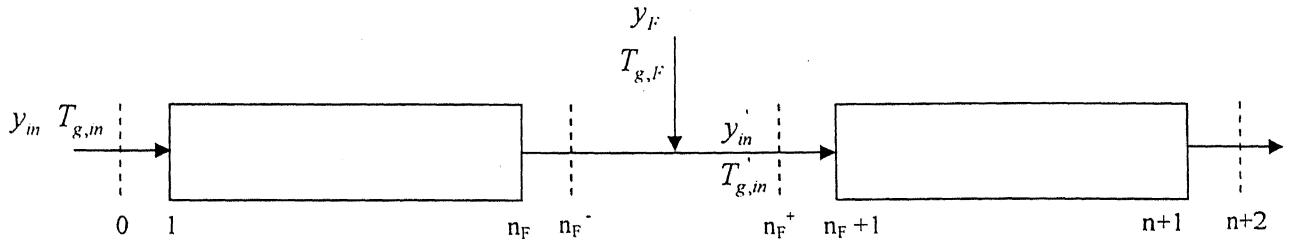
- at  $z = L$

$$\left. \frac{\partial y}{\partial z} \right|_{z=L} = 0 \Rightarrow y_{n+2} = y_n$$

$$\left. \frac{\partial P}{\partial t} \right|_{z=l.} = 0$$

$$\left. \frac{\partial T_g}{\partial z} \right|_{z=l.} = 0 \quad \Rightarrow \quad T_{g,n+2} = T_{g,n}$$

➤ *Cooling step*



- at  $z = 0$

$$\left. \frac{\partial y}{\partial z} \right|_{z=0} = -\frac{v_f}{D_L} (y_{in} - y|_{z=0}) \quad \Rightarrow \quad y_0 = y_2 + 2 \Delta z \left( \frac{v_f}{D_L} \right) (y_{in} - y_1)$$

$$\left. \frac{\partial P}{\partial z} \right|_{z=0} = -\frac{v_f}{K} \quad \Rightarrow \quad P_0 = P_2 + 2 \Delta z \left( \frac{v_f}{K} \right)$$

$$\left. \frac{\partial T_g}{\partial z} \right|_{z=0} = -\frac{v_f}{\alpha} (T_{g,in} - T_g|_{z=0}) \quad \Rightarrow \quad T_{g,0} = T_{g,2} + 2 \Delta z \left( \frac{v_f}{\alpha} \right) (T_{g,in} - T_{g,1})$$

- at  $z = z_{F^-}$

$$\left. \frac{\partial y}{\partial z} \right|_{z=z_{F^-}} = 0 \quad \Rightarrow \quad y_{n_F^-} = y_{n_F-1}$$

$$\left. \frac{\partial P}{\partial t} \right|_{z=z_{F^-}} = 0$$



$$\left. \frac{\partial T_g}{\partial z} \right|_{z=z_f^-} = 0 \quad \Rightarrow \quad T_{g,n_f} = T_{g,n_f-1}$$

- at  $z = z_f^+$

$$\left. \frac{\partial y}{\partial z} \right|_{z=z_f^+} = -\frac{v_f}{D_L} (y_m - y|_{z=z_f^+}) \quad \Rightarrow \quad y_{n_f^+} = y_{n_f+2} + 2\Delta z \left( \frac{v_f}{D_L} \right) (y_m - y_{n_f+1})$$

$$\left. \frac{\partial P}{\partial z} \right|_{z=z_f^+} = -\frac{v_f}{K} \quad \Rightarrow \quad P_{n_f^+} = P_{n_f+2} + 2\Delta z \left( \frac{v_f}{K} \right)$$

$$\left. \frac{\partial T_g}{\partial z} \right|_{z=z_f^+} = -\frac{v_f}{\alpha} (T_{g,m} - T_g|_{z=z_f^+}) \quad \Rightarrow \quad T_{g,n_f^+} = T_{g,n_f+2} + 2\Delta z \left( \frac{v_f}{\alpha} \right) (T_{g,m} - T_{g,n_f+1})$$

- at  $z = L$

$$\left. \frac{\partial y}{\partial z} \right|_{z=L} = 0 \quad \Rightarrow \quad y_{n+2} = y_n$$

$$\left. \frac{\partial P}{\partial z} \right|_{z=L} = 0$$

$$\left. \frac{\partial T_g}{\partial z} \right|_{z=L} = 0 \quad \Rightarrow \quad T_{g,n+2} = T_{g,n}$$

$z_f^-$  and  $z_f^+$  represents the bed position just before and after the feed inlet position respectively. Expression for composition and temperature of the mixed stream,  $y_m$  and  $T_{g,m}$  is given below.

From component mole balance at the mixing point we get,

$$y_m = \frac{T_{g,n_f+1}}{P_{n_f+1} v_{f,n_f+1}} \left( \frac{y_{n_f} P_{n_f} v_{f,n_f}}{T_{g,n_f}} + \frac{(F/t_F) y_F R}{\varepsilon A} \right)$$

where  $v_{f,n_F+1}$  is calculated from total mole balance at the mixing point as,

$$v_{f,n_F+1} = \frac{T_{g,n_F+1}}{P_{n_F+1}} \left( \frac{P_{n_F} v_{f,n_F}}{T_{g,n_F}} + \frac{(F/t_F)R}{\varepsilon A} \right)$$

In expression of  $v_{f,n_F+1}$ ,  $v_{f,n_F}$  is calculated by discretizing the Blake-kozeny equation using backward difference scheme as

$$v_{f,n_F} = -K \left( \frac{3P_{n_F} - 4P_{n_F-1} + P_{n_F-2}}{2\Delta z} \right)$$

## Appendix - B

### Integration scheme

For numerical integration, Newton-Cotes formula (degree of polynomial - 4) has been used which is given as (Joe D. Hoffman, *McGraw-Hill*, 1992)

$$I = \frac{4}{90} h (7f_1 + 32f_2 + 12f_3 + 32f_4 + 14f_5 + 32f_6 + 12f_7 + 32f_8 + 14f_9 + \dots \dots \dots + 32f_{n-2} + 12f_{n-1} + 32f_n + 7f_{n+1})$$

where  $n+1$  is the number of grid points and  $h$  is the length of the equally spaced grid element. Total number of grid elements,  $n$  must be integral multiple of four.